


2005

New Optimal High Efficiency Dsp-based Digital Controller Design For Super High-speed Permanent Magnet Synchronous Motor

limei Zhao
University of Central Florida

 Part of the [Electrical and Electronics Commons](#)
Find similar works at: <https://stars.library.ucf.edu/etd>
University of Central Florida Libraries <http://library.ucf.edu>

This Doctoral Dissertation (Open Access) is brought to you for free and open access by STARS. It has been accepted for inclusion in Electronic Theses and Dissertations, 2004-2019 by an authorized administrator of STARS. For more information, please contact STARS@ucf.edu.

STARS Citation

Zhao, limei, "New Optimal High Efficiency Dsp-based Digital Controller Design For Super High-speed Permanent Magnet Synchronous Motor" (2005). *Electronic Theses and Dissertations, 2004-2019*. 639.
<https://stars.library.ucf.edu/etd/639>

**NEW OPTIMAL HIGH EFFICIENCY DSP-BASED DIGITAL
CONTROLLER DESIGN FOR SUPER HIGH-SPEED PERMANENT
MAGNET SYNCHRONOUS MOTOR**

by

LIMEI ZHAO

A dissertation submitted in partial fulfillment of the requirements
for the degree of Doctor of Philosophy
in the Department of Electrical and Computer Engineering
in the College of Engineering and Computer Science
at the University of Central Florida
Orlando, Florida

Fall Term
2005

Major Professors: Dr. Thomas X. Wu, Dr. Chan Ham

© 2005 Limei Zhao

ABSTRACT

This dissertation investigates digital controller and switch mode power supply design for super high-speed permanent magnet synchronous motors (PMSM). The PMSMs are a key component for the miniaturic cryocooler that is currently under development at the University of Central Florida with support from NASA Kennedy Space Center and the Florida Solar Energy Center. Advanced motor design methods, control strategies, and rapid progress in semiconductor technology enables production of a highly efficient digital controller. However, there are still challenges for such super high-speed controller design because of its stability, high-speed, variable speed operation, and required efficiency over a wide speed range. Currently, limited research, and no commercial experimental analysis, is available concerning such motors and their control system design.

The stability of a super high-speed PMSM is an important issue particularly for open-loop control, given that PMSM are unstable after exceeding a certain applied frequency. In this dissertation, the stability of super high-speed PMSM is analyzed and some design suggestions are given to maximize this parameter.

For ordinary motors, the V/f control curve is a straight line with a boost voltage because the stator resistance is negligible and only has a significant effect around the DC frequency. However, for the proposed super high-speed PMSM the situation is quite different because of the motor's size. The stator resistance is quite large compared with the stator reactive impedance and cannot be neglected when employing constant a V/f control method. The challenge is to design an optimal constant V/f control scheme to raise efficiency with constant V/f control.

In the development, test systems and prototype boards were built and experimental results confirmed the effectiveness of the dissertation system.

Dedicated to God, my parents, my sister, and all people supporting me

ACKNOWLEDGMENTS

I would like to express my sincere gratitude to my advisors, Dr. Thomas X. Wu and Dr. Chan H. Ham, for their guidance, encouragement and continuous caring support during my graduate studies. Their extensive knowledge, vision, creative thinking, and careful research attitude have been the source of inspiration and encouragement for me throughout this work. They have been invaluable in improving everything from my writing and presentation skills to my general personality. Without their help, constant encouragement, and support, this work would not have been possible.

I am so grateful to Dr. Louis Chow for providing me with the opportunity to work with the NASA project. Many in-depth discussions with him have invaluable shaped every part of this work. He is so patient to teach me how to conduct a careful research. Besides, I would like to thank my other committee members, Dr. Jayanta Kapat, Dr. Kalpathy B. Sundaram, and Dr. Michael G. Haralambous for their help and encouragement on my research and education.

I must thank all my friends and the members of the project. I would like to thank Liping Zheng, Dipjyoti Acharya, and Lei Zhou for the friendship, enlightening discussions, valuable help, and innumerable number of hours we spent to work together.

Specially, thanks to the members of Florida Power Electronics Center, Mr. Xiangcheng Wang, Dr. Wenkai Wu, Dr. Hong Mao, and other students for the very helpful exchanges of thoughts and experiences.

Many thanks to other faculties, staffs, and students, especially to Ms. Arlene Ollivierre, for their wonderful help and support for this project. Also thanks to many

friends in church OCECC. Their friendship and pray made my stay at UCF pleasant, enjoyable and unforgettable.

Finally, special thanks go to my parents and my sister's family for their constant understanding and support during my educational career. Their love, encouragement, and inspiration have driven me to this point in my life and help to shape my future.

TABLE OF CONTENTS

| | |
|--|-----|
| LIST OF FIGURES | xii |
| LIST OF TABLES | xiv |
| CHAPTER ONE: INTRODUCTION | 1 |
| 1.1 Motivation and Objectives | 1 |
| 1.2 Review of Previous Research | 1 |
| 1.3 Dissertation Outline and Major Results | 6 |
| CHAPTER TWO: TECHNICAL REVIEW | 8 |
| 2.1 Permanent Magnet Motors | 9 |
| 2.1.1 Several Important Parameters | 11 |
| 2.1.2 Back EMF (Back ElectroMotive Force) | 13 |
| 2.2 Reference-Frame Theory | 14 |
| 2.2.1 Equations of Transformation | 15 |
| 2.2.2 Mathematical Modeling and Equivalent Circuit of PMSM | 18 |
| 2.3 Pulse Width Modulation Switching Scheme | 21 |
| 2.3.1 Sinusoidal PWM | 22 |
| 2.3.2 Space Vector PWM | 24 |
| 2.4 Power Transistors | 27 |
| 2.5 Adjustable-Speed Drive System | 29 |
| CHAPTER THREE: SUPER HIGH-SPEED PMSM STABILITY ANALYSIS | 31 |
| 3.1 Steady-State Equation of PMSM | 32 |
| 3.2 Stability Simulation and Analysis for Super High-Speed Motor 1 | 34 |

| | |
|--|----|
| 3.3 Stability Simulation and Analysis for Super High-Speed Motor 2..... | 38 |
| 3.4 Conclusion | 43 |
| 3.5 Design Parameters of Proposed Super High-Speed PMSMs..... | 44 |
| CHAPTER FOUR: OPTIMAL CONSTANT V/f CONTROL..... | 47 |
| 4.1 Constant V/f Control Criterion..... | 48 |
| 4.2 Derivation of an optimal V/f curve..... | 53 |
| 4.3 Optimal V/f Control Simulation and Analysis for Super High-Speed Motor | 58 |
| CHAPTER FIVE: DSP_BASED DIGITAL CONTROLLERS..... | 67 |
| 5.1 Analog Controller and Digital Controller..... | 67 |
| 5.2 DSP-based Digital Controller | 69 |
| 5.3 Motor Control | 71 |
| 5.4 Digital Control Portion | 72 |
| 5.5 Architecture of TI C2000..... | 73 |
| 5.5.1 TI TMS320F240 | 74 |
| 5.6 PWM Generators and ADC of TMS320LF2407A | 76 |
| 5.7 The Generation of Sine Wave..... | 80 |
| CHAPTER 6: DESIGN AND OPTIMIZE DIGITAL CONTROL AND SWITCH MODE POWER SUPPLY SYSTEM..... | 82 |
| 6.1 Switch Mode Power Supply..... | 83 |
| 6.1.1 Three-phase Voltage Source Inverter | 83 |
| 6.1.2 Power MOSFET..... | 84 |
| 6.1.3 MOSFET Gate Charge..... | 85 |
| 6.2 Gate Drive System | 88 |

| | |
|--|-----|
| 6.2.1 Drive Chip IR 2110..... | 88 |
| 6.2.2 IR2110 Bootstrap Circuits Design Tips | 91 |
| 6.3 Configuration of Hardware System | 92 |
| 6.4 High Current Design | 94 |
| 6.4.1 Current Rating..... | 95 |
| 6.4.2 High Current Distribution Devices | 96 |
| 6.5 Loss Calculation..... | 98 |
| 6.6 Interface | 102 |
| 6.7 Controller Implementation with TMS320F2407A | 104 |
| 6.8 The Proposed Embedded System..... | 105 |
| 6.8.1 Main blocks..... | 108 |
| CHAPTER SEVEN: EXPERIMENTAL RESULTS AND ANALYSIS | 109 |
| 7.1 Calibration of Current Probe..... | 109 |
| 7.2 Experimental Results of Test Motor 1 | 111 |
| 7.3 Experimental Results of Test Motor 2 | 116 |
| 7.4 Load Test Results and Analysis..... | 117 |
| 7.5 Trouble Shooting | 121 |
| CHAPTER EIGHT: CONCLUSION | 124 |
| 8.1 Conclusion | 124 |
| LIST OF REFERENCES | 125 |

LIST OF FIGURES

| | |
|--|----|
| Figure 2.1 A typically radial Permanent Magnet Synchronous Motor [36] | 10 |
| Figure 2.2 An axial Permanent Magnet Synchronous Motor [37]..... | 10 |
| Figure 2.3 Permanent Magnet Synchronous Motor poles [36]..... | 11 |
| Figure 2.4 Reference-Frame Theory..... | 15 |
| Figure 2.5 Equivalent qd0 circuits of a permanent magnet synchronous motor | 20 |
| Figure 2.6 Principle of Sinusoidal PWM Method [38]..... | 23 |
| Figure 2.7 A typical three-phase voltage source inverter | 25 |
| Figure 2.8 Basic Space Vectors | 25 |
| Figure 2.9 SV PWM signal..... | 27 |
| Figure 2.10 Structure of adjustable-speed drive system [9] | 29 |
| Figure 3.1 Loci of super high-speed PMSM under different driving frequencies and R_s , with $L_s = 1.6 \mu H$. Speed range is from 0-100 Krpm. | 36 |
| Figure 3.2 Loci of super high-speed PMSM under different driving frequencies and L_s , with $R_s = 0.06 \text{ ohms}$. Speed range is from 0-100 Krpm. | 36 |
| Figure 3.3 Loci of super high-speed PMSM under different driving frequencies and L_s , with $R_s = 0.006 \text{ ohms}$. Speed range is from 0-100 Krpm. | 37 |
| Figure 3.4 Root Loci of super high-speed PMSM under different driving frequency, with $R_s = 0.06 \Omega$, $L_s = 1.6 \mu H$, and different load angle. Speed range is from 0-100 Krpm. | 38 |
| Figure 3.5 Loci of super high-speed PMSM under different driving frequencies and R_s , with $L_s = 1 \mu H$. Speed range is from 0-200 Krpm. | 40 |

| | |
|---|----|
| Figure 3.6 Loci of super high-speed PMSM under different driving frequencies and L_s , with $R_s = 0.0057 \Omega$. Speed range is from 0-200 Krpm..... | 41 |
| Figure 3.7 Root Loci of super high-speed PMSM under different driving frequency, with $R_s = 0.0057 \Omega$, $L_s = 1 \mu H$, and different load angle. Speed range is from 0-200 Krpm. | 42 |
| Figure 3.8 Cross section of the designed PMSM [36] | 44 |
| Figure 3.9 Components of proposed PMSM | 45 |
| Figure 4.1 Torque-speed curves at variable voltage and variable frequency [8]..... | 49 |
| Figure 4.2 Voltage and frequency in constant torque and field-weakening regions [8]... | 50 |
| Figure 4.3 A typical V/f profile | 52 |
| Figure 4.4 A modified V/f profile | 52 |
| Figure 4.5 PMSM steady state equivalent circuit and phasor diagram 1..... | 53 |
| Figure 4.6 PMSM steady state equivalent circuit and phasor diagram 2..... | 57 |
| Figure 4.7 The simulation of proposed optimal constant V/f control design..... | 58 |
| Figure 4.8 Configuration of module deta..... | 59 |
| Figure 4.9 Configuration of module I_s | 59 |
| Figure 4.10 Configuration of module F_{ai} | 60 |
| Figure 4.11 Configuration of module V_s | 60 |
| Figure 4.12 Configuration of module I_q and Torque..... | 61 |
| Figure 4.13 Linear constant V/f (Volt/Hz) control with boost voltage ($R_s = 0.001 \Omega$) .. | 62 |
| Figure 4.14 The proposed optimal V/f (Volt/Hz) profile for test motor. Speed range is from 0-100 Krpm. | 63 |

| | |
|---|-----|
| Figure 4.15 Optimal V/f (Volt/Hz) control with difference stator resistance and $L_s=1.6 \mu$ H, $K=0.0045$. Speed range is from 0-100 Krpm..... | 64 |
| Figure 4.16 Optimal V/f (Volt/Hz) control with difference inductance and $R_s = 0.06 \Omega$, $K=0.0045$. Speed range is from 0-100 Krpm..... | 65 |
| Figure 4.17 Optimal V/f (Volt/Hz) control with difference K and $R_s = 0.06 \Omega$, $L_s=1.6 \mu$ H. Speed range is from 0-100 Krpm..... | 66 |
| Figure 5.1 Typical digital controller configurations [31] | 73 |
| Figure 5.2 TI TMS320 development board [44]..... | 75 |
| Figure 5.3 TI TMS320LF2407A Evaluation Board [45]..... | 76 |
| Figure 5.4 Generating PWM waveform in TI TMS320LF2407A [28] | 78 |
| Figure 5.5 Symmetrical PWM signals generation [28] | 79 |
| Figure 5.6 Asymmetrical PWM signals generation [28] | 80 |
| Figure 6.1 The block diagram of the proposed controllers..... | 82 |
| Figure 6.2 A typical three-phase voltage source inverter | 84 |
| Figure 6.3 MOSFET equivalent circuits at high frequency | 86 |
| Figure 6.4 Gate and drive waveforms [50] | 87 |
| Figure 6.5 IR2110 function block diagram [56] | 89 |
| Figure 6.6 IR2110 typical connection [56]..... | 89 |
| Figure 6.7 The 2000 W PMSM controller hardware circuit schematic..... | 92 |
| Figure 6.8 Fairchild FDP047AN08A0 safe operating area (SOA) [57] | 93 |
| Figure 6.9 Typical switching waveforms of power transistors..... | 99 |
| Figure 6.10 Prototype of inverter with heat sink | 105 |
| Figure 6.11 Software configuration | 106 |

| | |
|---|-----|
| Figure 6.12 Software flow chart | 107 |
| Figure 7.1 Phase shift and attenuation of AM Meter..... | 110 |
| Figure 7.2 The real current value/ the reading value under different motor speed..... | 111 |
| Figure 7.3 PMSM phase current ring error with mechanical speed (normalized) -- Real test results comparison..... | 113 |
| Figure 7.4 Motor phase voltage V_a , V_b and phase current I_c waveforms at 50,000 RPM | 114 |
| Figure 7.5 Phase current I_c harmonic FFT analysis (normalized) | 115 |
| Figure 7.6 Input power to controller under different motor speed | 116 |
| Figure 7.7 LCR meter | 117 |
| Figure 7.8 Test connection resistance with LCR meter..... | 118 |
| Figure 7.9 Controller efficiency with load..... | 120 |
| Figure 7.10 Bootstrap supply schematic [33] | 122 |
| Figure 7.11 Ring effect of V_B and V_s on drive IR2110 [32]..... | 123 |
| Figure 7.12 Two methods of V_s undershoot immunity [32]..... | 123 |

LIST OF TABLES

| | |
|--|-----|
| Table 1.1 PM Specifications in [1] | 2 |
| Table 1.2 Super High-Speed Machines [2]..... | 3 |
| Table 1.3 Design Parameters of Experimental Motor [3]..... | 6 |
| Table 2.1 SV PWM switching states [39]..... | 26 |
| Table3.1: Proposed super high-speed motor parameters | 46 |
| Table 6.1 Relationship between bus bar size and current..... | 95 |
| Table 7.1 Load test results and analysis..... | 119 |

CHAPTER ONE: INTRODUCTION

1.1 Motivation and Objectives

With the aeronautics and spacecraft technology development, numerous applications for cryocoolers have been proposed and developed in recent years. As the key components of these cryocoolers, highly effective miniature compressors and super high-speed motors are attracting more and more attention. As a result, the demand for super high-speed motors has increased recently due to technology advancements and cost reduction in power electronics, permanent magnet materials, and motor design. Remarkably small and lightweight of the super high-speed permanent magnet synchronous machine (PMSM) leads to high ratios of power to mass and power to volume. The PMSM systems also have a very high efficiency, which suppresses heat generation, particularly in rotors.

The following proposed PMSM systems are key components of the reverse Brayton cryocooler that is currently under development at the University of Central Florida supported by NASA Kennedy Space Center and the Florida Solar Energy Center.

1.2 Review of Previous Research

Thanks to rapid progress in power, microelectronics, and advanced motor design methods, highly efficient super high-speed PMSM controllers are becoming possible.

However, no experimental results or analysis of such super high-speed (200 Krpm) is available.

SatCon as a member of a consortium of companies (Carrier Corporation, Allied-Signal, General Electric, DuPont and Lockheed-Martin Control Systems) is working towards the development of a 25-ton proof-of-concept centrifugal compressor. SatCon Technology Corporation of the design of two high speed motor drive systems for industrial applications: (1) a 28 hp, only 47,000 rpm prototype PM motor drive for deployment in the centrifugal compressor of a 25-ton, rooftop air-conditioning unit and (2) a 45 kW, 92,500 rpm induction machine to be used with the turbo-charger of a diesel military engine. Table 1.1 is its PM specifications. [1]

Table 1.1 PM Specifications in [1]

| | |
|----------------------------|--------|
| Output power (hp) | 30 |
| Speed (rpm) | 54,000 |
| Motor efficiency (%) | >95 |
| Motor drive efficiency (%) | 90 |
| Terminal voltage (V) | 460 |
| Number of phases | 3 |
| Frequency (Hz) | 60 |
| Motor coolant | R134a |

In [2], the authors proposed several super high-speed machines projects, whose maximum speed is only 180 Krpm for induction motor and only 100 Krpm for PM motor.

Table 1.2 Super High-Speed Machines [2]

| SUPER-HIGH-SPEED MACHINES | | | | |
|---------------------------|-------------|---------------|----------------------|-----------------------|
| Machine type | speed r/min | output kW/kVA | comment | super high/high speed |
| Sync | 5,250 | 30000 | ICI | Super HS |
| Sync | 4,900 | 4200 | ICI | HS |
| IM | 8,000 | 3500 | | HS |
| IM | 10,000 | 6750 | ICI | Super HS |
| IM | 11,000 | 3300 | compressor | Super HS |
| PM | 15,000 | 1000 | cogeneration | Super HS |
| IM | 30,000 | 556 | cogeneration | Super HS |
| PM | 45,000 | 70 | machine tool spindle | Super HS |
| SBM | 48,000 | 32 | fuel pump | Super HS |
| PM | 60,000 | 200 | test | Super HS |
| Claw | 80,000 | 50 | generator for maglev | Super HS |
| Claw | 90,000 | 31 | hybrid car | Super HS |
| Claw | 100,000 | 25 | helium pump | Super HS |
| PM | 100,000 | 2.6 | mobile generator | Super HS |
| IM | 180,000 | 10 | test machine | Super HS |
| IM | 180,000 | 1.6 | machine tool spindle | Super HS |

Many challenges are still posed for such super high-speed PMSM system controller designs because of their super high-speed and their variable speed operation over wide speed ranges.

At first, inverters were working with high switching frequency at high power ratings. The super high-speed PMSM system routinely operates in the speed range from 0 to 200,000 rpm, with an excitation frequency from several to a few thousand hertz. In order to obtain satisfactory performance it is required that the ratio of the inverter switching frequency to the motor fundamental frequency be kept relatively high, a ratio of 10 or more [5]. It has even been suggested that the switching frequency should be at least 10 times higher than that of the most significant harmonic [6]. However, a high switching frequency will increase switching loss, produce extra heat, and reduce efficiency, especially in low speed range.

Secondly, the stability of a super high-speed PMSM is an important issue particularly for an open-loop constant V/f control approach. In other types of motors,

damper windings are used to assure the synchronization of motion of the rotor with the stator frequency applied to avoid stability problems [7]. Due to manufacturing costs, design difficulties, and efficiency considerations, damper windings are not generally implemented in a PMSM. That means a PMSM may be unstable after exceeding a certain applied frequency. Little solid data is available on a PMSM open-loop V/f control and its stability analysis.

Thirdly, the control approaches used most commonly in PMSM control are scale control, vector or field-oriented control, and direct torque control (DTC). For high-performance motion control applications the vector control and DTC are used to achieve high dynamic performance in position, speed, and torque. However, when motor drives are used for applications like pumps, fans, and heating, where the load is predictable and high dynamic performance is not a demand, a simple constant V/f control strategy can be used instead of the much more complex vector or DTC control approach [5][8]. The constant V/f control can be used in both open-loop and close-loop control. Open-loop speed control can be used when accuracy in speed response is not a concern such as in ventilation, air condition and compressor. By far, the constant V/f control method is the most popular method of speed control because of its simplicity and ease of implementation [9]. However, limited research results have been reported on V/f control scheme application on PMSM, especially on super high-speed PMSM with consideration of stator resistor.

For ordinary motors, the V/f control curve is a straight line with a boost voltage because the stator resistor is negligible and only has significant effect around the DC frequency. However, for the proposed super high-speed PMSM, the situation is quite

different because of the motor's small size requirement. The stator resistance is quite large compared with the stator reactive impedance and cannot be neglected when employing a constant V/f control method. So, the technical challenge is how to develop an optimal V/f control algorithm for this kind of motor.

Because of system requirements (200 Krpm, 2000 W output power, 28 V input voltage, 65 A high input current), no commercial products or research results is available.

Semikron, as the market leader in the field of power electronics modules and enjoying a 33% share of the European market, can provide 3-phase digital control with 1452W and maximum switching frequency is only 20 KHz, which is not fast enough for our target super high-speed.

IR, the biggest company in power electronic industry, has IRAM family, which is optimized for 400W to 2500W motor drives and features IR's rugged NPT IGBT technology and its industry benchmark three-phase, high voltage gate driver ICs. However, the maximum current rating is only 20A and maximum switching frequency is only 20 KHz.

Motorola Freescale has 400V DC up to 5A and power rating up to 600W. The product of Siemens: SIMOREG Control Module 6RA70, is digitally controlled and field current supply only up to 40 Amps.

In [3], the authors designed and built a trial ultra-high speed drive system of 2 poles, 5kW, 240,000 rpm motor. However, the rated current is only 25A.

Table 1.3 Design Parameters of Experimental Motor [3]

| | |
|-----------------|-------------|
| Rated Output | 5 kW |
| Rated Voltage | 200 V |
| Rated Speed | 240,000 rpm |
| Number of Poles | 2 |
| Stator Length | 40 mm |

In [4], the maximal speed is about 200,000 rpm with a power of only 1kW on the mechanical shaft.

1.3 Dissertation Outline and Major Results

This dissertation analyzes the effect of the PMSM parameters on its dynamic characteristics including its stability and performance. It is presented that super high-speed PMSM stability can be achieved over the full operating speed range. The stator resistance, R_s , which cannot be neglected, is taken into account to design V/f control. An optimal nonlinear V/f control scheme is derived.

Experimental experience and results gained from DSP-based digital controllers for super high-speed PMSMs are introduced in this dissertation. Testing systems and prototype boards for the super-high speed PMSMs have been built and the feasibility of open-loop control modes has been examined.

The dissertation is arranged as follows.

There are eight chapters including an introduction. Chapter 2 describes the technical background about permanent magnet synchronous motors (PMSM) and

controller. Chapter 3 presents PMSM mathematic model and stability analysis. Chapter 4 investigates the constant V/f method while considering of the stator resistor. An approach for optimal constant V/f algorithm is proposed. Analysis of the effect of the components on the optimal design is performed as well in this chapter. Chapter 5 introduces the concept of DSP-based digital controllers. In chapter 6, the design and optimization of digital control system and switch mode power supply system are proposed. Experimental results and analysis are presented in chapter 7 to confirm the theoretical developments and demonstrate the feasibility of the practical implementation and test analysis. Finally, conclusions of this work and suggestions for future works are outlined in Chapter 8.

CHAPTER TWO: TECHNICAL REVIEW

Super high-speed motors are becoming more and more attractive in many applications, such as centrifugal compressors and spacecraft, in recent years. There are many kinds of motors that can be considered for such applications.

Induction motors are the most numerous in today's industry. Induction machines are simple, rugged and usually cheap to produce. They dominate in the applications where rotational speeds are not required to vary and are not important. However, they are with relatively low efficiency at high speed due to the higher iron loss in the rotor [9].

Synchronous motors have several advantages over induction motors such as high efficiency. Due to the fast development of power semiconductor industry, more and more induction motors are replaced by synchronous motors in industry applications. Several types of synchronous motor are employed mostly for high-speed application: Switched reluctance motor, brushless DC motor, and Permanent Magnet Synchronous Motor (PMSM).

Switched reluctance motors have high reliability with simple and robust rotor structure [9], however, the iron loss is critical at high speed. The brushless DC motor, which has a trapezoidal induced electromagnetic force (back EMF), evolved from the brush DC motor as power electronic devices became available to provide electronic commutation in place of the mechanical commutation provided by brushes.

Although Brushless DC motors tend to be more popular than AC synchronous motors due to its simplicity and high power density, the high efficiency requirement at high speeds makes it impossible for some applications such as cryogenic coolers.

Permanent Magnet Synchronous Motors (PMSM) were introduced in recent years. Permanent magnets are used in place of electromagnets to provide an excitation field. The advantage of this approach is the elimination of field copper loss, higher power density, lower rotor inertia, and more robust construction of rotor. However, the downside is the loss of flexibility of field flux control and possible demagnetization effect [8]. Due to low harmonics of the induced sine electromagnetic force (back EMF), no excitation power loss in the rotor and only low eddy current loss in the stator and rotor exist. Slotless stator structure also eliminates the cogging torque. All of these technical advantages make it possible to design a slotless PMSM for super high-speed with high efficiency.

2.1 Permanent Magnet Motors

In Permanent Magnet Synchronous Motor, the field of winding of the synchronous machine is replaced by permanent magnets. This approach increases the efficiency of the machine and reliability due to the elimination of rotor winding maintenance. It also results in smaller size, less weight and higher torque to size ratio.

A typically radial permanent magnet synchronous motor is shown as following [36].

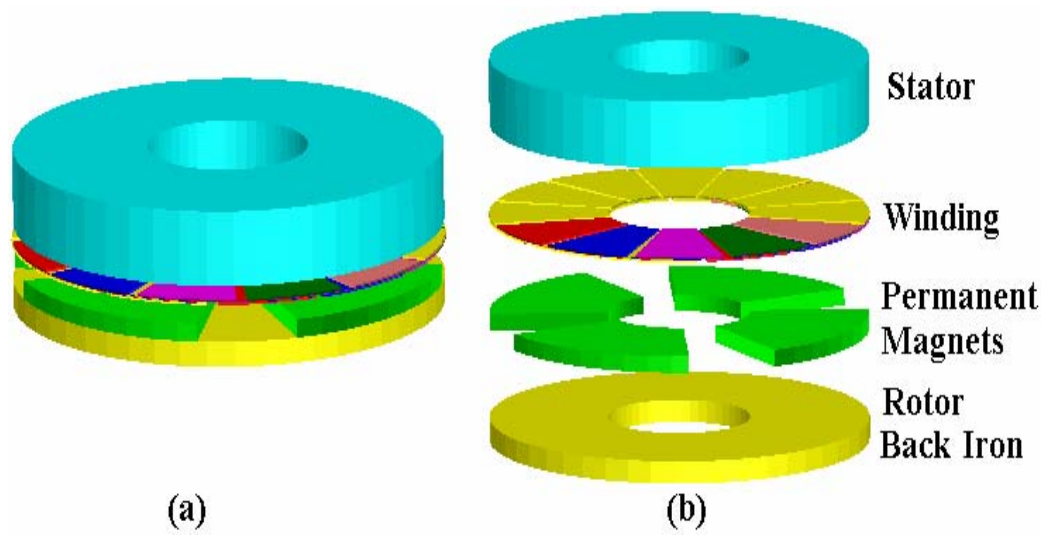


Figure 2.1 A typically radial Permanent Magnet Synchronous Motor [36]

Axial structure PMSM can be design as following [10][37]:

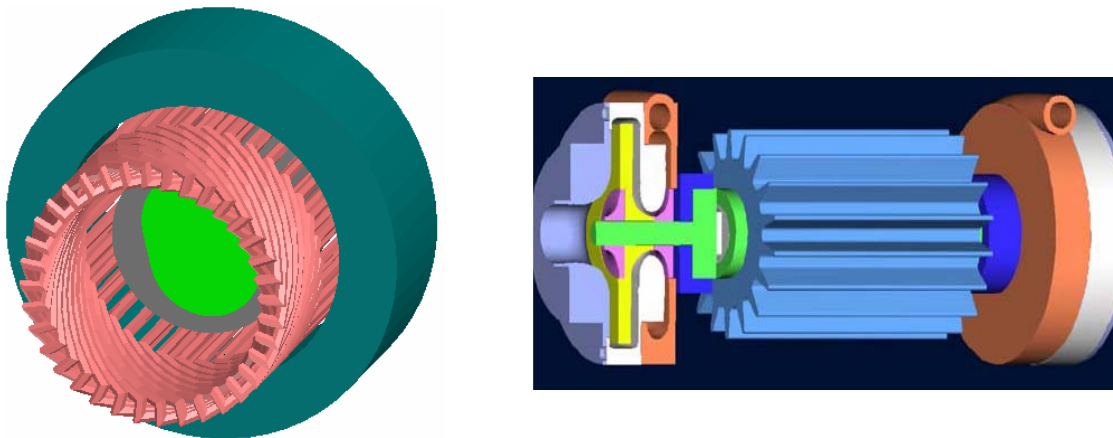


Figure 2.2 An axial Permanent Magnet Synchronous Motor [37]

2.1.1 Several Important Parameters

Number of Poles

For PM motor, the magnetic excitation is supplied by a permanent magnet. More PM poles will result in better spatial sinusoidal distribution of the air gap magnetic field. But too many poles will increase leakage and iron loss in the stator.

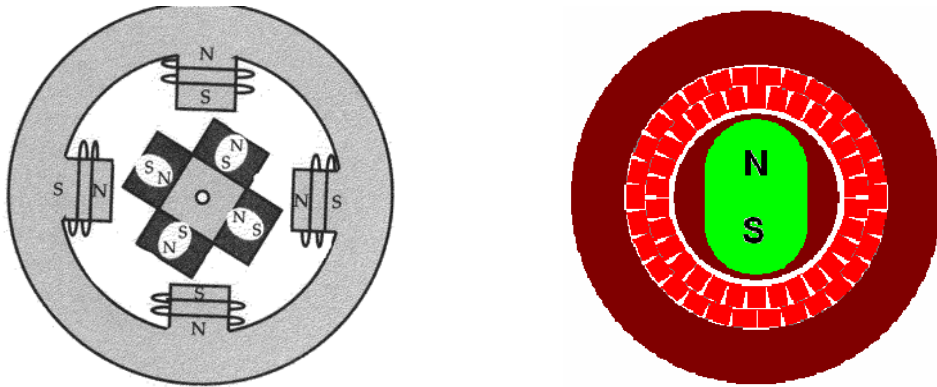


Figure 2.3 Permanent Magnet Synchronous Motor poles [36]

The number of poles is an important specification for PMSM. It has a directly reverse relationship with motor speed. The relationship of motor speed and the number of poles is:

$$S = 120 * f / p \quad (1)$$

S is motor speed, which is in RPM

f is motor input electrical frequency

p is the number of poles

With fewer poles, motors can be driven to higher speed in same condition. However, if the number of poles decreases, the size of the motor will increase.

Mechanical and Electrical Position and Speed

Mechanical position and speed are the respective position and speed of the rotor output shaft. Electrical position is defined such that the movement of the rotor by 360 electrical degrees puts the rotor back in an identical magnetic orientation. The relationship between mechanical and electrical position and speed can be stated as

$$\theta_e = N_p \cdot \theta_m \quad (2)$$

$$\omega_e = N_p \cdot \omega_m \quad (3)$$

where θ_e and θ_m are electrical and mechanical positions, respectively,

ω_e and ω_m are electrical and mechanical frequencies, respectively, and

N_p is the number of magnetic pole pairs.

The mechanical speed S in terms of revolutions per minute (RPM) can be stated as

$$S = \frac{30}{\pi} \omega_m \quad (4)$$

2.1.2 Back EMF (Back ElectroMotive Force)

When an electric motor is running, its armature windings are cutting through the magnetic field of the stator. Thus the motor is acting also as a generator. According to Lenz's Law, the induced voltage in the armature will oppose the applied voltage in the stator. This induced voltage is called back EMF (electromotive force). 'Back' because it tends to cancel out the applied voltage so that the actual voltage (pressure) across the armature is the difference between the applied voltage and the back EMF. The value of the back EMF is determined by the speed of rotation and the strength of the magnet(s) such that if the magnet is strong the back EMF increases and if the speed increases, so too does the back EMF.

Back EMF is very important in electric motors. When the motor is first turned on, there is no back EMF inasmuch as the armature is not yet turning. This means that the motor will have a high starting torque since there is no opposition to the applied voltage. Then when the motor is running at speed, the back EMF will oppose much of the applied voltage and the net result is a relatively small amount of power consumption. If a load is applied, speed will slow down. The back EMF will decrease so the difference between applied voltage and back EMF will increase. It is this difference that causes the current in the armature to flow - so the current will increase if increasing the mechanical loading and more power is applied to maintain the torque.

Many methods can be used to calculate the back EMF of the motor. The back EMF value can be calculated as

$$e_b = \frac{d\Lambda}{dt} = \frac{d\Lambda}{d\theta} \cdot \frac{d\theta}{dt} \quad (5)$$

and we also have

$$\frac{d\theta}{dt} = \frac{S}{60} \times 360^\circ \quad (6)$$

where S is the mechanical speed in RPM.

We can also calculate the back EMF using the analytical method according to the following equation

$$E_{rms} = \frac{2\pi}{\sqrt{2}} f k_w N \phi_u \quad (7)$$

where f is the electrical frequency,

k_w is the winding factor,

N is the number of coils per group,

ϕ_u is the useful flux per pole.

This equation shows clearly that back EMF has a direct relationship with electrical frequency.

2.2 Reference-Frame Theory

A change of variable is often used to reduce the complexity of these differential equations. The general transformation refers machine variables to a frame of reference,

which rotates at an arbitrary angular velocity. All known real transformations are obtained from this general transformation by simply assigning the speed of rotation of the reference frame.

In electric machine and controller system, the reference-frame transformation plays an important part in analysis currents, voltages and fluxes. The reference-frame transformation basically uses the method of changing variables to change from one reference frame to another one. This method reduces the computation and analysis complexity. The variables are presented in a reference frame rotating at synchronous speed. Hence, they are transformed to the synchronous rotating reference frame by a change of variables. [11]

2.2.1 Equations of Transformation

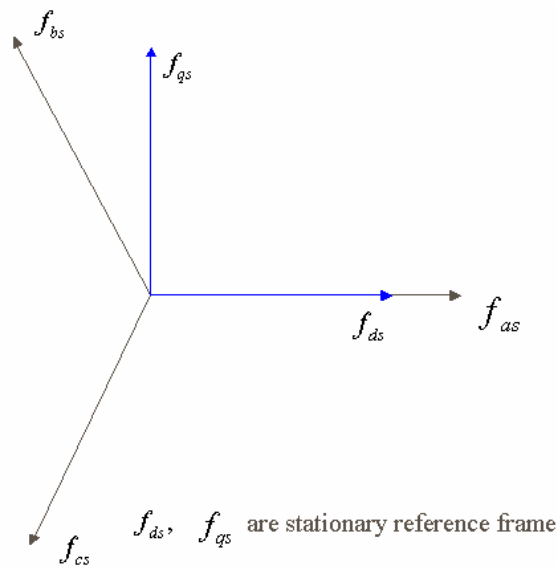


Figure 2.4 Reference-Frame Theory

For transforming three-phase frame system to two-phase (stator) frame system, we have the instantaneous values of the actual phase vector as

$$\begin{aligned} i_s &= i_{as} + i_{bs} [\cos(2\pi/3) + j\sin(2\pi/3)] + i_{cs} [\cos(4\pi/3) + j\sin(4\pi/3)] \\ &= i_{ds} + j i_{qs} \end{aligned} \quad (11)$$

So, i_{ds} and i_{qs} can be presented as

$$\begin{bmatrix} i_{ds} \\ i_{qs} \end{bmatrix} = \begin{bmatrix} 1 & \frac{-1}{2} & \frac{-1}{2} \\ 0 & \frac{\sqrt{3}}{2} & \frac{-\sqrt{3}}{2} \end{bmatrix} \begin{bmatrix} i_{as} \\ i_{bs} \\ i_{cs} \end{bmatrix} \quad (12)$$

The derived matrix equation expresses the $abc \rightarrow dq$ transformation.

For three-phase system, we also have

$$i_{as} + i_{bs} + i_{cs} = 0 \quad (13)$$

Put (13) into (12) and (12) can be rewritten as the following expansion of the matrix equation:

$$\begin{bmatrix} i_{ds} \\ i_{qs} \\ 0 \end{bmatrix} = \begin{bmatrix} 1 & \frac{-1}{2} & \frac{-1}{2} \\ 0 & \frac{\sqrt{3}}{2} & -\frac{\sqrt{3}}{2} \\ 1 & \frac{2}{1} & \frac{2}{1} \end{bmatrix} \begin{bmatrix} i_{as} \\ i_{bs} \\ i_{cs} \end{bmatrix} \quad (14)$$

Now, we can achieve the inverse $dq \rightarrow abc$ transformation by the matrix equation:

$$\begin{bmatrix} i_{as} \\ i_{bs} \\ i_{cs} \end{bmatrix} = \begin{bmatrix} \frac{2}{3} & 0 & \frac{1}{3} \\ -\frac{1}{3} & \frac{1}{\sqrt{3}} & \frac{1}{3} \\ -\frac{1}{3} & -\frac{1}{\sqrt{3}} & \frac{1}{3} \end{bmatrix} \begin{bmatrix} i_{ds} \\ i_{qs} \\ 0 \end{bmatrix} \quad (15)$$

It can be rewritten as

$$\begin{bmatrix} i_{as} \\ i_{bs} \\ i_{cs} \end{bmatrix} = \begin{bmatrix} \frac{2}{3} & \frac{0}{\sqrt{3}} \\ -\frac{1}{3} & \frac{1}{\sqrt{3}} \\ -\frac{1}{3} & -\frac{1}{\sqrt{3}} \end{bmatrix} \begin{bmatrix} i_{ds} \\ i_{qs} \end{bmatrix} \quad (16)$$

2.2.2 Mathematical Modeling and Equivalent Circuit of PMSM

With the reference-frame transformation, the mathematical modeling of PMSM can be shown as:

$$\begin{aligned}
 v_q &= r_s i_q + \frac{d\lambda_q}{dt} + \lambda_d \frac{d\theta_r}{dt} \\
 v_d &= r_s i_d + \frac{d\lambda_d}{dt} - \lambda_q \frac{d\theta_r}{dt} \\
 v_0 &= r_s i_0 + \frac{d\lambda_0}{dt} \\
 0 &= r'_{kd} i'_{kd} + \frac{d\lambda'_{kd}}{dt} \\
 0 &= r'_{kq} i'_{kq} + \frac{d\lambda'_{kq}}{dt}
 \end{aligned} \tag{17}$$

After transformation and derivation, the PMSM can be represented using the following equations and the flux linkage is:

$$\begin{aligned}
 \lambda_q &= L_q i_q + L_{mq} i'_{kq} \\
 \lambda_d &= L_d i_d + L_{md} i'_m \\
 \lambda_0 &= L_s i_0 \\
 \lambda'_{kd} &= L_{md} i_d + L'_{kd} i'_{kd} + L_{mq} i'_m \\
 \lambda'_{kq} &= L_{mq} i_q + L_{kq} i'_{kq}
 \end{aligned} \tag{18}$$

where

| | |
|-----------------------------------|--|
| V_q, V_d, V_0 | $qd0$ voltages |
| i_q, i_d, i_0 | $qd0$ currents |
| $\lambda_q, \lambda_d, \lambda_0$ | $qd0$ flux linkages |
| r_s | armature or stator winding resistance |
| θ_r | rotor angle |
| $L_{mq}, L_{md},$ | mutual inductance in q-axis and d-axis |
| L_{ls} | armature or stator winding leakage inductance |
| L_q | q-axis synchronous inductance, and $L_q = L_{mq} + L_{ls}$ |
| L_d | d-axis synchronous inductance, and $L_d = L_{md} + L_{ls}$ |
| r'_{kq}, r'_{kd} | equivalent q-axis and d-axis damper winding resistance |
| $\lambda'_{kq}, \lambda'_{kd}$ | equivalent q-axis and d-axis damper flux linkage |
| L'_{kdkd} | equivalent d-axis damper inductance |
| i'_{kq}, i'_{kd} | equivalent q-axis and d-axis damper current |
| i'_m | equivalent magnetizing current of permanent magnets |

So the equivalent $qd0$ circuit is given in Figure 2.5, where L_{rc} is the equivalent permanent magnet inductance which is associated with its recoil slope. It is lumped with the common d-axis mutual inductance of the stator and damper windings and the combined d-axis mutual inductance denoted still by L_{md} .

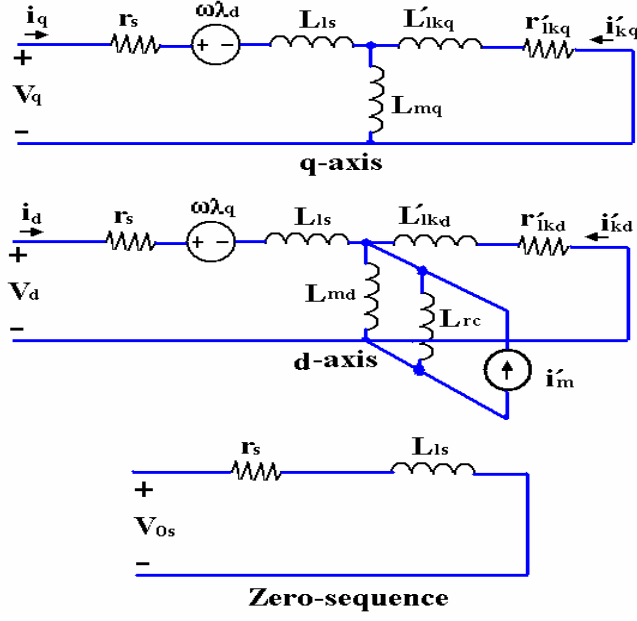


Figure 2.5 Equivalent qd0 circuits of a permanent magnet synchronous motor

The total power into the motor is given by

$$P_{in} = v_a i_a + v_b i_b + v_c i_c \quad (19)$$

or

$$\begin{aligned} P_{in} &= \frac{3}{2} (v_q i_q + v_d i_d) + 3v_0 i_0 \\ &= \frac{3}{2} (r_s (i_q^2 + i_d^2)) + \frac{3}{2} \left(i_q \frac{d\lambda_q}{dt} + i_d \frac{d\lambda_d}{dt} \right) + \frac{3}{2} \omega_r (\lambda_d i_q - \lambda_q i_d) \end{aligned} \quad (20)$$

where the first term is the ohmic losses and the second term is the rate of change in magnetic energy, and the last term is the electromagnetic power that will be converted to mechanical power

$$P_{em} = \frac{3}{2} \omega_r (\lambda_d i_q - \lambda_q i_d) \quad (21)$$

So the developed torque is

$$T_{em} = \frac{P_{em}}{\omega_{rm}} = \frac{3}{2} \frac{P}{2} (\lambda_d i_q - \lambda_q i_d) \quad (22)$$

where P is the number of magnetic poles.

2.3 Pulse Width Modulation Switching Scheme

One of the most widely utilized strategies for controlling the AC output of power electronic converters is the technique known as pulse width modulation (PWM), which varies the duty cycle of the converter switches at a high switching frequency to achieve a target average low-frequency output voltage or current [12]. This technique also allows

for the use of small and light transformers and reactive elements, because their sizes depend on the converter switching frequency rather than the AC line frequency. [21]

Because of the PWM inverter, it is possible to modulate both signal frequency and voltage magnitude in high switching frequency due to advances in microprocessor and semiconductor. The PWM inverter provides higher efficiency and better performance compared to fixed frequency controller [5][8]. Several PWM techniques are most commonly used: Sinusoidal PWM, hysteric PWM and Space Vector PWM. Sinusoidal PWM is very popular in applications. SVPWM is an advanced, computation-intensive PWM method with superior performance characteristics. It has been widespread applied in recent years due to the development of DSP technology [8].

2.3.1 Sinusoidal PWM

In sinusoidal pulse-width modulation, the output voltage is controller by varying the on-off periods so that the on periods (pulse width) are longest at the peak of the wave.

Sinusoidal PWM technique is very popular for industrial converters. Figure 2.6 explains the general principle of Sinusoidal PWM, where an isosceles triangle carrier wave of frequency f_c is compared with the fundamental frequency f_m of sinusoidal modulating wave, and the points of intersection determine the switching points of power devices and generate the resulting PWM waveform. The notch and pulse widths of voltage wave vary in a sinusoidal manner and the average of fundamental component frequency is the same as f and the amplitude is proportional to the command modulating voltage [8]. The same carrier wave can be used for all three phases.

Two control parameters that regulate the output voltage are the chopping ratio and the modulation index. The frequency ratio f_c/f_m is known as the chopping carrier ratio N . It determines the number of pulses in each of cycle of the inverter output voltage. The ratio V_m/V_c is called the modulated index M ($0 \leq M \leq 1$). It determines the width of the pulses and therefore the RMS value of the inverter output voltage. M is usually adjusted by varying the amplitude of the reference wave while keeping the carrier wave amplitude fixed. The inverter output frequency is varied by varying the reference wave frequency [13].

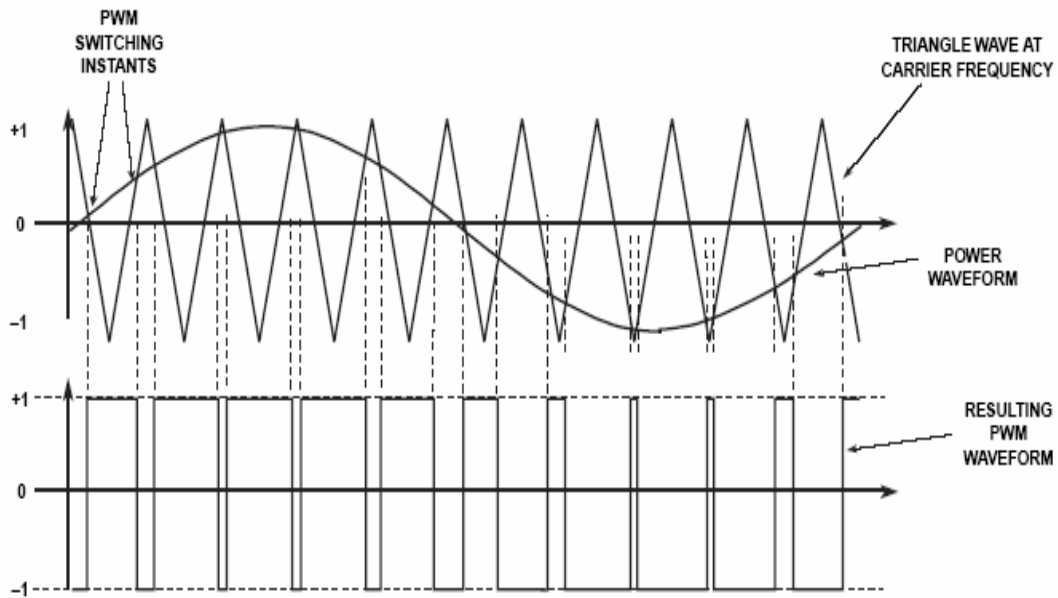


Figure 2.6 Principle of Sinusoidal PWM Method [38]

The inherent low-pass characteristic of the machine will filter out the high frequency components in the voltage waveform, leaving the desired sinusoidal current waveform only.

2.3.2 Space Vector PWM

The Space Vector Pulse Width Modulation (SV PWM) technique, which was proposed in recent years, refers to a special way to determine switching sequence of the three-phase voltage source inverters. It uses basic space vectors to generate the output voltages to the motor. The space vector PWM technique has been shown to generate less harmonic distortion in output voltages and currents. In addition, it provides a more efficient use of the supply voltage compared to sinusoidal PWM technique [8].

For a three-phase voltage source inverter (VSI), shown in Figure 2.7, V_a , V_b and V_c are the output voltage, which will modulate PMSM speed. M_1 , M_2 , ... through M_6 are power transistors which are controlled by gate signal and decide the output. When the upper transistors are turned on, i.e. a , b or c is 1, the lower sides are turned off, i.e. a^* , b^* or c^* is 0. SV PWM is to determine the switching sequence of upper sides. The on and off status of the three upper transistors compose eight possible vectors. The eight vectors are called the Basic Space Vectors. They are denoted by U_0 , U_{60} , U_{120} , U_{180} , U_{240} , U_{300} , O_{000} and O_{111} , as shown in Figure 2.8. There are six non-zero vectors and two zero vectors. The six nonzero vectors form a hexagon. The angle between any two adjacent non-zero vectors is 60 degrees. The two zero vectors are at the original point.

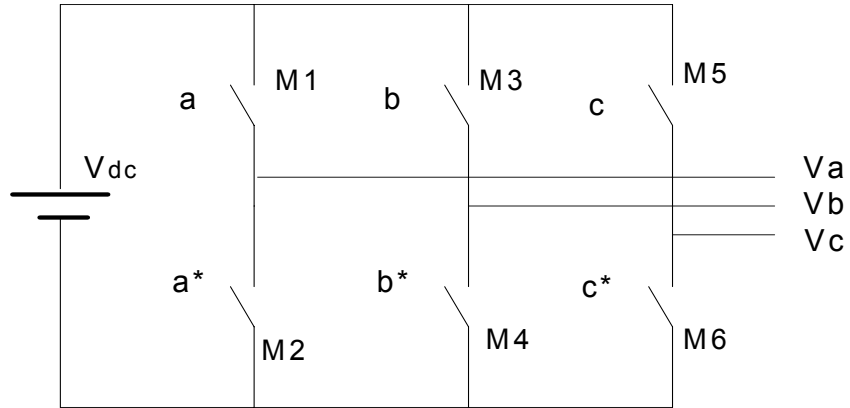


Figure 2.7 A typical three-phase voltage source inverter

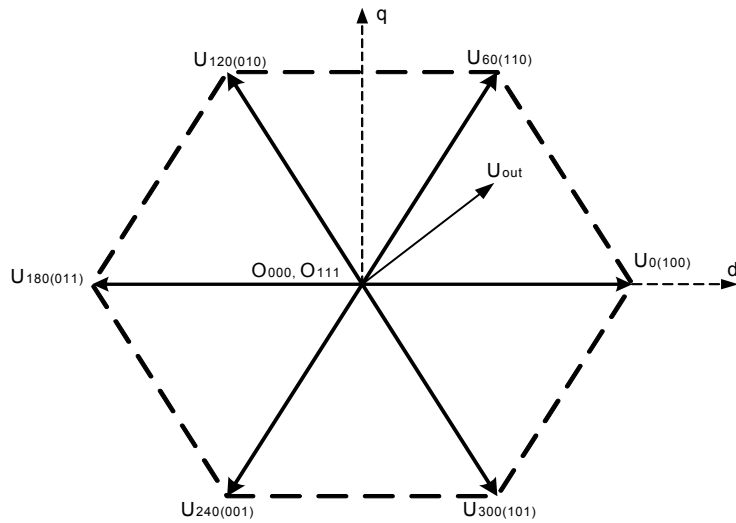


Figure 2.8 Basic Space Vectors

In the basic space vectors diagram, the rotating reference VSI output voltage, denoted U_{out} , can be shown on a stationary locus between two adjacent space vectors for any short amount of time. The combination of two switching states can be used to instantaneously represent the reference voltage as long as this period of time is much smaller than the reference voltage rotating speed.

Table 2.1 gives a summary of the switching states and the corresponding phase voltages and phase-to-phase voltages after normalized by DC voltage V_{dc} of the three-phase voltage source inverter.

Table 2.1 SV PWM switching states [39]

| a | b | c | v_a | v_b | v_c | v_{ab} | v_{bc} | v_{ca} |
|---|---|---|--------|--------|--------|----------|----------|----------|
| 0 | 0 | 0 | 0 | 0 | 0 | 0 | 0 | 0 |
| 1 | 0 | 0 | $2/3$ | $-1/3$ | $-1/3$ | 1 | 0 | -1 |
| 1 | 1 | 0 | $1/3$ | $1/3$ | $-2/3$ | 0 | 1 | -1 |
| 0 | 1 | 0 | $-1/3$ | $2/3$ | $-1/3$ | -1 | 1 | 0 |
| 0 | 1 | 1 | $-2/3$ | $1/3$ | $1/3$ | -1 | 0 | 1 |
| 0 | 0 | 1 | $-1/3$ | $-1/3$ | $2/3$ | 0 | -1 | 1 |
| 1 | 0 | 1 | $1/3$ | $-2/3$ | $1/3$ | 1 | -1 | 0 |
| 1 | 1 | 1 | 0 | 0 | 0 | 0 | 0 | 0 |

Figure 2.9 is the simulation SV PWM signal. The space vector concept adds third-harmonic quantities to the basic regular sampled PWM method. However, the third harmonics can be balanced by three-phase systems. As a result, we can see a 15% increase in available bus voltage when comparing the maximum bus voltages between SV PWM method and Sinusoidal PWM method [8].

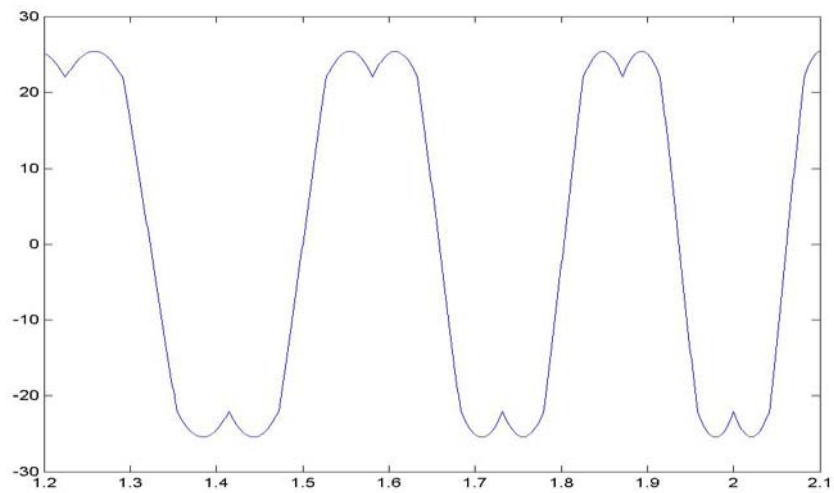


Figure 2.9 SV PWM signal

Motor controllers based on space-vector modulation might look similar to traditional sinusoidal-commutation products, but they can bring advantages to new systems. However, it is normally a DSP-based system due to the complicated calculation of SV PWM method.

2.4 Power Transistors

Power semiconductor devices constitute the heart of modern power electronic and motor control. The switching mode power supply provides high efficiency and also generates harmonics at both the supply and load sides due to the nonlinear of switches.

Three types of power transistors are mostly used in motor drive systems: bipolar junction transistors (BJT), MOSFETs, and insulated gate bipolar junction transistors (IGBT). BJT are the least expensive of the three. BJT devices are minority carrier devices that require charge storage within the device to function. This charge storage may cause problem and slow the switch speed when switching off. As a result, BJT is not widely used in switching application.

The power MOSFET is a transconductance, majority carrier device. It has two prominent advantages: fast switching and low average drive current. Power MOSFET can switch very quickly because it is a majority carrier device. The advantage of high input impedance and faster switching speed of the power MOSFET make it the displacement of the bipolar power transistor in most applications. However, the current-handling capability of the power MOSFET, which degrades rapidly when the structure is designed to support high voltages, limits its application at high voltage. These characteristics make it a good choice for high-speed, low to middle voltage applications. Typically, MOSFETs are used in motor drives when voltage rating is less than 200V. MOSFETs are extremely popular in low-voltage, and low power, and high frequency switching applications. Power MOSFET has dominating applied over computer power supplies and peripheral drives, telecommunications, and automotive electronics [14].

In order to overcome the poor current-handling capability of power MOSFETs at high operating voltages, the concept of merging MOS gate technology with bipolar current conduction was introduced in 1980s. The most commercially successful structure was the insulated gate bipolar transistor (IGBT). It has performance similar to BJT and is driven like a power MOSFET, which enable the efficient control of very high current and

voltage together with high input impedance. However, IGBT's special turnoff characteristic limits its switching frequency to about 40 kHz [15]. Some of the important applications for IGBT are heating, ventilating/air-conditioning (HVAC) systems, factory automation/numerical controls/robotics, lighting ballasts, appliance controls, and electrical vehicle drives [14].

2.5 Adjustable-Speed Drive System

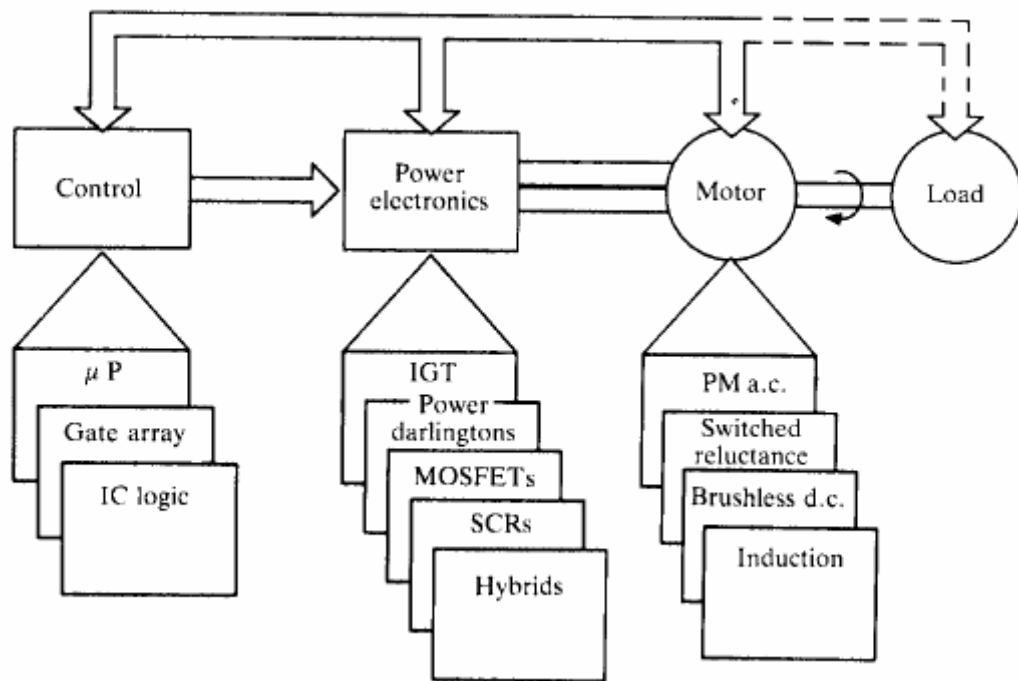


Figure 2.10 Structure of adjustable-speed drive system [9]

Figure 2.10 is the structure of adjustable-speed drive system. It is composed by several parts: control, power converter, motor, and load.

Adjustable-speed control can be realized by microprocessor, FPGA, or customer IC. Power converter is essentially a device for creating a variable AC frequency output from DC input. The frequency of the output voltage or current is readily established by simple switching for equal time periods to the positive and the negative DC bus and appropriately adjusting the half-cycle period. However, the variable frequency ability is nearly always accompanied by a corresponding need to adjust the amplitude of the fundamental component of the output waveform as the frequency changes, i.e. voltage control [12].

There are single phase converter and also three-phase converter. It depends on the structure of load system.

CHAPTER THREE: SUPER HIGH-SPEED PMSM STABILITY ANALYSIS

When PMSM drives are used for pumps, fans, compressors, and other applications where the load is predictable and high dynamic performance is not a requirement, a simple V/f scale control strategy can be used instead of the more complex vector or DTC control [7][16]. Open-loop V/f control is an attractive solution for super high-speed PMSM for the inherent lack of any shaft mechanical sensors [8]. However, the stability of super high-speed PMSM is an important issue particularly for open-loop V/f control, given that PMSM are unstable after exceeding a certain applied frequency. When operated with an open-loop control mode PMSM, without damper windings in the rotor, does not assure the synchronization of motion of the rotor with the stator frequency applied that may cause instability problem [10]. Due to manufacturing costs, design difficulties, and efficiency considerations, damper windings are not generally implemented in PMSM. Therefore, different approaches need to be developed in order to solve the instability problem. One approach is the DC link feedback method [17][18], but this still requires some current sensor. Little solid data is available on PMSM open-loop V/f control and its stability analysis.

This chapter analyzes the effect of the PMSM parameters on its dynamic characteristics including its stability and performance. It is presented that super high-speed PMSM stability can be achieved over the full operating speed range.

The stator resistor R_s and inductance L_s are the main parameters influencing the stability. While the super high-speed PMSM satisfies the design requirements, there are enough design choices in selection of R_s and L_s values. The final values ensure the motor

stability over its operating speed range. As the result, stable axial flux slotless PMSM can be designed that demonstrates the effectiveness of the proposed design method.

3.1 Steady-State Equation of PMSM

The steady-state equations of PMSM are as following:

$$\begin{aligned}
\frac{di_q}{dt} &= -\frac{R_s}{L_q}i_q - \frac{L_d}{L_q}i_d\omega_r - \frac{\lambda_m}{L_q}\omega_r + \frac{V_s}{L_q}\cos\delta \\
\frac{di_d}{dt} &= -\frac{R_s}{L_d}i_d + \frac{L_q}{L_d}i_q\omega_r - \frac{V_s}{L_d}\sin\delta \\
\frac{d\omega_r}{dt} &= \frac{3P^2}{2J}\left[\lambda_m i_q + (L_d - L_q)i_q i_d\right] - \frac{P}{J}T_l - \frac{B_m}{J}\omega_r \\
\frac{d\delta}{dt} &= \omega_s - \omega_r
\end{aligned} \tag{23}$$

where ω_s is supply frequency, ω_r is the rotor electrical synchronous speed, L_d and L_q are the inductance values for the d- and q- axes respectively, V_s is supplied voltage, R_s is the stator resistance, i_d and i_q are the d- and q- axes currents respectively, δ is load angle, P is the number of pole pairs, and λ_m is permanent magnet flux, J is the moment of inertia, B_m is the coefficient of viscous friction, and T_L is the load torque.

The linearized system equation of (23) is given by

$$\dot{\Delta x} = A(x)\Delta x + B(x)\Delta u \quad (24)$$

where, $\Delta x = [\Delta i_q \quad \Delta i_d \quad \Delta \omega_r \quad \Delta \delta]^T$, x and u are the state variable and the input vectors respectively, and matrices A and B are given as

$$A = \begin{bmatrix} -\frac{R_s}{L_q} & -\frac{L_d}{L_q}\omega_r & -\frac{\lambda_m + L_d i_d}{L_q} & -\frac{V_s}{L_q}\sin(\delta) \\ \frac{L_q}{L_d}\omega_r & -\frac{R_s}{L_d} & -\frac{L_q}{L_d}\omega_r & -\frac{V_s}{L_d}\cos(\delta) \\ \frac{3P^2}{2J}[\lambda_m + (L_d - L_q)i_d] & \frac{3P^2}{2J}(L_d - L_q)i_d & -\frac{B_m}{J} & 0 \\ 0 & 0 & -1 & 0 \end{bmatrix}$$

and

$$B = \begin{bmatrix} 0 & 0 & -\frac{n}{2J} & 0 \end{bmatrix}$$

The general solution of the homogenous or force-free linear differential equation (24) is given by

$$x = Ke^{At} \quad (25)$$

K is a vector formed by an arbitrary set of initial conditions. The state transition matrix e^{At} represents the unforced response of the system.

The eigenvalues provide a simple means of predicting the behavior of the PMSM at any balanced operating condition. The eigenvalues of the state matrix in equation (25) form two groups. One group is comprised of well-damped complex conjugated pairs. The second group is composed of either lightly damped or negatively damped complex conjugate pairs. Since the well-damped group has no effect on the stability analysis, the stability study was focused on the second pair, under-damped or negative damped group, which has the dominant influence on the stability characteristics.

3.2 Stability Simulation and Analysis for Super High-Speed Motor 1

From equation (25) and matrix A , it is clear that the eigenvalues are functions of R_s , L_d , L_q , λ_m , J and B_m . In this research, R_s , L_d and L_q are considered as design variables within certain lower and upper limits, while the overall requirement and performance of the super high-speed PMSM are satisfied. Before calculating the eigenvalues of the state matrix, the values of the parameters contained in the elements of the state matrix must be determined for the particular steady state operating point.

For reasons of simplicity, no load condition was initially considered, and then extended to include various load angles for the super high-speed PMSM in this analysis. Note that the motor developed in this paper is an axial flux slotless surface permanent magnet type with $L_d=L_q=L_s$. The proposed PMSM major parameters are given in Table 3.1.

Loci of the developed super high-speed PMSM, for different applied frequencies and different R_s with $L_s = 1.6 \mu\text{H}$ are shown in Figure 3.1.

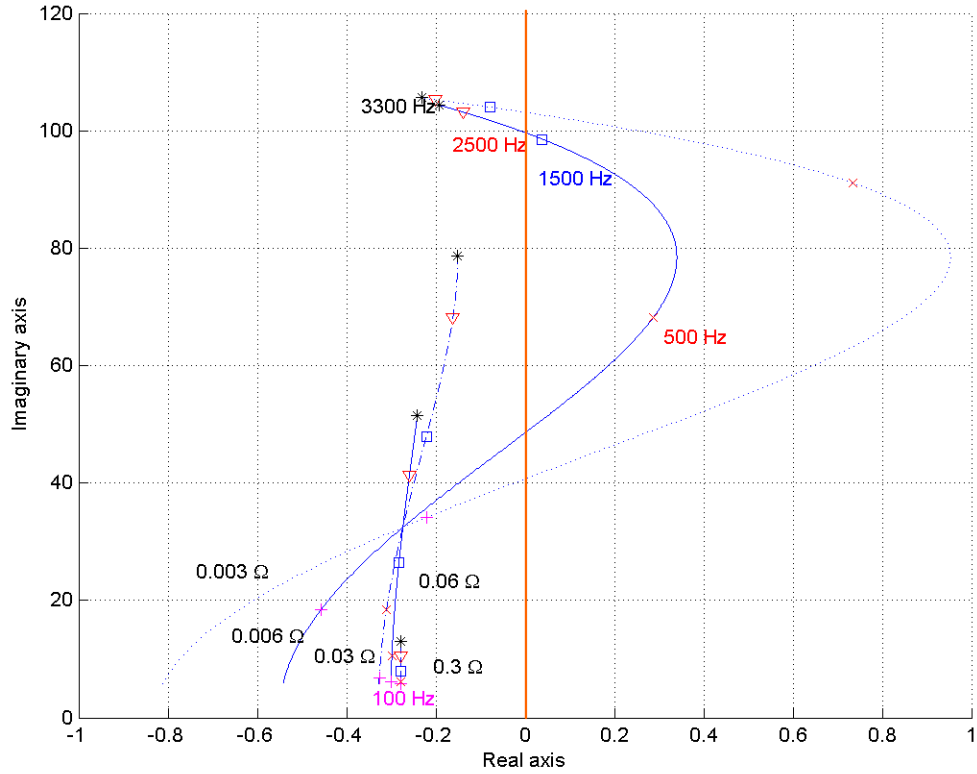


Figure 3.1 Loci of super high-speed PMSM under different driving frequencies and R_s , with $L_s = 1.6 \mu\text{H}$. Speed range is from 0-100 Krpm.

It shows that resistor R_s has a strong effect on the eigenvalues location, i.e. the stability. A larger stator resistance is favorable for stability, but results in higher copper loss. When R_s has exceeds some value, no prominent improvement of stability even further increasing R_s .

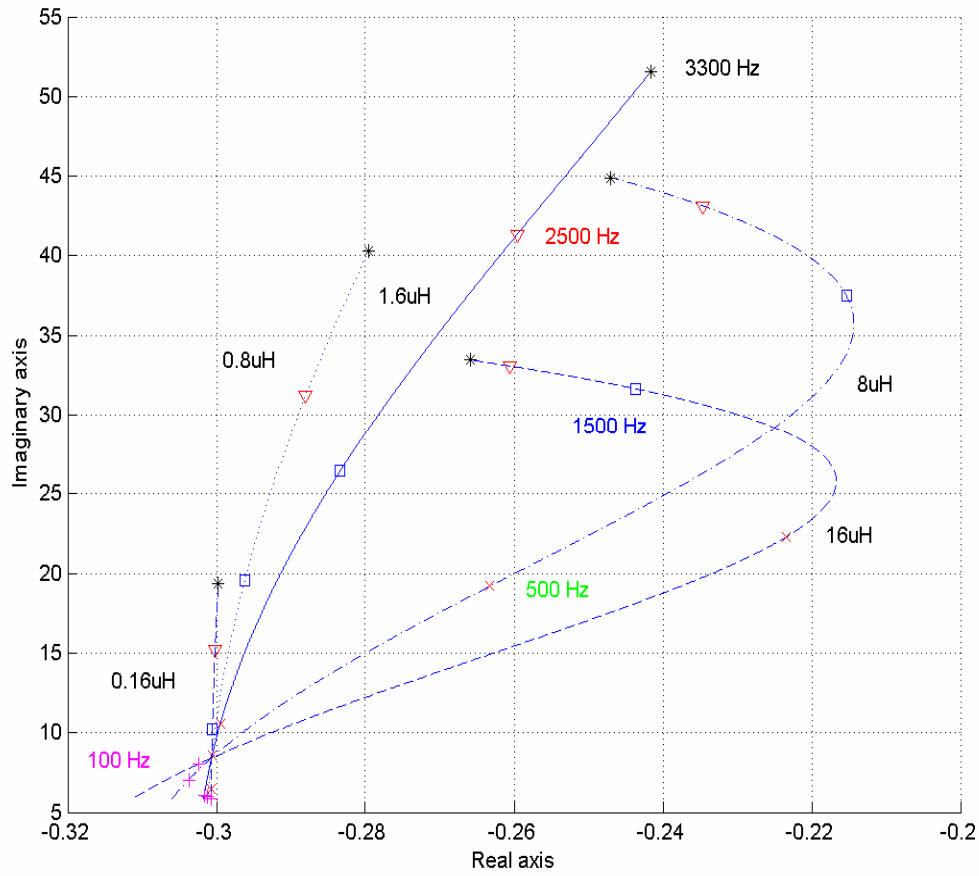


Figure 3.2 Loci of super high-speed PMSM under different driving frequencies and L_s ,
with $R_s = 0.06$ ohms. Speed range is from 0-100 Krpm.

Figure 3.2 indicates that inductance L_s also has an effect on the root location. With suitable selection of R_s , the effect on the stability is not dominant, but proper selection of L_s will give enough margins for stability with the selected R_s value. The motor is stable with $R_s = 0.06 \Omega$, $L_s = 1.6 \mu H$ (satisfies the design requirements) under no load condition.

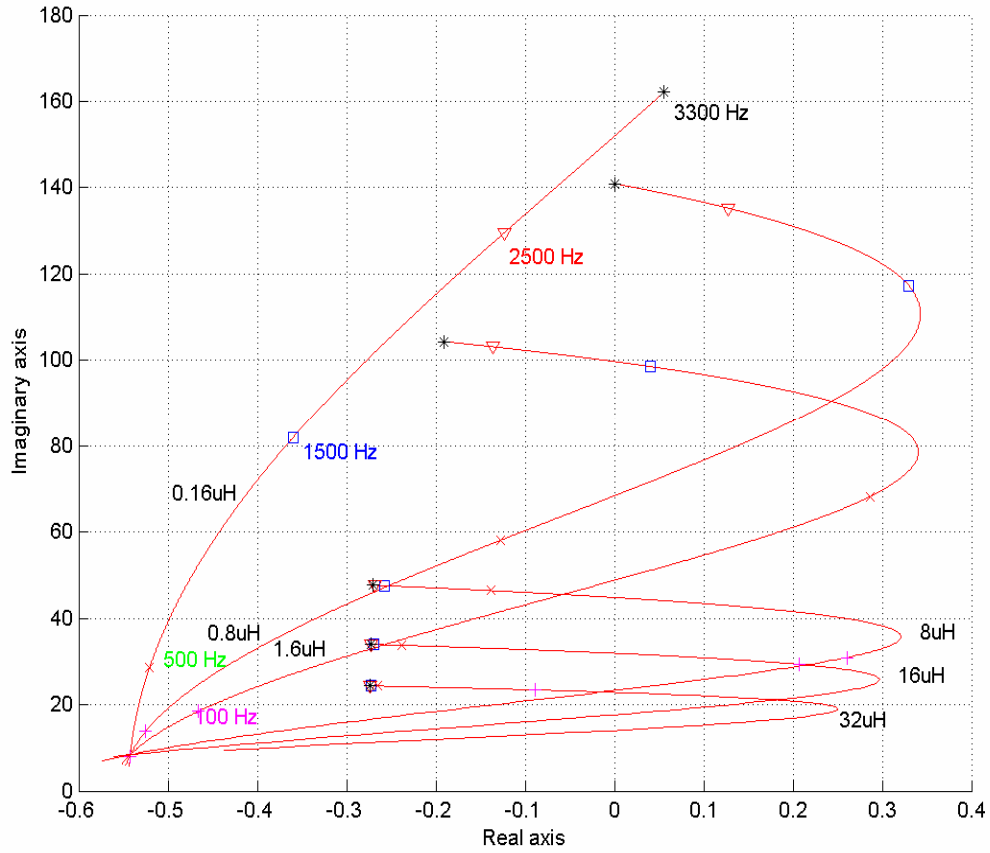


Figure 3.3 Loci of super high-speed PMSM under different driving frequencies and L_s , with $R_s = 0.006$ ohms. Speed range is from 0-100 Krpm.

Figure 3.3 reveals that the inductance L_s has a strong effect on the root location and stability, when R_s is too small. In our design, 0.06 ohms stator resistance is chosen considering stable margin and other design requirements.

Figure 3.4 shows the stability of the test super high-speed PMSM 1 over its full operating speed range, even up to 3,333 Hz, with $R_s = 0.06 \Omega$, $L_s = 1.6 \mu H$ under different load angles, which demonstrates the effectiveness of the proposed scheme. Since the motor inductance and resistor both are functions of the drive voltage, current, and

temperature, a significant margin in motor stability is required in order to guarantee the performance.

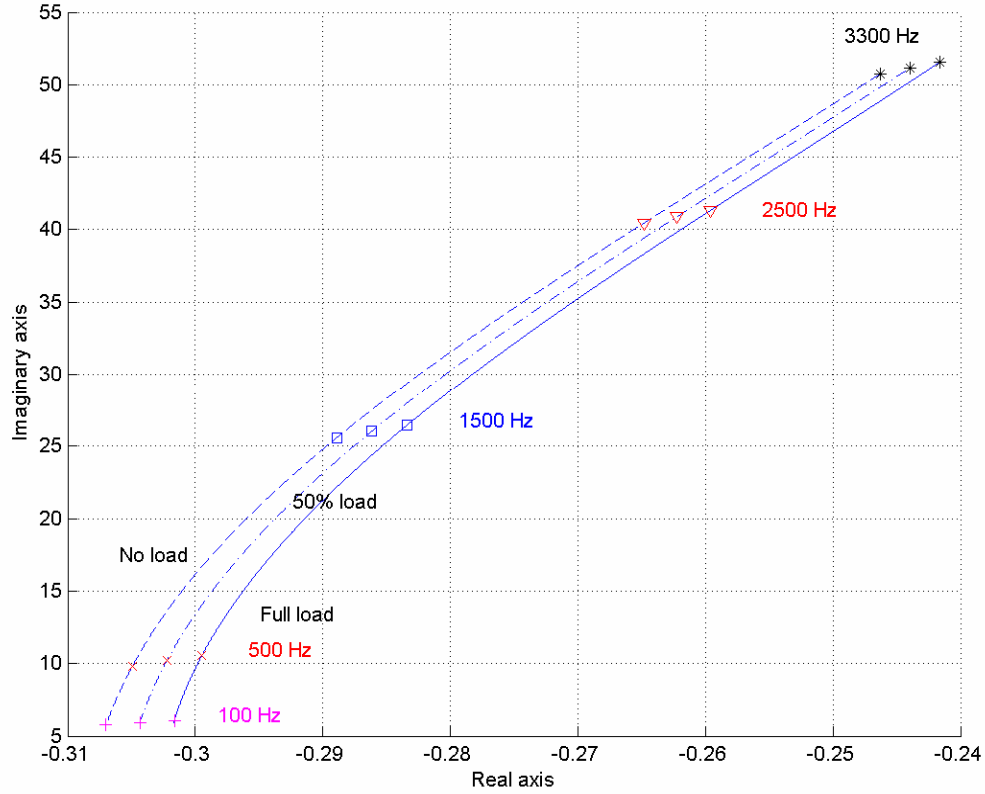


Figure 3.4 Root Loci of super high-speed PMSM under different driving frequency, with $R_s = 0.06 \Omega$, $L_s = 1.6 \mu H$, and different load angle. Speed range is from 0-100 Krpm.

3.3 Stability Simulation and Analysis for Super High-Speed Motor 2

Similarly, stability simulation and analysis are done for super high-speed test motor 2. Loci of the developed super high-speed PMSM 2, for different applied

frequencies and different R_s with $L_s = 1 \text{ uH}$ are shown in Figure 3.5. It verifies again that resistor R_s has a strong effect on the root location, partially for smaller inductance. Compared with the analysis results of the super high-speed motor 1, smaller inductance increases the opportunity of instability. Figure 3.6 indicates that inductance L_s has a little effect on the root location when the resistance becomes smaller. If the ratio of the inductance over the resistance increases, the root locus will have a sharper curve in mid-frequency or mid-range. The motor is stable with $R_s = 0.0057 \text{ } \Omega$, $L_s = 1 \text{ } \mu \text{ H}$ (satisfies the design requirements) under no load condition.

Figure 3.7 shows the stability of the test super high-speed PMSM 2 over its full operating speed range, even up to 3,333 Hz, with $R_s = 0.0057 \text{ } \Omega$, $L_s = 1 \text{ } \mu \text{ H}$ under different load angles, which demonstrates the effectiveness of the proposed scheme. Since the motor inductance and resistor both are functions of the drive voltage, current, and temperature, a significant margin in motor stability is required in order to guarantee the performance.

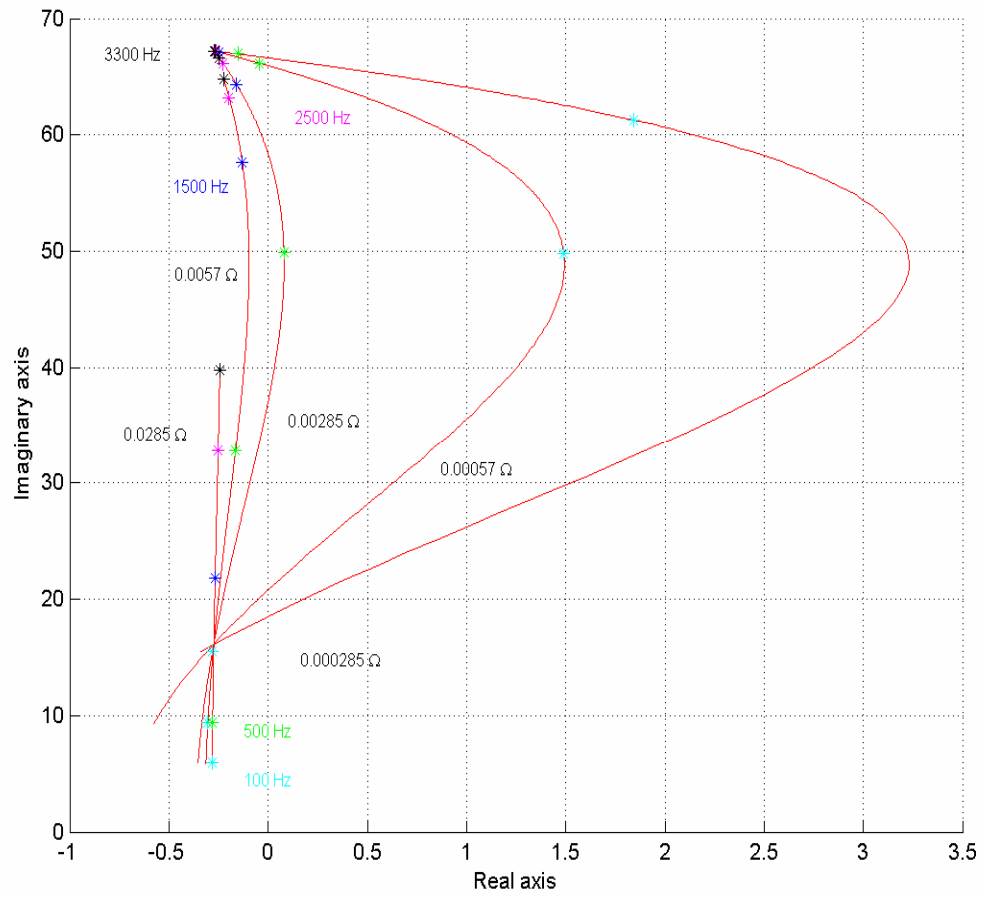


Figure 3.5 Loci of super high-speed PMSM under different driving frequencies and R_s ,
with $L_s = 1\mu\text{H}$. Speed range is from 0-200 Krpm.

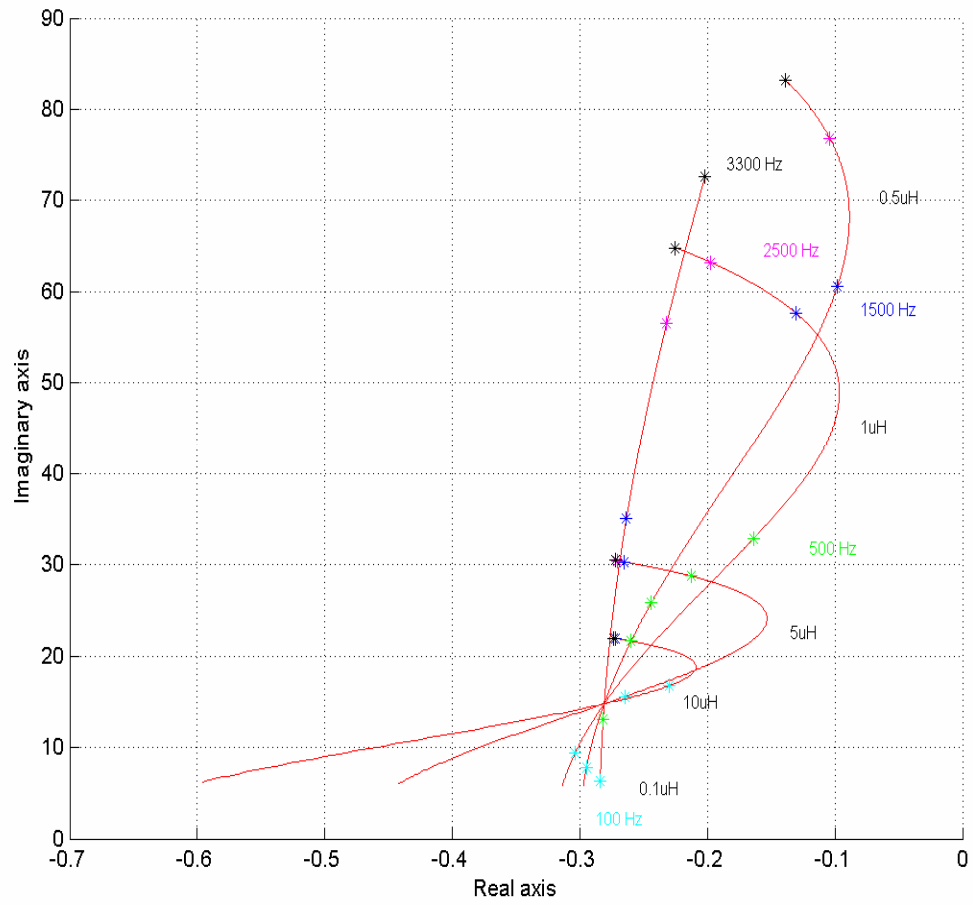


Figure 3.6 Loci of super high-speed PMSM under different driving frequencies and L_s ,
with $R_s = 0.0057 \Omega$. Speed range is from 0-200 Krpm.

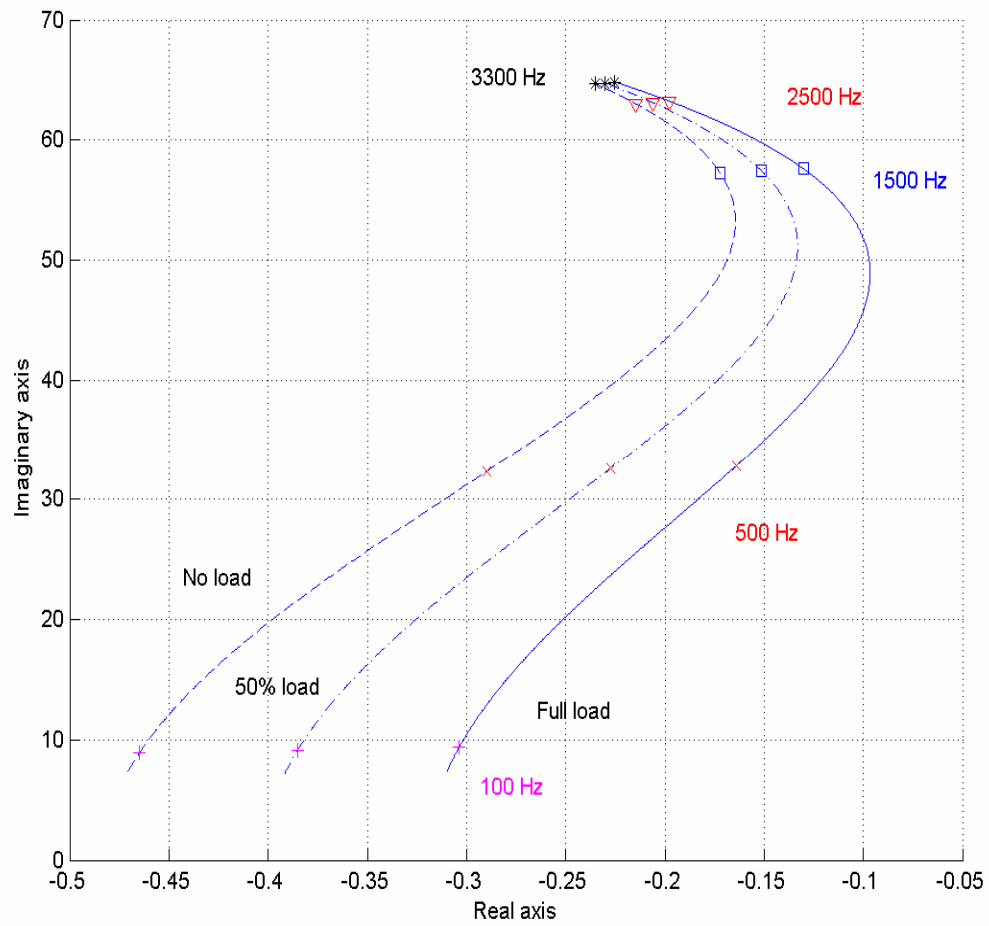


Figure 3.7 Root Loci of super high-speed PMSM under different driving frequency, with $R_s = 0.0057 \Omega$, $L_s = 1 \mu H$, and different load angle. Speed range is from 0-200 Krpm.

3.4 Conclusion

This chapter has presented the stability analysis and simulation for super high-speed PMSMs. The R_s and L_s of motor can be considered as design variables chosen to satisfy the performance requirements and proper stability margin. Another stability analysis approach presented in [19], it provided comprehensive stability analysis based on how the various motor and drive parameters affect stability on the torque-speed curve. It is clear that the eigenvalues are functions of motor parameters and the stability depends only on the time-constant of motor, L_s/R_s . The higher the value of Stator resistor R_s , the faster the motor will run to the stability boundary. The analysis results are in concordance with our conclusion. So, R_s and L_s are considered as design variables within certain lower and upper limits, while the design requirement and performance of the super high-speed PMSM are satisfied. It showed that the stability of super high-speed PMSMs can be guaranteed over their operating speed range without damper windings on the rotor under careful design. This stability made an open-loop V/f control possible for the super high-speed PMSMs.

3.5 Design Parameters of Proposed Super High-Speed PMSMs

Two super high-speed motors and corresponding controllers are designed according to the project requirement and stability analysis.

The permanent magnet is centrally located inside the hollow shaft. The rotor was assembled by heating the shaft and cooling the permanent magnet. For 200 Krpm super-high speed, 2-pole configuration is preferred since the required electrical frequency is the lowest for the same speed. Low electrical frequency can reduce switching loss of the controller. The number of turns per phase and the pitch factor were considered based on the requirements such as dc supply voltage, shaft speed and desired back-EMF.

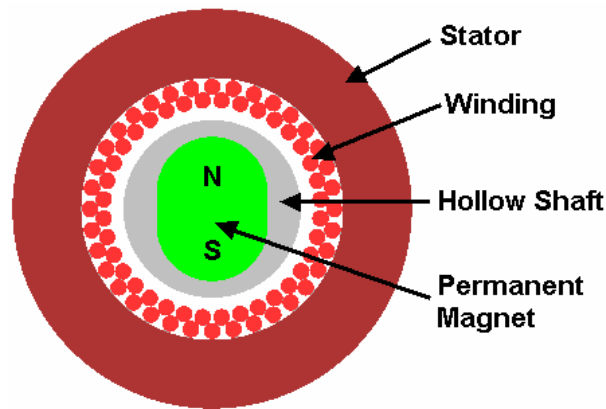


Figure 3.8 Cross section of the designed PMSM [36]

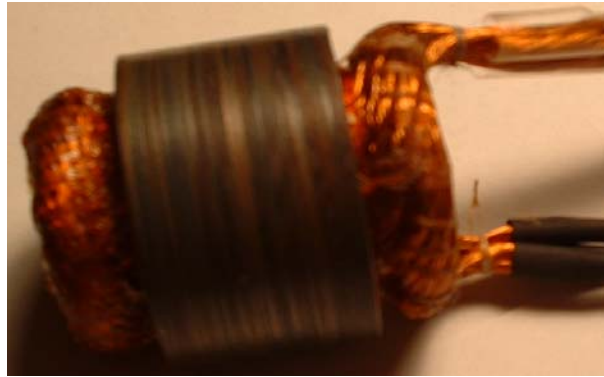
The designed PMSM electric motor consists of a hollow shaft with a magnet inside it. The direction of flux flow is radial. The cross-section of the shaft with magnet inside is as shown in Figure 3.8 and Figure 3.9 a. The non-uniform shape of the magnet prevented it from slipping inside the shaft while rotating. Two plugs of same material of

the shaft were designed to support the magnet at the center from two sides. The bearings were mounted on the plugs.

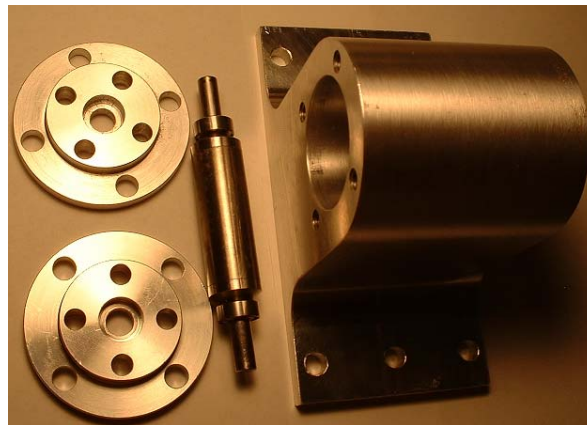
The components of the PMSM were fabricated.



a.



b.



c.

Figure 3.9 Components of proposed PMSM

a. Hollow shaft and magnet

b. Stator and winding

c. Casing, caps and the assembled shaft [37]

Table3.1: Proposed super high-speed motor parameters

| Parameters | Super high-speed PMSM 1 | Super high-speed PMSM 2 |
|---|-------------------------|-------------------------|
| Number of Poles | 4 | 2 |
| Rated Voltage (phase to phase peak value) | 28 V | 28 V |
| Rated Current (RMS) | 5 A | 65A |
| Rated speed | 100,000 RPM | 200,000 RPM |
| Rated frequency | 3333 HZ | 3,333 HZ |
| L_d | 1.6 μ H | 1 μ H |
| L_q | 1.6 μ H | 1 μ H |
| R_s | 0.06 ohms | 0.0056 ohms |

CHAPTER FOUR: OPTIMAL CONSTANT V/f CONTROL

A constant volts/hertz (V/f) method is employed to produce controlling voltage responding to frequency because of its easy to realize and advantage at middle to high speed applications. The purpose of constant V/f control is to generate required phase voltage V_s^* which is maintained proportional to the frequency so that the stator flux remains constant. This permits for nearly maximum available torque per ampere of the stator current and fast transient response for the V/f control. As a result, higher efficiency and better performance can be permitted. For normal motor system, constant V/f control is a linear control because stator resistance is small compared with motor inductance and can be neglected [5][8].

For ordinary PMSM V/f control design, the analysis is always based on a smaller stator resistance compared with the reactive impedance after speed increases over some value. The stator resistance is neglected and taken into account by a boost voltage only. But, for the proposed motor, the two values are the same only after electrical frequency increasing over 5KHz (150,000 rpm). The stator resistance effect cannot be neglected anymore in these cases.

In constant V/f control, the phase voltage command V_s^* is generated from a function generator, where the voltage is maintained proportional to the frequency so that the stator flux remains constant, which permits for nearly maximum available torque per ampere of the stator current and fast transient response for the V/f control [9].

4.1 Constant V/f Control Criterion

It can be shown that the torque sensitivity per ampere of stator current is high, permitting fast transient response of the drive with the stator current control. In variable-frequency, variable-voltage operation of a drive system, the machine usually has low slip characteristics, giving high efficiency. In spite of the low inherent starting torque for base frequency operation, the machine can always be started at maximum torque. The absence of a high in-rush starting current in a direct-start drive reduces stress and therefore improves the effective life of the machine.

By far, the majority of variable-speed ac drives operate with a variable-frequency, variable-voltage power supply. The different operating region of torque-speed curves for a variable-speed drive system with a variable-frequency, variable-voltage supply and the corresponding voltage-frequency relation is shown in Figure 4.1 and Figure 4.2. The figures also show torque, stator current, and slip as functions of frequency [8].

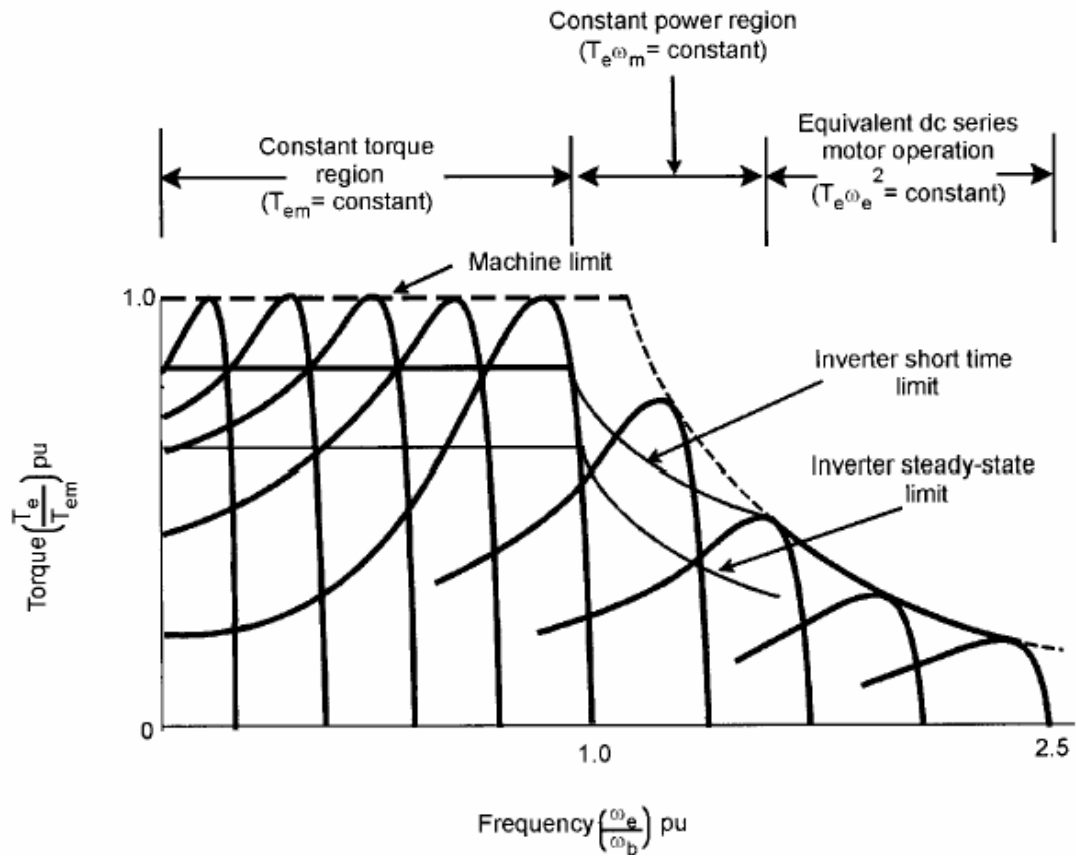


Figure 4.1 Torque-speed curves at variable voltage and variable frequency [8]

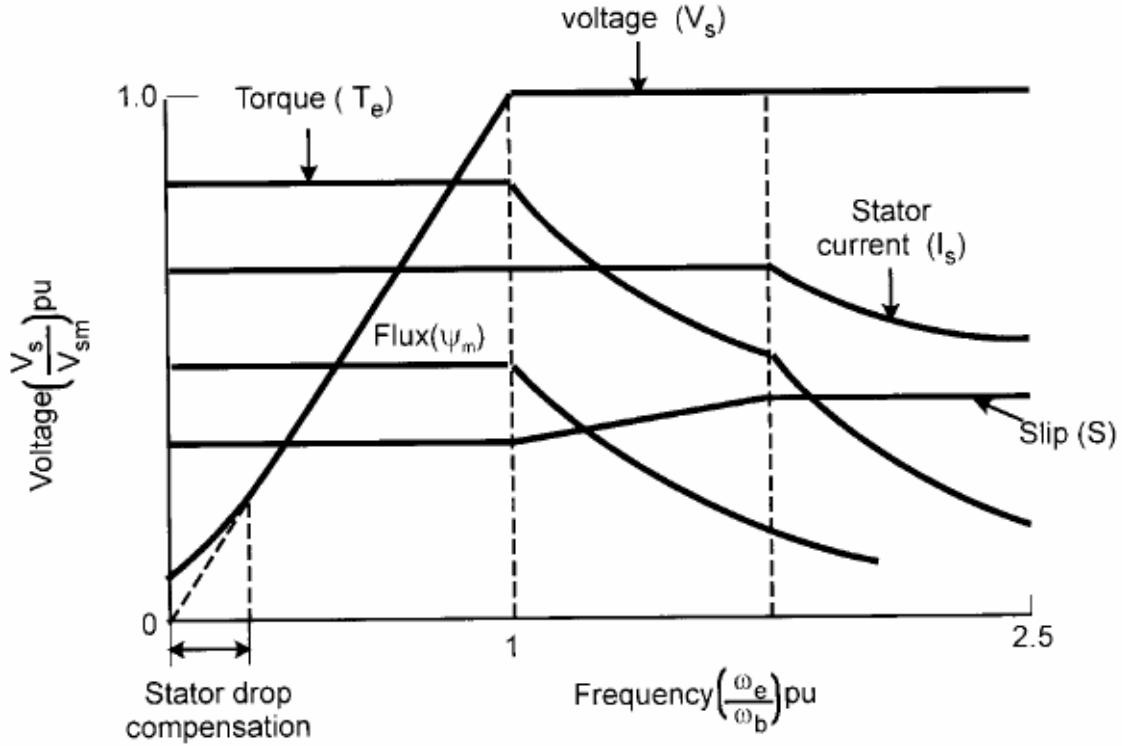


Figure 4.2 Voltage and frequency in constant torque and field-weakening regions [8]

V/f control approach is employed frequently in industry application due to low cost and simple design, which is advantageous in the middle to high-speed range [6]. This method consists of controlling the speed of the rotating magnetic field of the stator by changing the supply frequency.

In the V/f control method, motor speed is controlled by both the magnitude and frequency of stator voltages, which always maintain the air gap flux at the desired steady-state level. The stator waveforms are assumed to be sinusoidal with adjustable frequency and magnitude under V/f control method. The magnetizing current, denoted as I_m , that generates the air gap flux λ_m , can be approximately presented by the ratio of stator voltage to frequency. At steady state status, its phasor equation can be written as:

$$\begin{aligned}
I_m &\cong \frac{V}{\omega L_m} = \frac{V}{2\pi f L_m} \\
I_m &= \frac{\Lambda_m}{L_m}
\end{aligned} \tag{26}$$

L_m is a constant because motor is assumed to be operating in linear magnetic region. So, we can get

$$\Lambda_m \propto \frac{V}{f} \tag{27}$$

To keep the air gap flux Λ_m a constant, that is to keep the magnetizing current I_m as a constant, the ratio of stator voltage over the corresponding frequency must be a constant at different speeds. This approach is also called constant volts per hertz control. As the motor speed increases, the stator voltage need be proportionally increased in order to keep the ratio V/f constant. If motor speed is higher than the motor rated frequency, f_{rated} , the V/f ratio cannot be kept at a constant value because of the limit of the stator voltage. Therefore, the air gap flux is reduced consequently. This reduces the output torque further. This region is usually called the field-weakening region. A typical V/f profile is shown in Figure4.3.

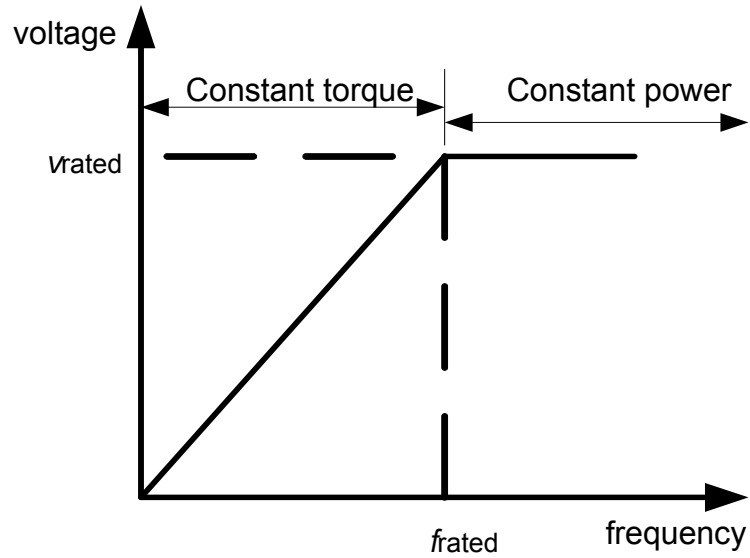


Figure 4.3 A typical V/f profile

In practice, at low frequency and voltage, voltage drop across the stator resistance cannot be neglected and it must be compensated. So, it is important to have a suitable starting voltage. Correspondingly, the V/f profile is modified as Figure 4.4.

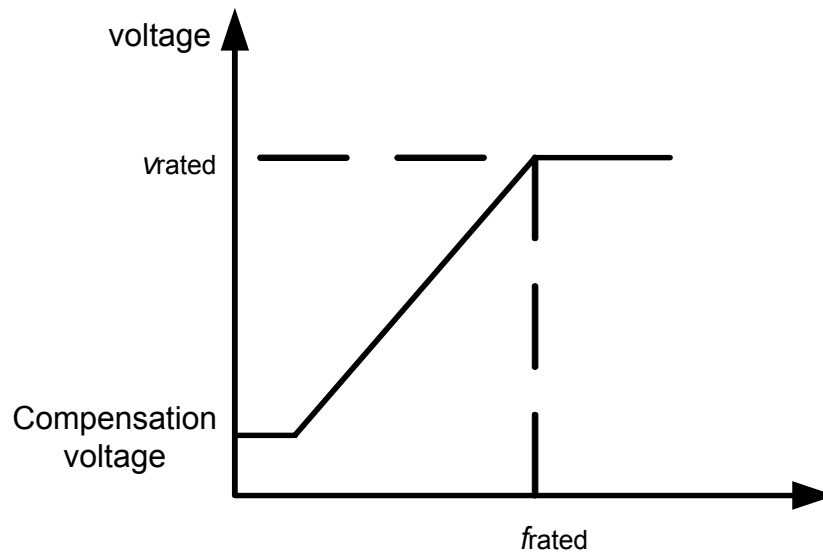


Figure 4.4 A modified V/f profile

4.2 Derivation of an optimal V/f curve

The steady state equivalent circuit and phasor diagram of the PMSM with neglecting the core loss is show in Figure 4.5. V_s is supply voltage, I_s is stator current, R_s is stator resistance, X_s is the synchronous reactance and with $X_{ds}=X_{qs}$ for nonsalient pole machine, δ is electrical angle between V_s and the induced EMF E_f from the magnet, which is positive for motoring. E_s is the stator voltage neglected R_s .

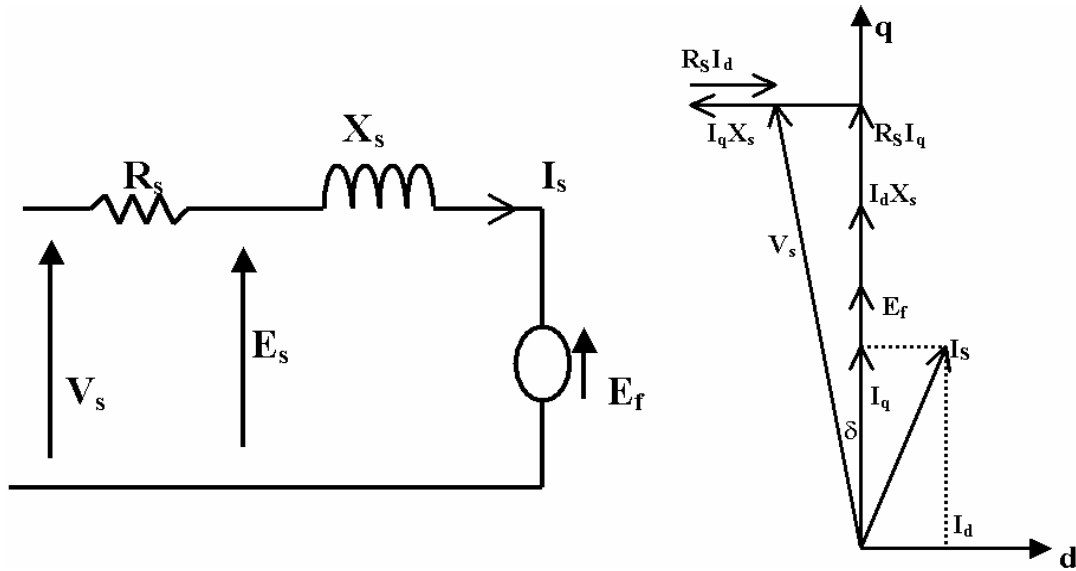


Figure 4.5 PMSM steady state equivalent circuit and phasor diagram 1

The steady state equation can be derived as

$$\begin{bmatrix} V_d \\ V_q \end{bmatrix} = \begin{bmatrix} R_s & -\omega L_s \\ \omega L_s & R_s \end{bmatrix} \begin{bmatrix} I_d \\ I_q \end{bmatrix} + \begin{bmatrix} 0 \\ E_f \end{bmatrix} \quad (28)$$

where ω is the electrical speed, L_s is the motor inductance, R_s is the stator resistance. I_d , I_q , V_d and V_q are the d- q- axes stator current and voltage, respectively. Solving for I_q , substituting with $V_d = -V_s \sin \delta$ and $V_q = V_s \cos \delta$, we can get:

$$I_q = \frac{R_s V_s \cos \delta - R_s E_f + \omega L_s V_s \sin \delta}{R_s^2 + \omega^2 L_s^2} \quad (29)$$

Then, the developed torque is

$$\begin{aligned} T_e &= \frac{3P_{out}}{\omega_m} = \frac{3pE_f I_q}{\omega} \\ &= \frac{3pE_f}{\omega} * \frac{R_s V_s \cos \delta - R_s E_f + \omega L_s V_s \sin \delta}{R_s^2 + \omega^2 L_s^2} \end{aligned} \quad (30)$$

Where, P_{out} is the motor developed power, p is the number of motor pole pairs, ω_m is the mechanic speed.

From Figure 4.6, we can get I_s

$$\begin{aligned}
I_s &= \frac{V_s - E_f \angle \delta}{R_s + j\omega L_s} \\
&= \frac{V_s - (E_f \cos \delta + jE_f \sin \delta)}{R_s + j\omega L_s} \\
&= |I_s| \angle \phi
\end{aligned} \tag{31}$$

where,

$$|I_s| = \frac{\sqrt{(V_s - E_f \cos \delta)^2 + (E_f \sin \delta)^2}}{\sqrt{R_s^2 + \omega^2 L_s^2}}$$

and

$$\phi = -\tan^{-1} \frac{\omega L_s V_s + R_s E_f \sin \delta - \omega L_s E_f \cos \delta}{R_s V - R_s E_f \cos \delta - \omega L_s E_f \sin \delta}$$

ϕ is power factor angle.

In order to find δ_{\max} (maximum available torque per ampere of the stator current

occurring δ value), we can get $\frac{T_e}{|I_s|}$ as following equation:

$$\begin{aligned}
\frac{T_e}{|I_s|} &= \frac{\omega}{\sqrt{(V_s - E_f \cos \delta)^2 + (E_f \sin \delta)^2}} * \frac{R_s V_s \cos \delta - R_s E_f + \omega L_s V_s \sin \delta}{R_s^2 + \omega^2 L_s^2} \\
&= \frac{3pE_f}{\omega \sqrt{R_s^2 + \omega^2 L_s^2}} * \frac{R_s V_s \cos \delta - R_s E_f + \omega L_s V_s \sin \delta}{\sqrt{(V_s - E_f \cos \delta)^2 + (E_f \sin \delta)^2}}
\end{aligned} \tag{32}$$

Then, we differentiate equation (32) with respect to δ , and set it equal to zero.

The corresponding δ_{\max} can be got from following equation, which can be easily realized by Simulink.

$$\omega L_s V_s \cos \delta_{\max} = \omega L_s E_f + R_s V_s \sin \delta_{\max} \tag{33}$$

V_s can also be written as

$$V_s = |I_s| R_s \cos \phi + \sqrt{|E_s|^2 - (|I_s| R_s \sin \phi)^2} \tag{34}$$

In order to accomplish true constant V/f , at any frequency f , the required value of E_s is set as [20]:

$$E_s = V_{so} / f_r * f \tag{35}$$

where V_{so} is the magnitude of E_s at rated frequency f_r , which is a constant defined by rated conditions. E_f also can be substituted by $E_f = K * f$, where K is a constant determined by system.

We can rewrite V_s into

$$V_s = |I_s| R_s \cos \phi + \sqrt{\left(\frac{V_{so}}{f_r} * f\right)^2 - (|I_s| R_s \sin \phi)^2} \quad (36)$$

Using $\delta = \delta_{\max}$, we can get the optimal V/f control when stator resistance cannot be neglected.

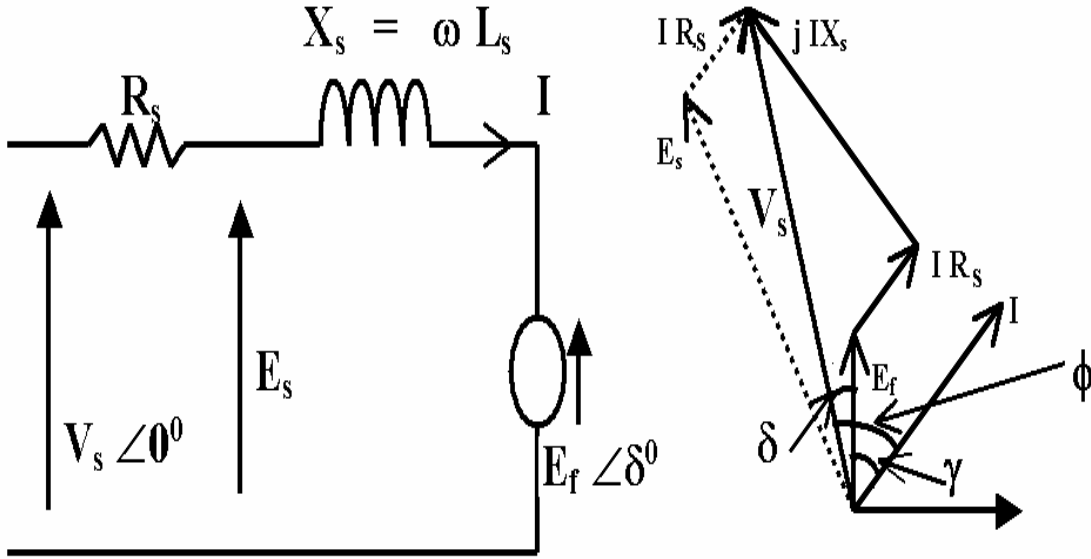


Figure 4.6 PMSM steady state equivalent circuit and phasor diagram 2

4.3 Optimal V/f Control Simulation and Analysis for Super High-Speed Motor

The simulation is done by SIMULINK.

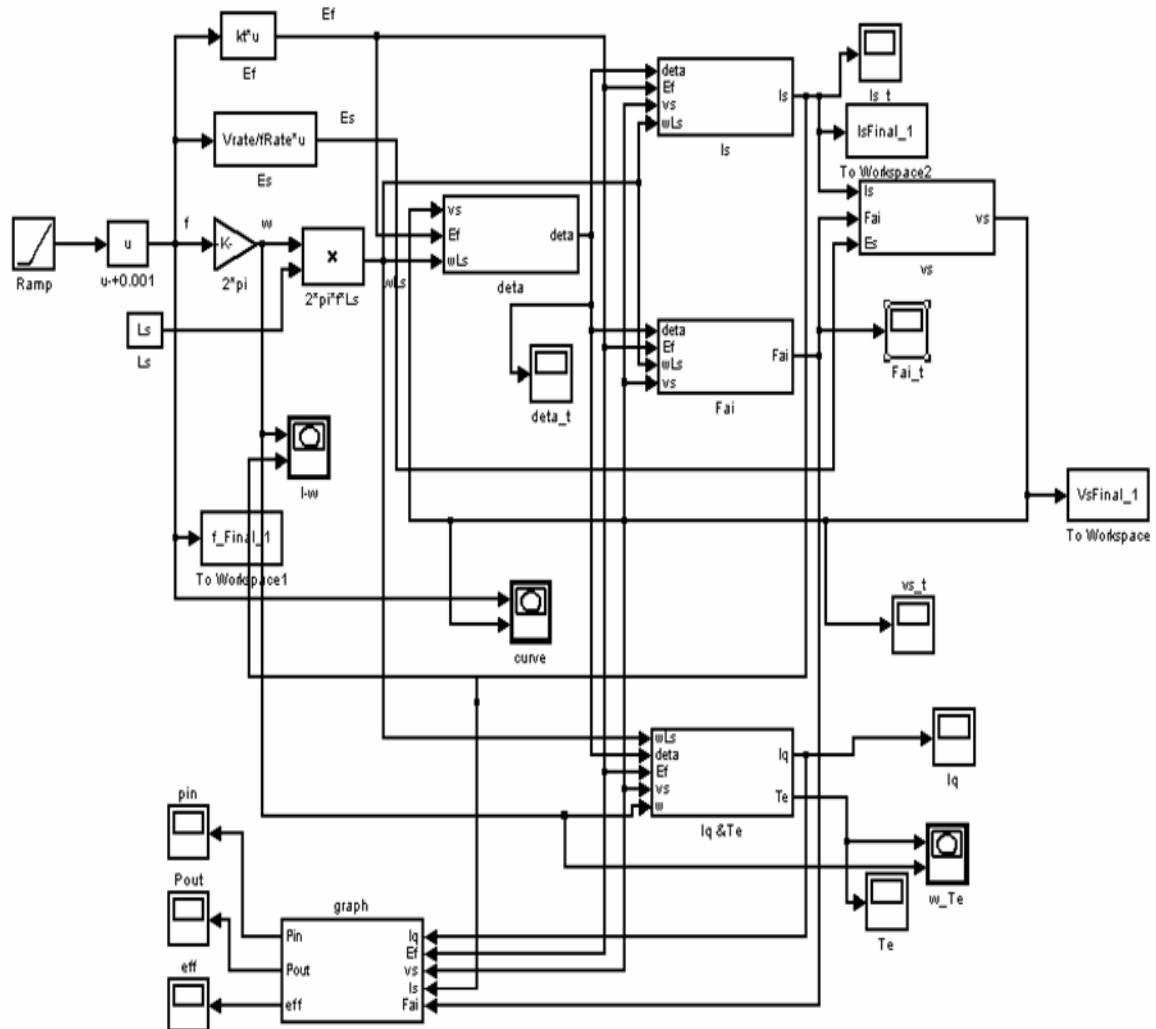


Figure 4.7 The simulation of proposed optimal constant V/f control design

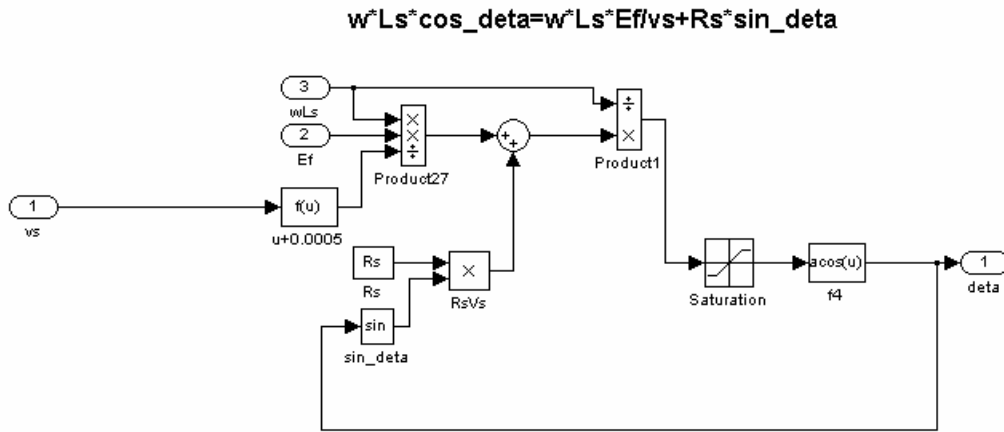


Figure 4.8 Configuration of module deta

$$I_s^2 = (v_s - E_f \cos(\text{deta}))^2 + (E_f \sin(\text{deta}))^2 / (R^2 + (wL_s)^2)$$

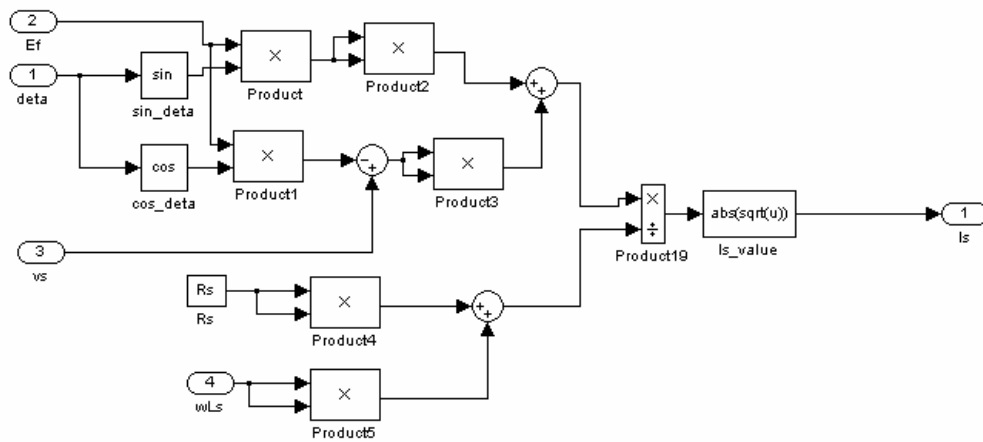
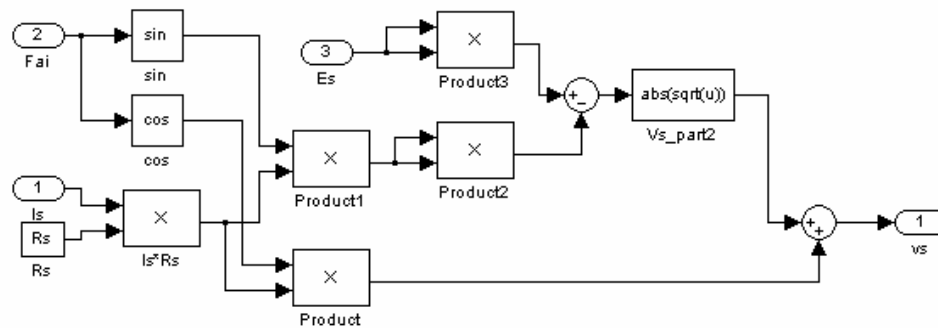


Figure 4.9 Configuration of module Is

$$v_s = I_s R_s \cos_{_Fai} + (E_s^2 - (I_s R_s \sin_{_Fai})^2)^{0.5}$$


60

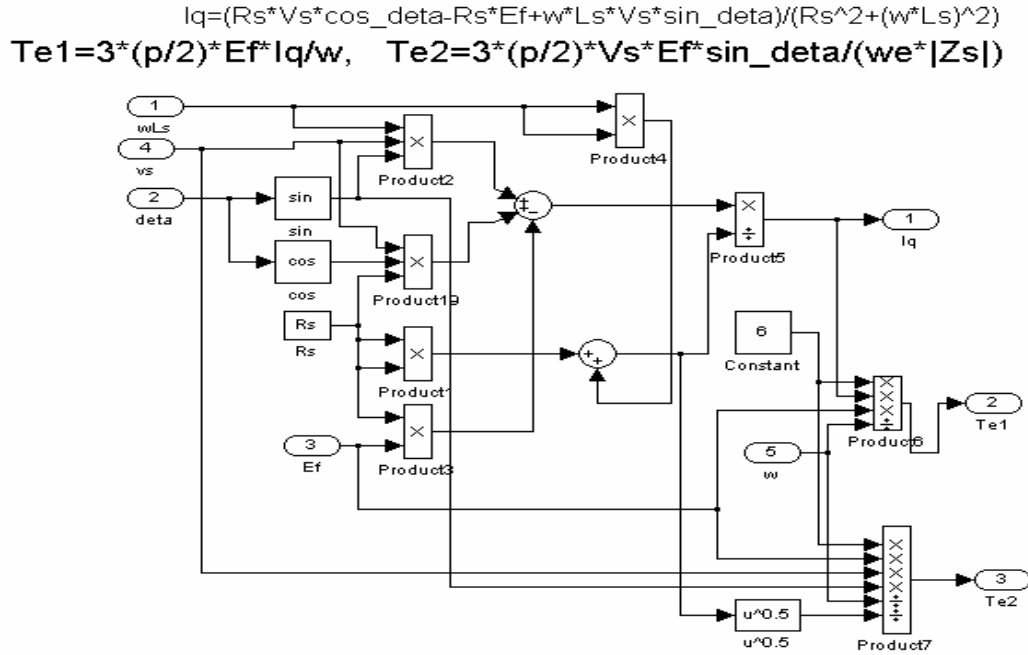


Figure 4.12 Configuration of module Iq and Torque

From Figure 4.13, when R_s is small enough, its effect is small and linear V/f control only with a boost voltage can be used. Figure 4.14 is the proposed optimal V/f control profile for the super high-speed motor 1. Different stator resistor value effect was analyzed in Figure 4.15. As shown, the proposed optimal constant V/f control profiles are quite different from the originally linear V/f control profile. The stator resistance affects the schematic substantially during the whole proposed motor speed range. Its effect fades with increasing frequency and the scheme becomes linear after the frequency passes some value. The proposed curves have a clear decreasing trend at low frequencies because the voltage drop on the stator resistor is faster than that increment on the reactance at low frequency. When increasing stator resistance, boost voltage increases quickly. At the same time, the optimal control scheme has a much sharper curve and with

a larger nonlinear frequency range, which can be found from Figure 4.15. The slope of linear part also decreases.

The inductance L_s also plays an important role to the optimal curve as well. When L_s increases, the boost voltage drops oppositely because stator resistor effect becomes smaller (Figure 4.16). Otherwise, if the inductance voltage increases, the boost voltage will increase dramatically and the bending trend becomes gentle (Figure 4.17).

In addition, the relationship of the stator resistance and the voltage drop effect are nonlinear. The effect weakens quickly when the frequency increases. Simulation results also verify stator resistance critically affects the dynamic stability. An almost linear V/f control scheme happens far before the cut-off frequency, where it was originally thought the stator resistance effect disappears.

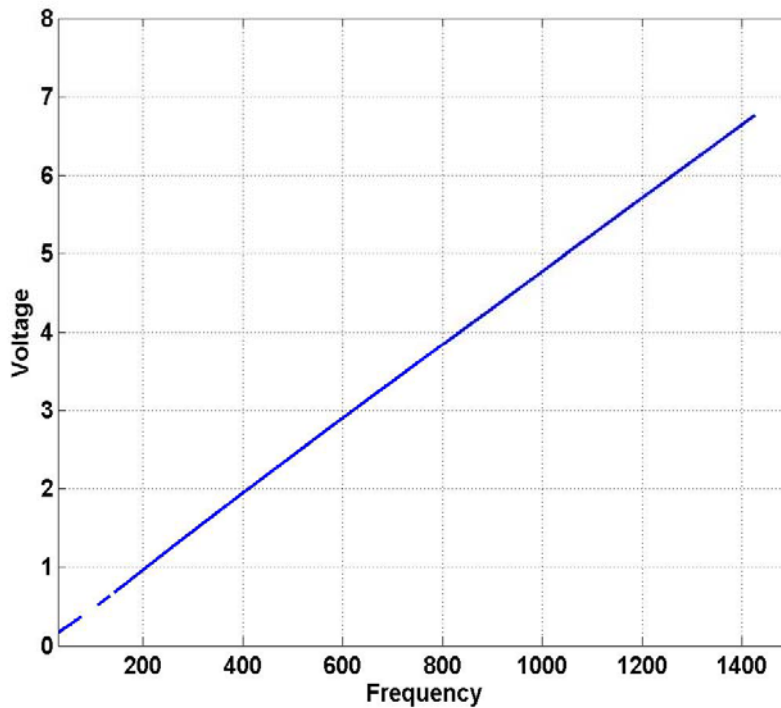


Figure 4.13 Linear constant V/f (Volt/Hz) control with boost voltage ($R_s=0.001 \Omega$)

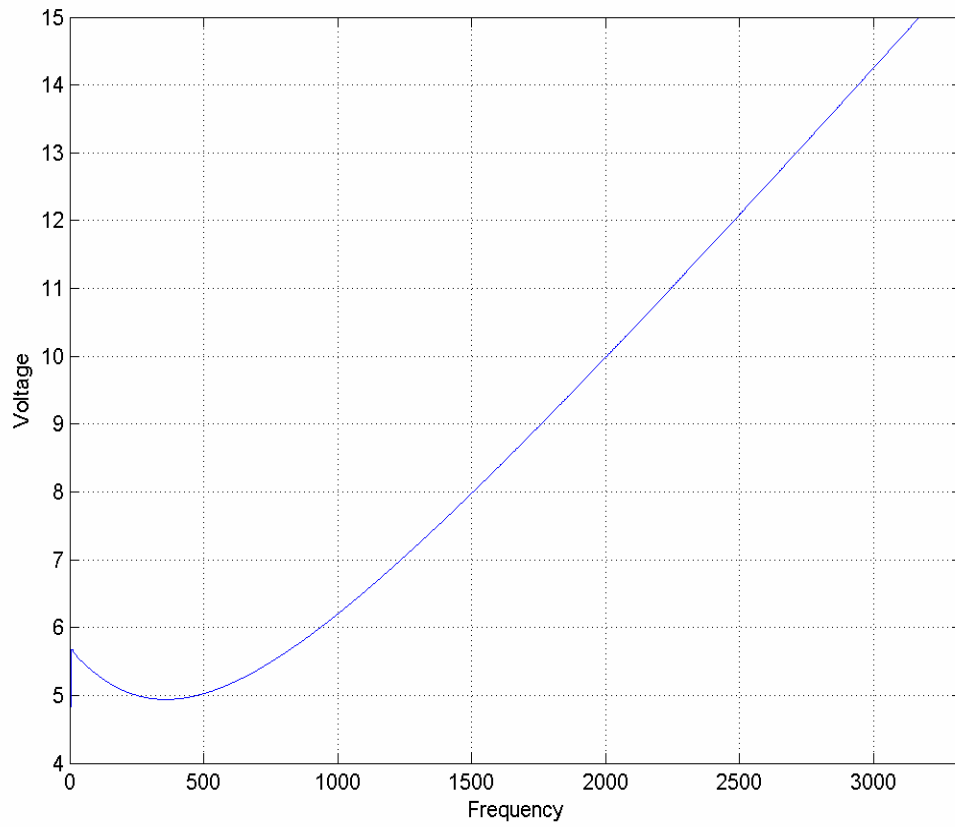
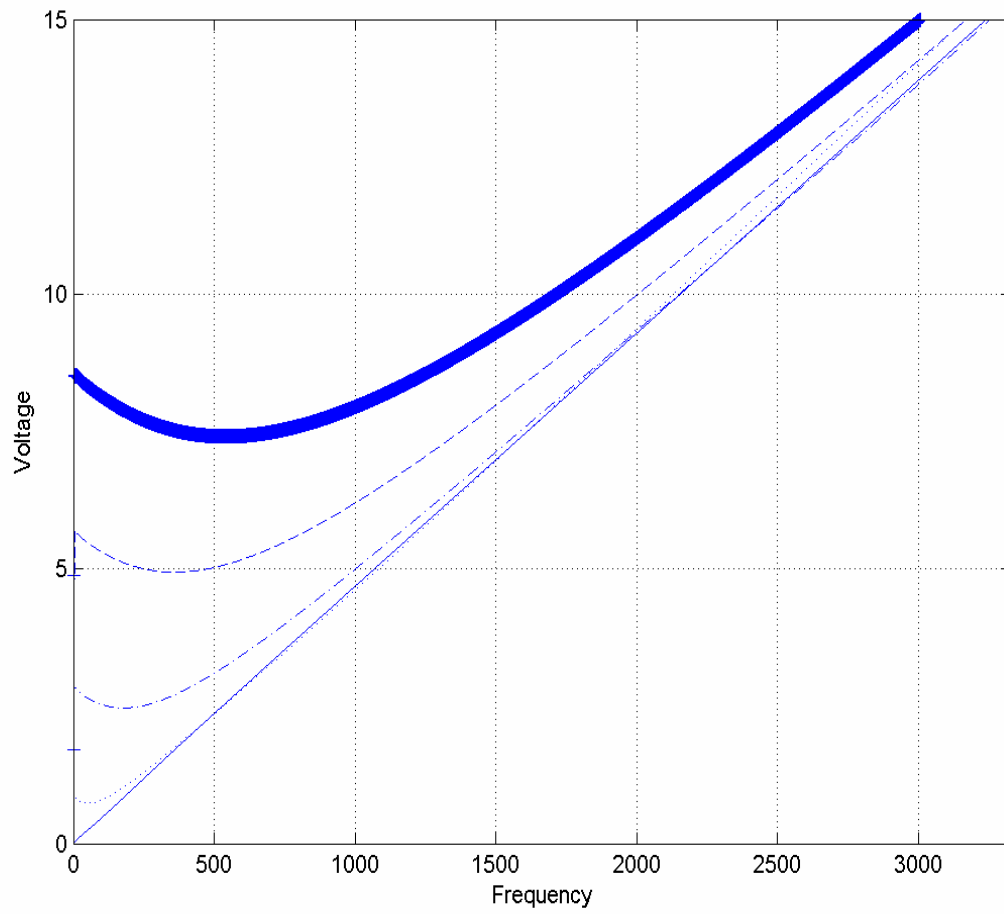


Figure 4.14 The proposed optimal V/f (Volt/Hz) profile for test motor.

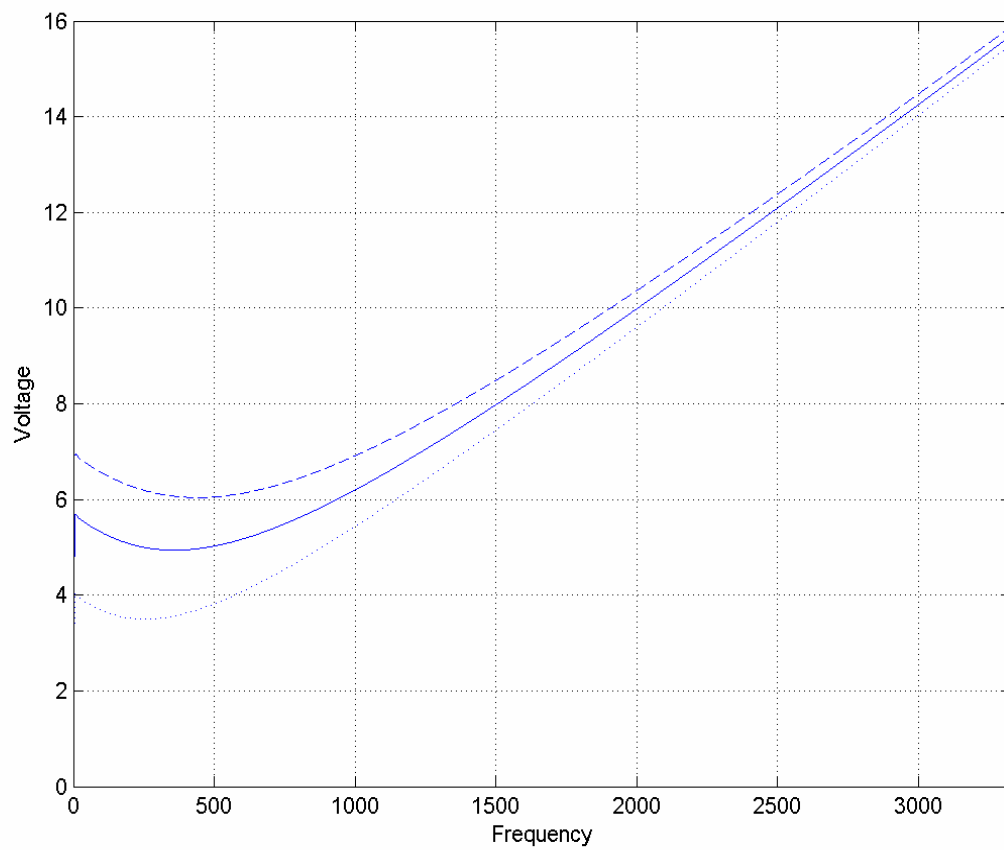
Speed range is from 0-100 Krpm.



- bold line is $R_s=0.09 \Omega$
- dashed line is $R_s=0.06 \Omega$
- dashdot line is $R_s=0.03 \Omega$
- dotted line is $R_s=0.01 \Omega$
- solid line is $R_s=0.001 \Omega$

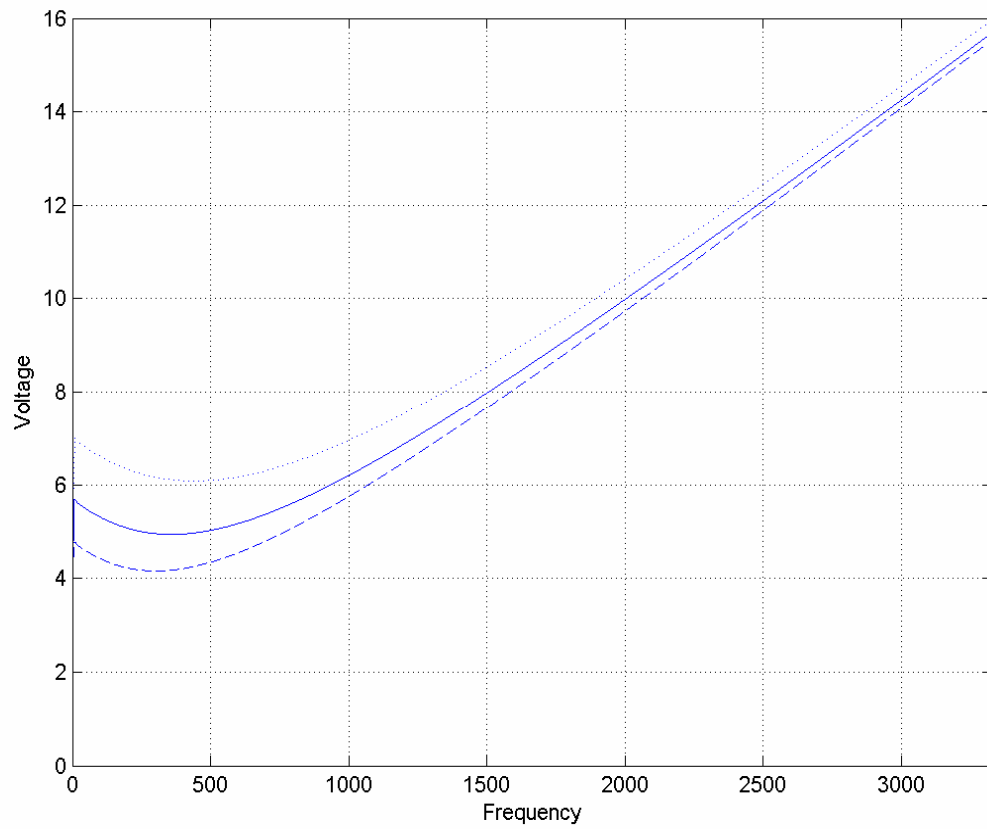
Figure 4.15 Optimal V/f (Volt/Hz) control with difference stator resistance and $L_s=1.6 \mu$

H, $K=0.0045$. Speed range is from 0-100 Krpm.



- dashed line is $L_s=1.3 \mu H$
- solid line is $L_s=1.6 \mu H$
- dotted line is $L_s=1.9 \mu H$

Figure 4.16 Optimal V/f (Volt/Hz) control with difference inductance and $R_s = 0.06 \Omega$, $K=0.0045$. Speed range is from 0-100 Krpm.



- dotted line is $K=0.00445$
- solid line is $K=0.0045$
- dashed line is $K=0.00455$

Figure 4.17 Optimal V/f (Volt/Hz) control with difference K and $R_s = 0.06 \Omega$, $L_s = 1.6 \mu H$.

Speed range is from 0-100 Krpm.

CHAPTER FIVE: DSP_BASED DIGITAL CONTROLLERS

The advent of programmable digital signal processors (DSPs) in recent years is creating new opportunities in power electronics. The special architecture and high performance of DSPs make it possible to implement a wide variety of control and measurement algorithms at a high sampling rate and reasonable cost. Power electronics systems are typically a complex combination of linear, nonlinear and switching elements. High-frequency converters add another dimension of complexity because of their fast dynamics. Real-time power electronics systems, therefore, demand the use of high-speed data-acquisition and control. DSPs meet the processing requirements posed by such systems. As a result, DSP are widely used in multiple applications in power electronics including AC motor drives, high-frequency converter control, motion control, robotics and real-time testing and monitoring.

5.1 Analog Controller and Digital Controller

The primary advantages of traditional analog controllers are high bandwidth, high resolution, are easy to understand and use, and they are relatively low in cost. But analog controllers suffer from serious limitations, such as sensitivity to noise, temperature change, component drift, and are not flexible. Large part count is also common for complex analog systems. Components age and change values over temperature and

various environmental conditions defect the performance of analog controllers. As far as predictability, one cannot obtain two components that are exactly alike. They have to be tweaked and trimmed. To modify a system one has to replace components. Board layouts also become a consideration that must be taken into account, and it is difficult, sometimes impossible, to implement some functions. Hence, the trend has moved towards digital control schemes, which offer multitudinous benefits.

There are many advantages to digital control. For example, digital controllers are less sensitive to the environment, they are highly reliable, and they are software programmable, which translates to greater flexibility. Digital controllers are precise, and offer more predictable behavior. Advanced control is also possible – enabling non-linear and multi-variable control. Designers can also perform multiple loops, and other unique functions.

Power control schemes have been revolutionized over the past few decades due to digital controller. Digital controllers for switching power supplies offer a number of advantages including a reduction of the number of passive components, programmability, implementation of more advanced control algorithms and additional processing options, as well as reduced sensitivity to parameter variations [15].

Digital controllers have some drawbacks, however. Those include bandwidth limitations, numerical problems like quantization errors, data converter limitations, CPU performance limitations, and system cost concerns. More recently, many of the "traditional" negatives associated with digital controllers are disappearing. DSP controller technology is rapidly improving while prices are reaching levels where even cost-sensitive equipments benefit.

5.2 DSP-based Digital Controller

Digital controller has many advantages over its analog counterpart. There are no hardware adjustments, fewer components, less aging effects, and smaller temperature drifts. With a digital controller, adjustment of control parameters for adapting to different electrical environments is easy and flexible. DSP provides more advantages such as full digital control, fewer components, high noise/EMI immunity, high reliability, reduced heating of power switches, lower harmonics, less filtering, faster fault response, no dc components, and higher efficiency. Additionally, it is easy to include other system level functions such as battery charging, power factor correction, reactive power compensation, fuzzy logic control, parallel operation, and on-the-fly frequency change to adapt to different environments and applications. Secure remote communication, data acquisition and display, device overload protection, maximum power tracking, and state control can all easily be implemented.

The innovation of DSP-based digital control into power electronic designs is an excellent example of the advantages provided by major technological advances. Digital signal processor (DSP) controller is the combination of a high-speed mathematical core, memory, and a set of peripheral devices. With an appropriate set of peripherals for the application, it is possible to reach a single chip solution with minimum or even no external interface components. Today's DSP controllers that are created for complex motor speed and servo control are widely used in industry due to continuously dropping

cost and performance improving. Their features include single-cycle multiplication and accumulation, on-chip pulse-width modulation (PWM) mechanism, and analog to digital converters (ADCs), to implement sophisticated control techniques required [27][31][41].

With the improvement in math-intensive functions and high execution speed, faster control response and correction to achieve desired parameters yields a better performing system. The DSP software allows for automation of the testing process, thus reducing the labor content of the technical staff. The software within the DSP can be easily modified to optimize the application and provide diagnostic once in use in the field or if the application changes once the unit is installed. The application that the equipment addresses can be easily modified via software changes as opposed to hardware design changes. This also increases in-house design flexibility. Development time is reduced, since software is easier to revise than manufactured hardware.

With advanced DSP control, fewer components are required. This results in a simple system configuration, high reliability, low cost, smaller footprint, and lighter weight. DSP controller will reduce the material cost of the customer's equipment, labor content, and overhead related to both materials and labor (purchasing transactions cost, accounting transactions costs, factory overhead). Technological advancements allow equipment to become smaller and lighter which translates into cost reduction, labor, transportation, and materials.

5.3 Motor Control

Traditionally motor control was designed with analog components as they are easy to design and can be implemented with relatively inexpensive components. However, there are several drawbacks with analog systems. Aging and temperature reduce system reliability and increase maintenance cost. Tolerance issues and difficulty to upgrade also are important problems.

Digital systems offer improvements over analog designs. Drift is eliminated since most functions are performed digitally, upgrades can easily be made in software and part count is also reduced since digital systems can handle several functions on chip.

Digital Signal Processors further provide high-speed, high-resolution control algorithms resulting in reducing system costs. Generally, fixed point DSPs are preferred for motor control for two reasons. Firstly, for most applications a dynamic range of 16 bits is enough. If and when needed, the dynamic range can be increased in a fixed-point processor by doing floating-point calculations in software. Secondly, the cost of fixed point DSP is much less than that of floating point DSP.

The performance of an AC synchronous motor is strongly dependent on its control. DSP controllers enable enhanced real time algorithms. The combination of both allows a reduction in the number of components and optimizes the design to reduce system cost [15].

Over analog controller for power converters digital controller has some limitations. Due to digital controller's inevitable involving of ADC, the system's performance must be affected by the ADC. A complete analog system is simpler than a high speed and high resolution ADC. Moreover, available microcontroller or DSP now are still too slow and too costly for the power converters. A high speed and high resolution of DPWM is also too costly for some simple power application. Furthermore, digital controller increases the complexity of the system due to ADC and digital processing. As a result, DSP controllers are only applied when necessary.

5.4 Digital Control Portion

A general structure to incorporate digital control for a plant, such as a power stage, is shown in Figure 5.1. Data converters are necessary to transfer a signal from analog to digital domain, and vice versa. The analog-to-digital converter (ADC) and digital-to-analog converter (DAC) perform those functions, respectively. Calculation is done inside the digital controller, which can be a DSP, FPGA [22], etc.

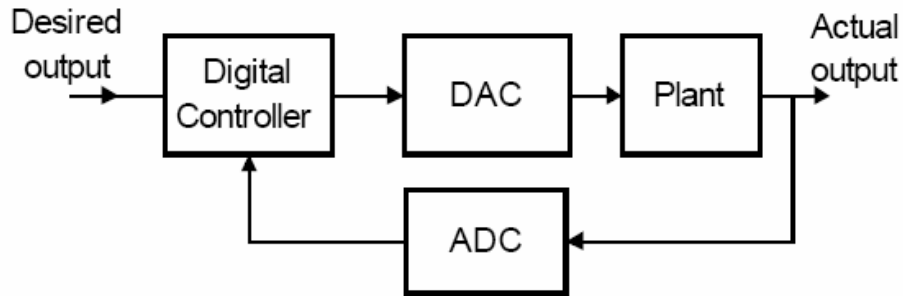


Figure 5.1 Typical digital controller configurations [31]

Initial modeling of the data converters' characteristics can include effects, such as static performance, delay effect, sample-and-hold, quantization, and input impedance, and etc. [31]. To achieve better modeling of the data converter, experimental data can be incorporated into the simulation. Dynamic characteristics, such as frequency response, can be performed experimentally and then modeled on the computer for ease of further analysis.

5.5 Architecture of TI C2000

TI has developed the DSP solutions that are driving digital control by providing the industry's high performing and code efficient DSPs. The TMS320C2000 family of DSP controllers set the standard for performance and peripheral integration by offering a unique combination of on-chip peripherals such as flash memory, ultra-fast A/D converters, PWM modules and robust CAN modules.

The TMS320C2000 family is optimized for digital motor control applications. The DSP controllers combine the enhanced TMS320 architectural design of the C2xLP core CPU for low-cost, high-performance processing capabilities and several advanced peripherals optimized for motor or motion control applications. Notable related features of this family are as follows [44]:

- 20 MHz clock speed
- 16K Words \times 16 Bits of On-Chip Program Flash EEPROM
- 12 Compare/Pulse-Width Modulation (PWM) Channels
- Three 16-Bit General-Purpose Timers with Six Modes
- Three 16-Bit Full-Compare Units with Dead band
- Dual 10-Bit ADC Module with 6.1 μ s conversion time
- 28 Individually Programmable, Multiplexed I/O Pins

5.5.1 TI TMS320F240

Texas Instruments introduced TMS320F240 in 1996, and this chip has successfully demonstrated its power in many applications since then.

The Evaluation Module (EVM) of TMS320F240, as shown in Figure 5.2, containing the TMS320F240 chip with external peripherals is available from Texas Instruments. The EVM includes 4 channels 12 bits DAC, external memory, DIP switches, etc. The resolution of the DAC relates directly to the step size. Extra components on the EVM board and the accompany software: Code Composer, facilitate in the debugging process.

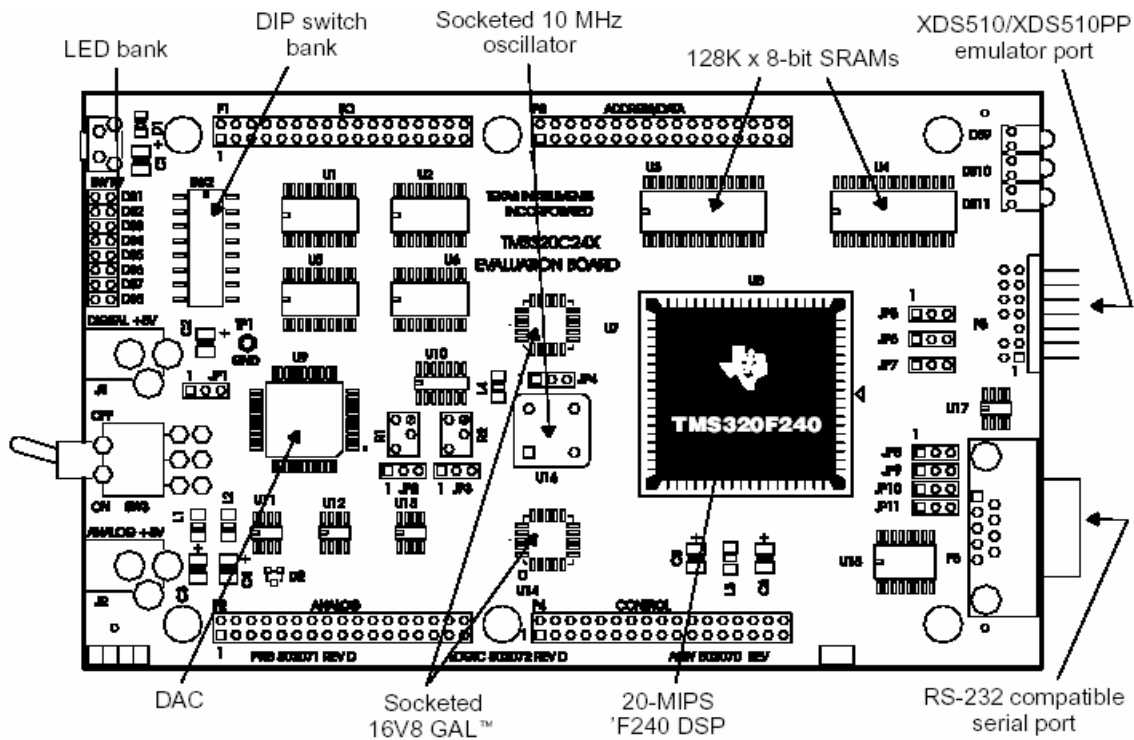


Figure 5.2 TI TMS320 development board [44]

The 16-bit TMS320LF240 from Texas Instrument was chosen as the microprocessor for our prototype. This embedded device provides suitable processing power for this application. To achieve high level of performance and to explore the complicated control schemes and features made possible by operating with a digital controller [44].

5.6 PWM Generators and ADC of TMS320LF2407A

With digital power applications, ADC and PWM modules are the most important peripheral devices inside the DSPs. TMS320LF2407A provides high performance ADC and PWM generators and makes it possible to meet the high requirement of converters.

The TMS320LF2407A [45] is specifically designed for the digital motor control segment. This device combines a 16-bit 40MHz processor with fixed point calculation capability. The DSP chip has a 16 channels multiplexed 10-bit ADC with a built-in sample-and-hold (S/H) circuit. The minimum conversion time is 500ns.

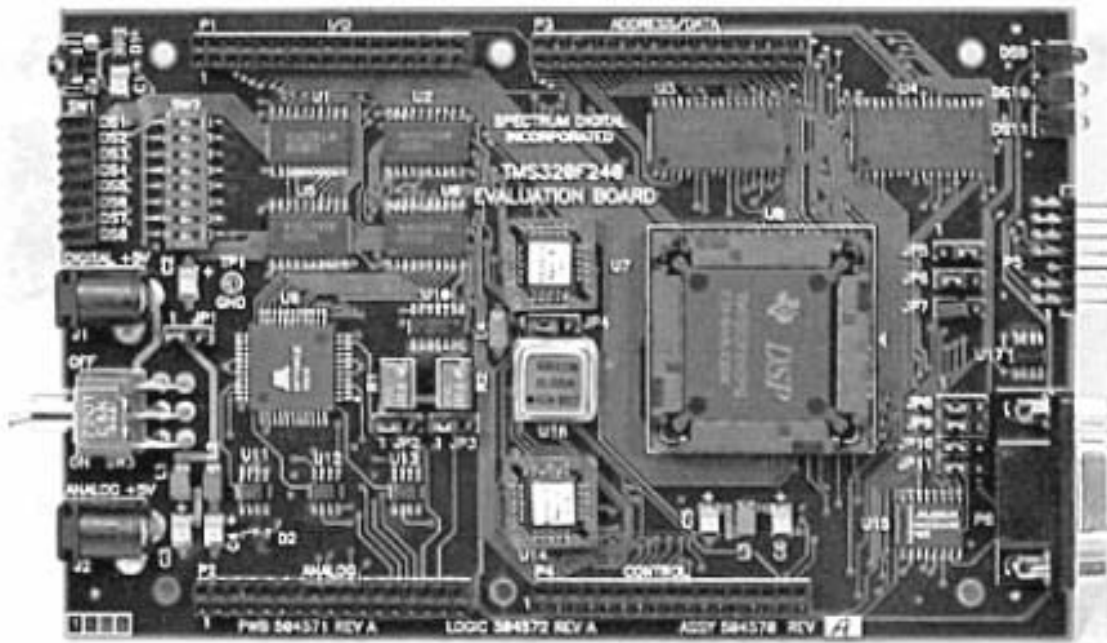


Figure 5.3 TI TMS320LF2407A Evaluation Board [45]

The ADC of TMS320LF2407A provides 12-bit core with built-in dual sample-and-hold (S/H) modes, very fast conversion time (running at 40 MHz), ADC clock, and 16-channel, multiplexed inputs and 16 result registers to store conversion values.

The PWM modules of TMS320LF2407A are designed to generate pulse width modulated waveforms used in motor control and motion control applications. The PWM waveform generation capability of each event manager module (A and B) is summarized as follows.

There are five independent PWM outputs — three of which are generated by the compare units, while the other two are generated by the GP timer compares — plus three additional PWM outputs, dependent on the three compare unit PWM outputs. This make possible to realize multiple motor control using a single DSP TMS320F2407A [41]. It provides programmable dead-band for the PWM output pairs, and the minimum dead-band duration of one device clock cycle (6.67ns) [47]. The minimum PWM pulse width and pulse width increment/decrement is one clock cycle. The PWM supports 16-bit maximum PWM resolution and programmable generation of asymmetric and symmetric PWM waveforms. Figure 5.4 is an example of generating the PWM waveform with the controlled dead time based on the given PWM period and initial values.

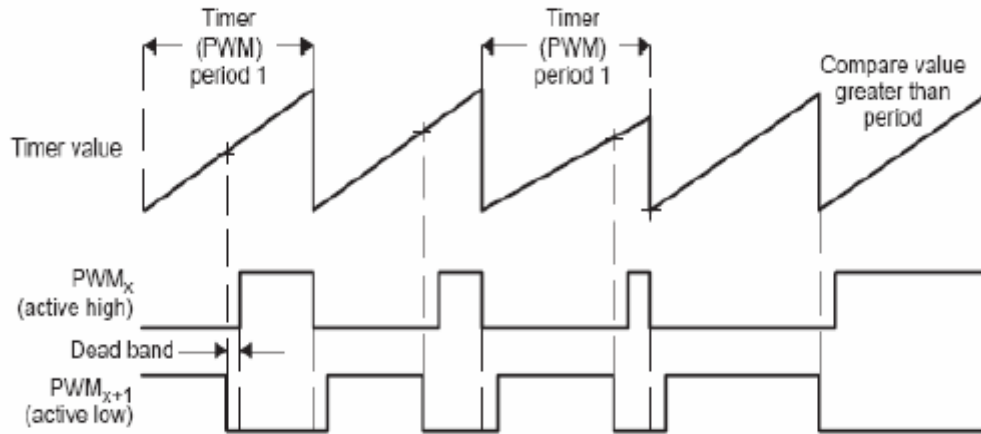


Figure 5.4 Generating PWM waveform in TI TMS320LF2407A [28]

The PWM modules of TMS320LF2407A can set up the period register TxPR and configure register TxCON to initialize the frequency and configuration of PWM. To generate the gate driver signals for the DC-AC converter, the PWM frequency is designed to be equal to the switching frequency. To avoid the limit cycle, the resolution PWM must be greater than the resolution of ADC. The PWM signal of TMS320LF2407A has 16-bits resolution, while the resolution ADC is 12 bits. Therefore, TMS320LF2407A provides the most reasonable resolution for the digital controller implementation.

There are two kinds of cases for PWM signals, which includes symmetrical and asymmetrical. For symmetrical PWM, the gate signals of primary side have the same duty cycle ratio but with 180-degree phase shift. For asymmetrical PWM, the gate signals of the primary side are complimentary signals with dead time. The complementary signals should be generated with controlled dead time for the secondary side signals.

The Figure 5.5 and Figure 5.6 show how to generate the primary and secondary PWM signals with PWM generator of TMS320LF2407A. To get the accurate dead time and phase shift of the signals, we generate the signals based on the same timer, which is set up in Event Manager A. The symmetrical ramp signals are achieved by using Event Manager A timer in a PWM module. Using given duty cycle values from the compensator calculation, the four compare values are calculated to get responding values, and then the compare registers are set up respectively.

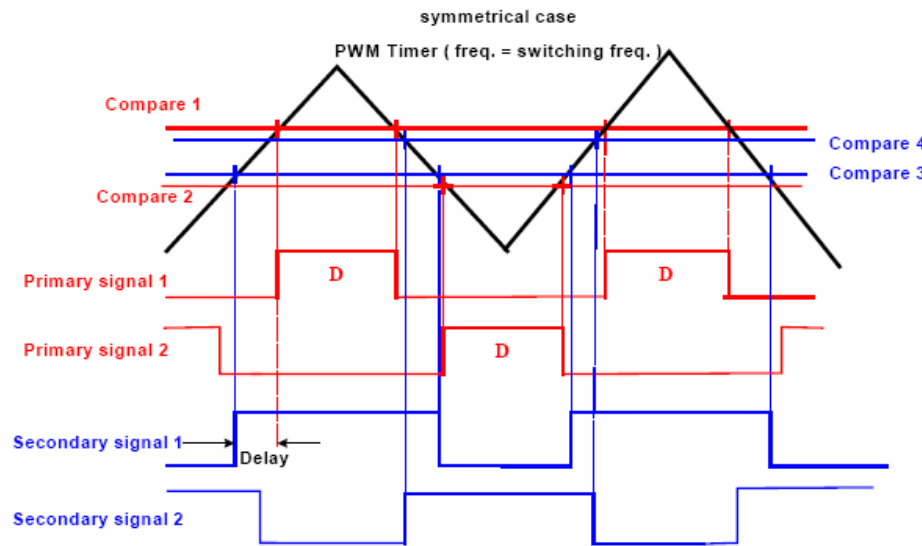


Figure 5.5 Symmetrical PWM signals generation [28]

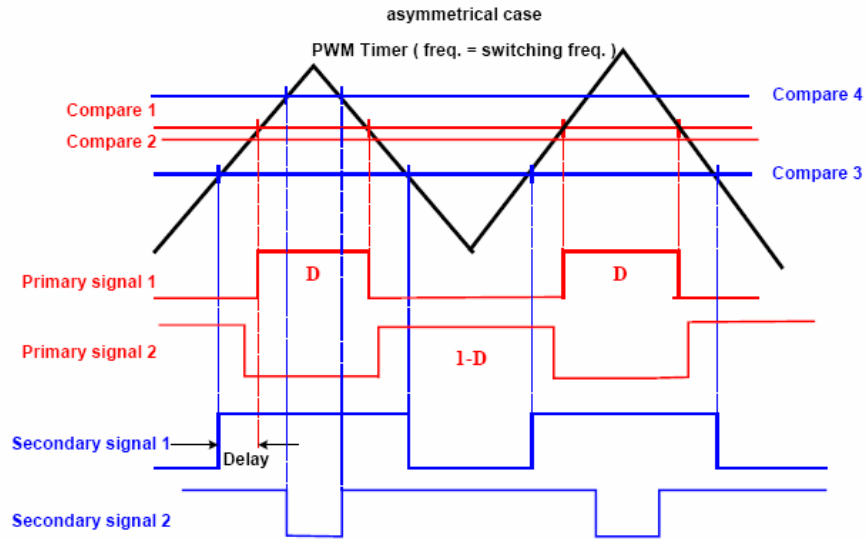


Figure 5.6 Asymmetrical PWM signals generation [28]

The ADC of TMS320LF2407A could be triggered by the software, EVA/B or the external pins. In our DSP platform, we set up the ADC triggered by the Event Timer A, whose frequency is suppose to be equal to the sampling frequency of ADC.

5.7 The Generation of Sine Wave

The generation of the sine wave is performed using a look up table. To be able to control the frequency of the modulation with some accuracy, a method based on the modulo mathematical operation is used. The modulo mathematical operation is used when there is overflow in the accumulator from the lower word to the upper word. When an overflow occurs, only the remainder (lower word) is stored. A 16-bit counter is used to

determine the location of the next value. A step value is added to the counter every time a new value from the sine table is to be loaded. By modifying the value of the step, the frequency of the sine wave is changed. The frequency of the sine wave is proportional to the step size and inversely proportional to the size of the counter register and the period at which the routine is accessed and can be calculated by [48]

$$f(step) = \frac{step}{T_s \times 2^n} \quad (37)$$

where $f(step)$ is the desired frequency, T_s is the time period between each update, n is the number of bits in the counter register, and $step$ is the step size used. Phase shift can be realized by specifying the starting point for the counter. A separate timer is used to vary the amplitude of the dither signal periodically, when desired.

CHAPTER 6: DESIGN AND OPTIMIZE DIGITAL CONTROL AND SWITCH MODE POWER SUPPLY SYSTEM

The proposed super high-speed PMSM controller is based on TI Digital Signal Processor TMSLF2407A. The controller includes hardware and software systems. Hardware is switching mode power supply system to provide suitable driven power to the motor. Software is embedded real-time control system to generate PWM signals. The block chart of the proposed controllers is shown in Figure 6.1. The controller design is based on space vector PWM method and switch mode method to realize high efficiency real-time control and power supply.

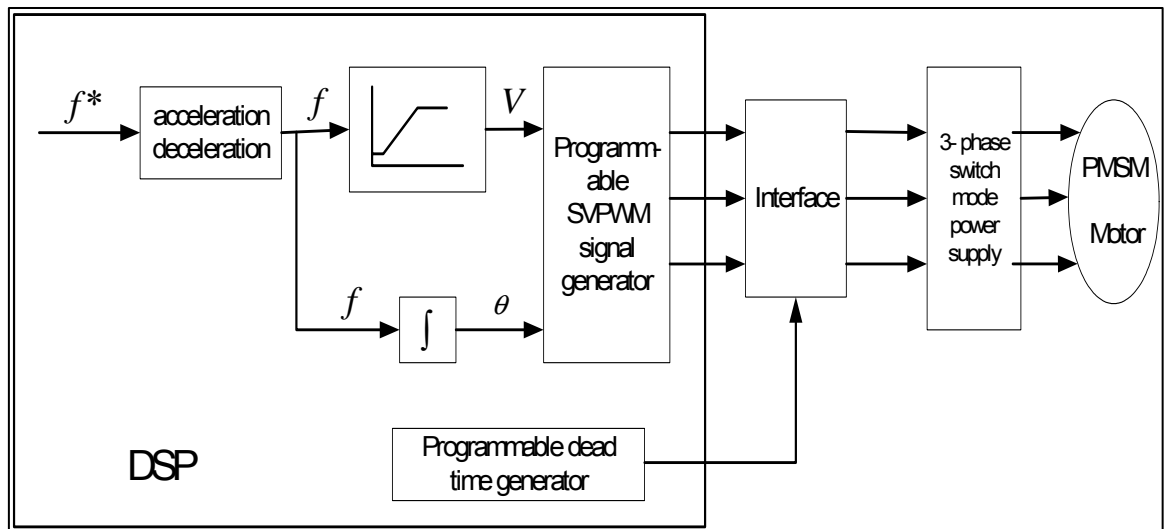


Figure 6.1 The block diagram of the proposed controllers

6.1 Switch Mode Power Supply

The converter is a required element of a motor drive system. It is responsible for supplying the motor with power as well as commutation pulses to allow for rotation. The commutation pulses come from the semiconductor transistor switch. The most widely accepted converter for a single-phase load is the asymmetric bridge design. The asymmetric bridge begins with an ac supply fed into a bridge rectifier connected to a DC link. This is then fed to the bridge, which consists of two transistor switches and two diodes. This design involves four semiconductor devices for each phase, two transistors and other two working as power diodes [15].

6.1.1 Three-phase Voltage Source Inverter

When the load is a multi-phase system, the power supply system must be multi-phase system to supply suitable driver signals. Power electronic inverters can be thought as networks of semiconductor power switches. Depending on types, the switches can be divided as uncontrolled, semi-controlled and fully controlled [15].

Switching is used to control the output voltage in this application. Inverters convert DC power into AC power at a desired output voltage or current and frequency. Voltage source inverter (VSI) is the most commonly used type of inverters [8]. In a VSI, the input DC voltage source is essentially constant and independent of the load current drawn.

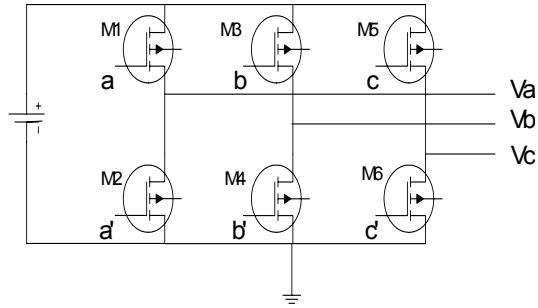


Figure 6.2 A typical three-phase voltage source inverter

Power devices in industrial drives typically constitute about one-third of the cost. However, the cost can rise substantially when motors larger than 5 kW [15]. Motor topologies dictate the power device configuration, and the supply voltage affects the choice of power devices.

6.1.2 Power MOSFET

Power MOSFET is a fast-switching transistor, suited to low-power (up to a few kilowatts), high-frequency (up to 100K HZ) applications [15]. MOSFET is major component in inverter. Performance of the MOSFET will directly affect the efficiency and performance of controller.

The thermal ratings for MOSFET should be carefully followed. These parameters directly affect the reliability of the device. A good prototyping method is to select a heat sink that is 2 to 5 times larger than expected [15].

Minimizing the MOSFET power dissipation lowers its junction temperature. The lowest power dissipation device will almost always be the most expensive, but it will reduce heat sink size and offer good long reliability.

When a power MOSFET is used as a switch and is in the on condition, it is forced to operate in the ohmic region. Therefore for switching application, the on-state resistance ($R_{DS(ON)}$) is a very important parameter, since it determines the conduction power loss for a given value of the load current. The lower the value of $R_{DS(ON)}$, the lower the on-state voltage drop, the lower the power dissipation, and the higher the current-carrying capability of the device.

Although MOSFETs are fairly robust power devices and can sustain some excessive drain-to-source voltage spikes, it is a good practice to ensure that the maximum voltage, current and energy ratings are not exceeded in applications. If possible, the device should be derated by 30 to 50 percent to ensure long-term reliability [49][50][52].

The phase current peak value of the 200 Krpm motor is about 91 amperes at full load and phase voltage peak value is 16 volts. Considering the safety margin, the wanted MOSFET must satisfy that the maximum voltage should be at least 50 V and maximum current be at least 180 A. Paralleling MOSFETs prototype is employed to increase the current capacity and reduce the on-state resistance ($R_{DS(ON)}$) and responding reduce conduction loss.

6.1.3 MOSFET Gate Charge

Selecting a fast-switching power semiconductor helps reduce switching loss. This has a point of diminishing return on power semiconductor switching speed, since the

stray inductance will set an upper limit on switching speeds [50]. It is very important for high switching frequency application. The Figure 6.3 shows MOSFET equivalent circuit at high frequency.

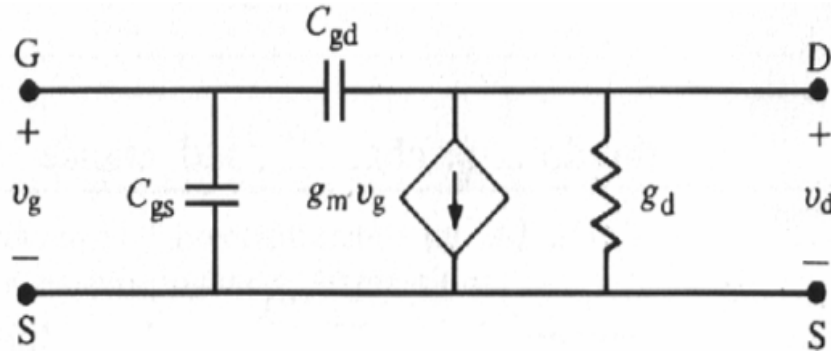


Figure 6.3 MOSFET equivalent circuits at high frequency

The switching performance of a device is determined by the time required to establish voltage changes across capacitances. Gate-to-drain capacitance, C_{gd} , is a nonlinear function of voltage and is the most important parameter because it provides a feedback loop between the output and the input of the circuit. C_{gd} is also called the Miller capacitance and causes the total dynamic input capacitance to become greater than the sum of the static capacitances.

Although the gate-to-drain capacitance is an important value, it is actually more difficult to deal with because of its non-linear capacitance affected as a function of voltage. To account for both gate-to-source and gate-to-drain capacitance in a way readily usable by designers, gate charge can be used to calculate drive circuit requirements. Gate charge, Q , is defined as the charge that must be supplied to the gate,

either to swing the gate by a given amount, or to achieve full switching. The lower the charge, the lower is the gate drive current needed to achieve a given switching time [29][30][50][51][52] .

The advantage of using gate charge is that the designer can easily calculate the amount of current required from the drive circuit to switch the device on in a desired length of time because $Q = C \cdot V$ and $I = C \cdot dv/dt$, the $Q = \text{Time} \cdot \text{current}$. For our case, a 50 kHz switcher is required to achieve a switching time of 200 nanoseconds. Two parallel MOSFETs with gate charge of 194nC can be turned on in 1usec if 200mA is supplied to the gate or they can turn on in 200nsec if the gate current is increased to 1A. These simple calculations would not have been possible with input capacitance values.

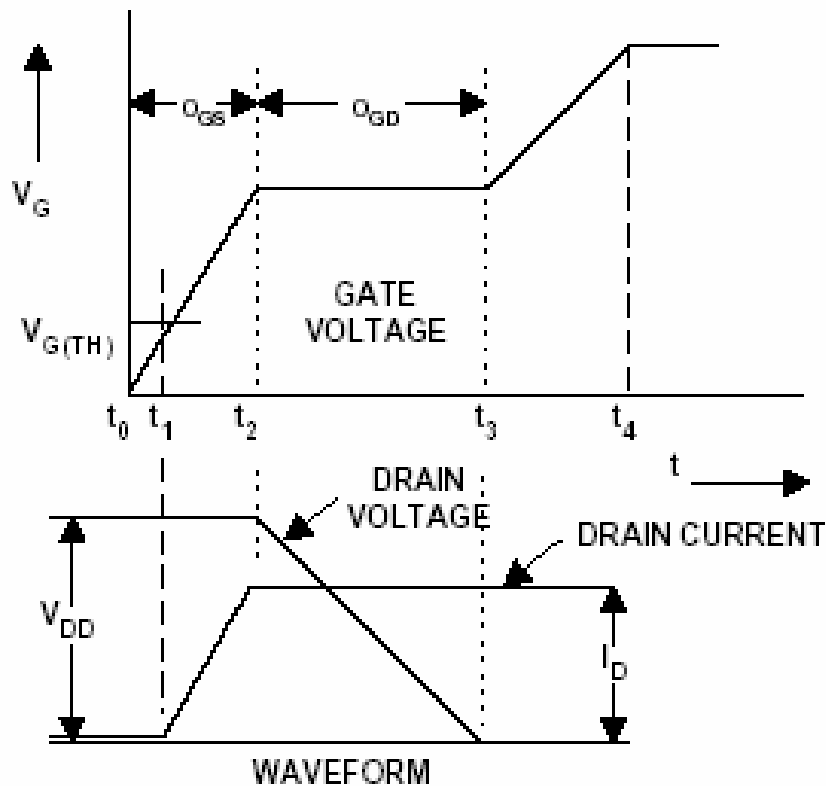


Figure 6.4 Gate and drive waveforms [50]

6.2 Gate Drive System

To design a gate drive circuit, electrical characteristics of the involved devices (DSP, optocouplers, and power switches) need to be checked. These values will be used to determine the current limiting resistances used in both the input and output circuits of the optocouplers. The current limiting resistors will limit the both the output current of the DSP pins and the collector-emitter current of the optocoupler from exceeding the maximum [54].

Drive chip is one important component in the controller system, which critically affects MOSFET dynamic characteristic. Enough drive current is essential condition to make MOSFET work correctly and also helps to high efficiency.

6.2.1 Drive Chip IR 2110

Well-known IR 2110 is used for the 2000W motor controller, which is capable of 2A sink and 2A source maximum gate driving current. Drive chip IR2110 and a 3-phase voltage-fed inverter provide enough input power to motor.

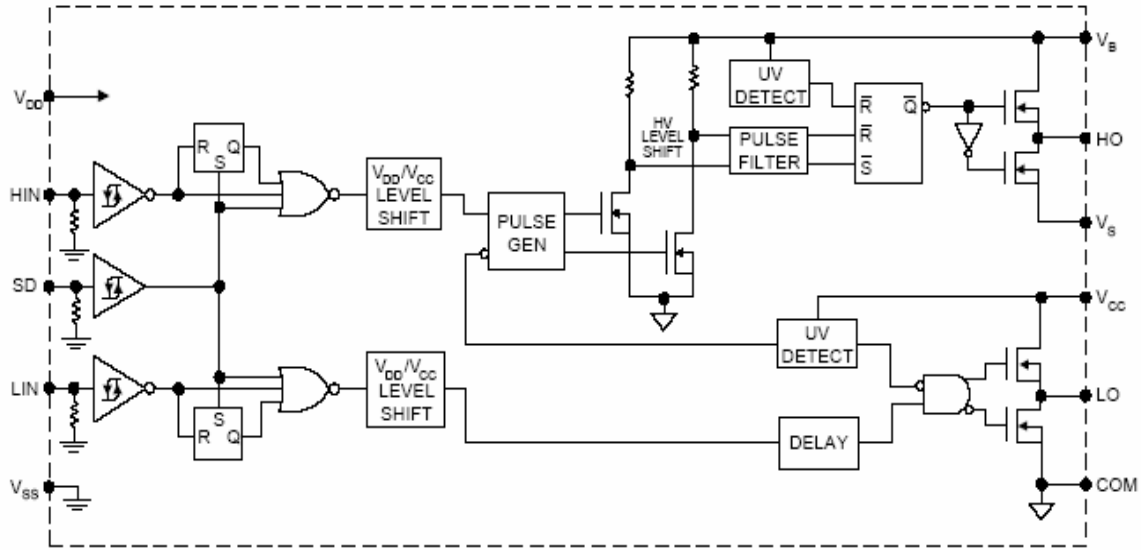


Figure 6.5 IR2110 function block diagram [56]

Typical Connection

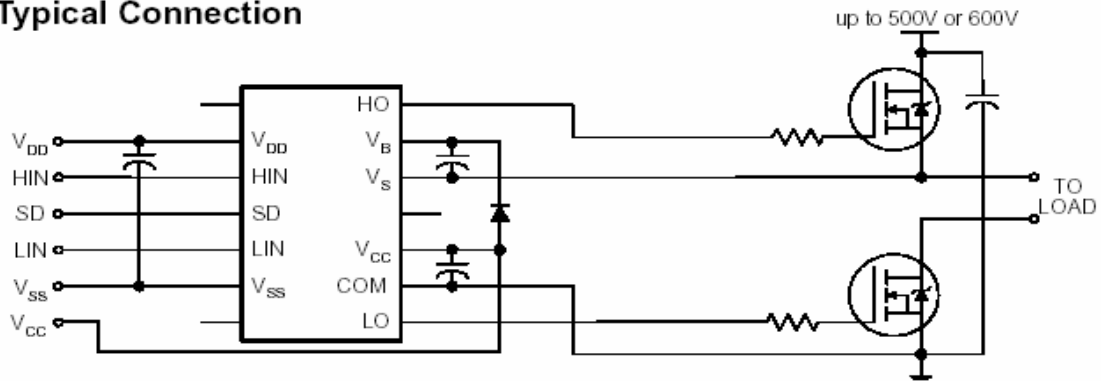


Figure 6.6 IR2110 typical connection [56]

To make drive chip work, the bootstrap circuit needs to be design at first. To design the bootstrap circuit for IR2110, two components are mainly considered. The first is a suitable bootstrap capacitor, which can be calculated by [54]:

$$C = 15 \times \frac{2 \left[2Q_g + \frac{I_{qbs(max)}}{f} + (I_{lson} + I_{lsoff})t_w + \frac{I_{cbs(leak)}}{f} \right]}{V_{cc} - V_f - V_{LS}} \quad (38)$$

where:

Q_g =Gate charge of high side FET

f =frequency of operation

I_{lson}/I_{lsoff} =level shift currents required to switch on or off

t_w =pulse width of level shift currents

$I_{cbs(leak)}$ =Bootstrap capacitor leakage current

V_f = Forward voltage drop across the bootstrap diode

V_{LS} = Voltage drop across the low side FET or load

We can calculate that bootstrap capacitance C_{bs} should equal or greater than 879.85nF. 0.1uF capacitors are taken for convenience.

Another component needed to design is a fast recovery diode, which requires $t_{rr} < 100ns$. A super fast recovery diode ($t_{rr} = 35ns$) is chosen for bootstrap circuit in this design.

6.2.2 IR2110 Bootstrap Circuits Design Tips

There are some design tips to avoid latch up the drive chip. First, avoid overcharging the gate of the power switch because the higher the gate voltage is the longer it takes to turn off the device. In addition, more charge must be transferred, which dissipates more power both in the IR2110 and in the switch device [29][30][31][32].

The upper bias is maintained by the Bootstrap Capacitor C_F between refresh cycles. A refresh cycle is defined as the time that elapses between conduction periods of the lower power switch and/or its body diode or flyback diode. Sometimes compromises on the value of the bootstrap capacitor must be made. For example, the capacitance should be neither so large to require a long refresh period nor so small that the voltage drops below the undervoltage trip point during the period of upper switch conduction.

In any event, capacitor C_F must have sufficient charge to dump into the bootstrap capacitor when V_s moves toward COM. This happens when the lower switch is on and when the upper switch has just been turned off. But long $R_G \times C_F$ time constant causes extra switching loss.

If R_G is too small, it tends to reduce the effective dead time and increase shoot-through tendency. In addition, switching dv/dt increases EMI. However, if R_G is too large, it may fail to hold the gate low when the opposing power device turns on, either tending to turn on the device prematurely or slow desired turn-off, due to the Miller Effect. One may need to bypass R_G with an anti-parallel signal diode [33][34].

important to leave some extra space on voltage rating and leave quite a larger extra space on current rating based on design requirement. Heat dissipation is another substantial effect when considering package and specifying electrical elements.

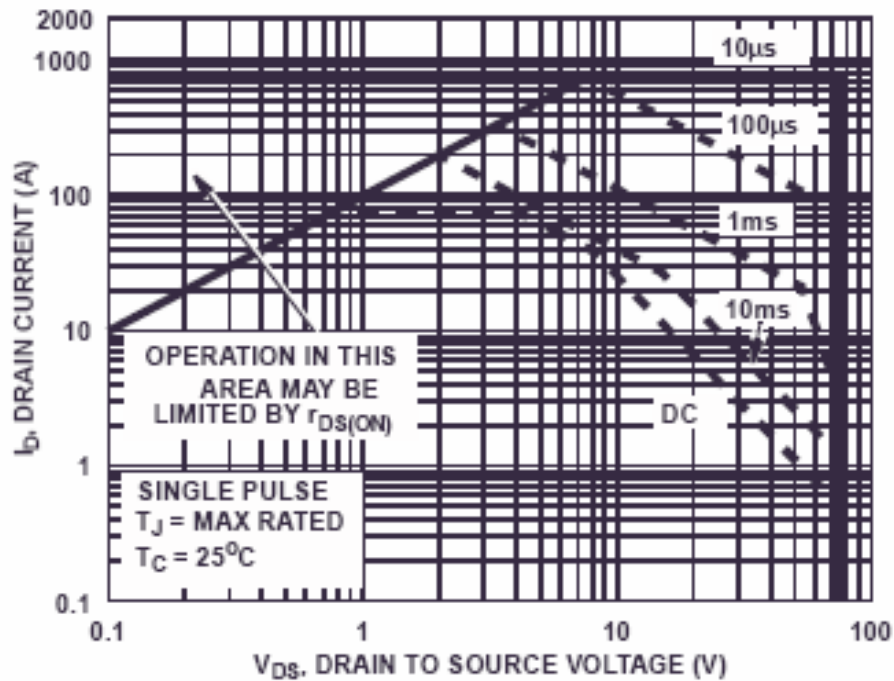


Figure 6.8 Fairchild FDP047AN08A0 safe operating area (SOA) [57]

MOSFET is a good power semiconductor device for parallel due to its physical characteristic, which is good for increasing current rating and reducing conduction resistance. However, the build-in capacitor may introduce some limitation. The build-in capacitors are charging and discharging when the switch is on and off. The speed of charging and discharging depends on the capacitance and the drive current and it is important to short these time delays to make switching work properly and achieve good

system performance. It is a tradeoff in real design. And also with consideration of cost, two or three MOSFETs will be paralleled to work as one switch.

6.4 High Current Design

For high current board design, heat dissipation and conduction loss is noticeable. Some problems are caused by high current. Electronic components are more sensitive to temperature extremes. Semiconductor long-term reliability is directly affected by operating temperatures. The maximum junction temperature is the critical design point for motor control power stages. Reliability research suggests that for each 10°C rise in junction temperature, the long-term reliability is decreased by about 50 percent [15]. As a result, special design and rules need to be considered.

Larger converter footprint does not necessarily imply good hot-spot design. Leadless copper pad style packages, such as Power Pak for power semiconductors, provide better thermal performance than leaded packages like SO8. Thermally effective packages have a much lower junction-to-case thermal resistance. Proper thermal via placement within a brick layout will provide lower resistance to heavy copper planes within its PCB. 3, 4 or 5 oz. copper conductors and planes help spread heat throughout the PCB making the module temperature more homogeneous and reducing hot spots. This allows each electrical device to be closer to the average PCB temperature. Heat can then be convectively coupled to the passing air stream as well as coupled through well-designed power terminations to the host PCB.

6.4.1 Current Rating

In general, a bus bar design consists of one or more flat electrical conductors laminated and electronically insulated by a thin dielectric material, which is encapsulated or sealed along the edges. Input and output tabs are placed at convenient points to minimize interconnections.

To determine the proper size of copper conductors, refer to the following table for specific current and cross sectional areas needed to minimize voltage drop:

Table 6.1 Relationship between bus bar size and current

| Wire Gauge (AWG) | Circ. mils | Sq. mils | Rated Current* (amperes) |
|------------------|------------|----------|--------------------------|
| 16 | 2583 | 2025 | 5.63 |
| 14 | 4110 | 3230 | 8.96 |
| 12 | 6530 | 5130 | 14.24 |
| 10 | 10380 | 8155 | 22.65 |
| 8 | 16510 | 12970 | 36.02 |
| 6 | 26240 | 20610 | 57.27 |
| 4 | 41740 | 32780 | 91.06 |
| 2 | 66360 | 52120 | 144.80 |
| 0 | 105600 | 82910 | 230.17 |
| 00 | 133100 | 104500 | 290.38 |
| 000 | 167800 | 131800 | 366.08 |
| 0000 | 211600 | 166200 | 461.64 |

The current (amperage) rating is based upon the cross-sectional area of the conductor. This directly reflects the temperature rise at given amperage. A general rule of thumb for determining the current carrying capacity is:

$$I = [(W)(T)]/.00036 \quad (39)$$

I = Amperage , W = Width of conductor , T = Thickness of conductor

.00036 = 360 sq. mils per amp

In most cases this should result in less than a 30% rise at operating currents.

6.4.2 High Current Distribution Devices

There are several choices for high current board design with consideration of heat dissipation, such as bus-bar, heat pipe.

A heat pipe is a simple device that can quickly transfer heat from one point to another. They are often referred to as the "superconductors" of heat as they possess an extra ordinary heat transfer capacity and rate with almost no heat loss. It consists of a sealed aluminum or copper container whose inner surfaces have a capillary wicking material. The wick provides the capillary driving force to return the condensate to the evaporator. The quality and type of wick usually determines the performance of the heat pipe.

A laminated bus-bar system consists of planar conductors separated by insulating layers. The conductors are usually copper, plated with tin, nickel, or gold, depending on

system requirements. The stack of conductors and insulators is laminated together--often with the edges sealed--to form a monolithic, multi-conductor assembly that can be completely insulated on the outside.

Laminated bus-bar systems can also incorporate circuit elements such as capacitors, fuses, circuit breakers, diodes, resistors, IGBTs, and heat sinks, as well as all types of terminations and/or connectors. Flex circuit breakouts can also be implemented into the design of a laminated bus-bar assembly.

Laminated bus-bar systems handle high currents with less voltage drop, thereby better maintaining the regulation of the dc voltage across the system. The laminated design also reduces the amount of noise on the power buses, because the conductors can be interleaved with just the right sequence of voltage, polarities--or even ground planes--to minimize noise. The laminated conductors have lower inductance than conventional cables, minimizing the negative effects of power supply noise.

These laminated assemblies are widely used in the following products, Telecom Power, Computer Power Supplies, UPS Systems, Inverters, Motor Drives, Motor Controls and Locomotives.

When current levels exceed several hundred amperes per circuit, it is necessary to use heavy-gauge cables, 2 /0 AWG or heavier, which are very stiff and difficult to bend into the optimum shape to fit in an enclosure.

6.5 Loss Calculation

The main heat dissipation of this controller is from DC/AC inverter, which means from MOSFET. It is worth to calculate efficiency of this part and design the heat sink. There are two main resource causing power losses for MOSFETs working as switch. The total power loss includes power loss in resistive (conduction loss) and power loss in switching (switching loss).

In power electronics, power semiconductors devices are generally operated as switches. These switches can be made to operate at high frequency to convert and control power with high efficiency and high resolution. The power loss in the switch itself is very small since the voltage is nearly zero when it is on and the current is nearly zero when it is off. Typical switching waveforms for a practical switch are shown in Figure 6.9.

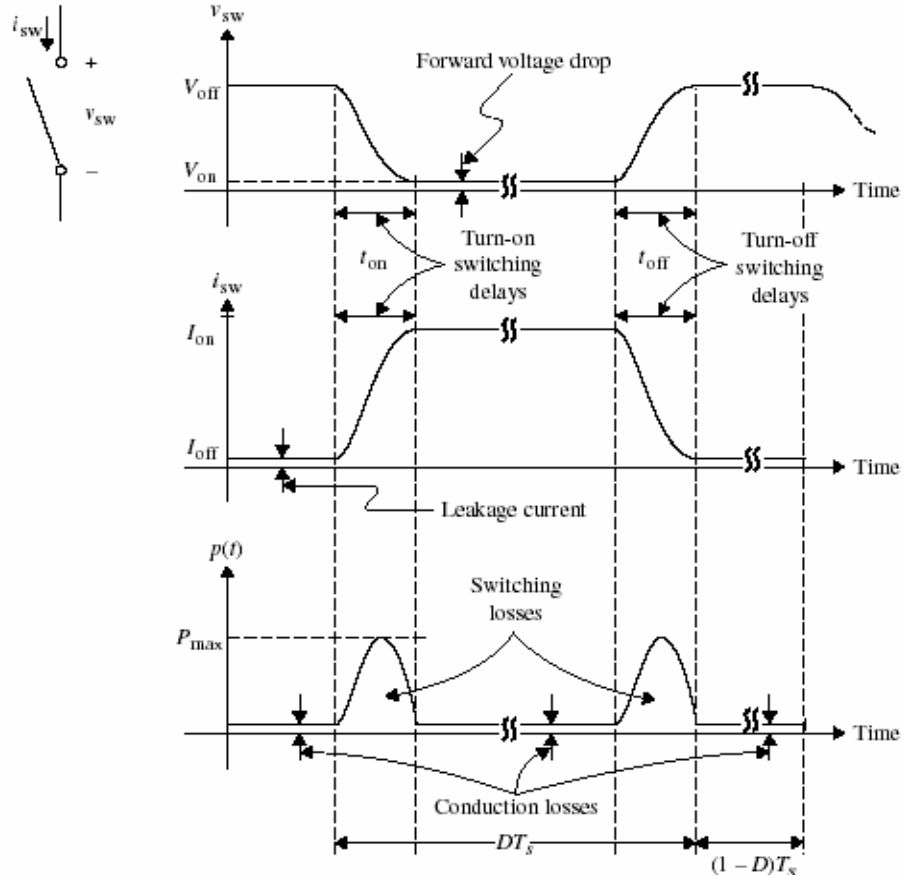


Figure 6.9 Typical switching waveforms of power transistors

The average power dissipation, P_{ave} , over one switching cycle is given by [42]

$$P_{ave} = \frac{1}{T_s} \int_0^{T_s} i_{sw} v_{sw} dt = P_{ave,swit} + P_{ave,cond} \quad (40)$$

Where $P_{ave,swit}$ is the average switching losses and $P_{ave,cond}$ is the average conduction losses, given by

$$P_{ave,swit} = \frac{1}{T_s} \left[\int_0^{t_{on}} i_{sw} v_{sw} dt + \int_{DT_s - t_{off}}^{DT_s} i_{sw} v_{sw} dt \right] \quad (41)$$

$$\begin{aligned} P_{ave,cond} &= \frac{1}{T_s} \left[\int_{t_{on}}^{DT_s - t_{off}} I_{on} V_{off} dt + \int_{DT_s}^{T_s} I_{off} V_{on} dt \right] \\ &= I_{on} V_{off} \left(D - \frac{t_{on} + t_{off}}{T_s} \right) + I_{off} V_{on} (1 - D) \end{aligned} \quad (42)$$

Conduction loss on MOSFET is main loss in controller. It greatly depends on $R_{ds(on)}$ value. (MOSFET conduction loss is main loss for switching frequency $< 1\text{M HZ}$ [15].) It will dramatically change even $R_{ds(on)}$ just changes a little when load current is huge.

For high-side MOSFET, the conduction loss is [59]:

$$P_{cond} = I_{out}^2 * R_{ds(on)} * D \quad (43)$$

The switching loss is:

$$P_{sw} = \frac{1}{2} V_{in} * I_{out} * f_{sw} * (t_{s(L-H)} + t_{s(H-L)}) \quad (44)$$

There are several additional losses that are typically much smaller than the aforementioned losses. In order of importance, the first two are the power to charge the gate and the power to charge the MOSFET's output capacitance. They can be calculated by

$$P_{gate} = V_{in} * Q_g * f_{sw} \quad (45)$$

$$P_{cos s} = \frac{1}{2} C_{oss} * V_{in}^2 * f_{sw} \quad (46)$$

For low-side, we have conduction loss:

$$P_{cond} = I_{out}^2 * R_{ds(on)} * (1 - D) \quad (47)$$

Low-side switching losses:

$$P_{sw} = t_{s(H-L)} * V_F + t_{s(L-H)} * \frac{1}{2} (V_F + 1.1 * I_{out} * R_{ds(on)}) * I_{out} * f_{sw} \quad (48)$$

Dead-time is needed to avoid short circuit. During the time, the body diode is in forward conduction. The conduction loss is:

$$P_{diode} = V_F * I_{out} * f_{sw} * T_{deadtime} \quad (49)$$

For DC/AC inverter applications, switching frequency do not need so high as DC/DC converter, where switching loss may play an important role. When switching loss is not so dominant, soft-switching technology may not necessary because of its complicated and causing additional loss in real world.

Substituted with the motor controller parameters, the controller efficiency can be assumed about 95% in theory. Real test results and analysis will introduce in Chapter 7.

6.6 Interface

For most power switches, microprocessor pins cannot provide enough power to drive their gates/bases to implement switching operation. Therefore, a specially designed interface circuit is necessary to drive the gates/bases according to the output low power signals from the microprocessor.

Furthermore, in order to protect the microprocessor electrically from possible over-voltage or over-current fault, it is necessary to isolate the low power circuitry from high power one electrically while the signal is still allowed to pass through. An optical isolator (optocoupler) is an ideal device for this application. An optocoupler consists of a primary side circuit and a secondary side circuit. The primary circuit is an LED and the secondary side is a photo transistor or light sensitive logic circuit. When the LED is lit, the secondary transistor is conducting. There is no electrical connection between the two sides. The grounds should be separate also.

Electrical noise (EMI or RFI) from the power stage can all too easily feed back into the sensitive control stage and cause havoc. From a voltage safety viewpoint, it is advantageous to use voltage isolation between the logic control and the power stage. This allows safer troubleshooting of the logic control and minimizes the chances of voltage spikes that will upset the logic. Price wise, optocouplers are low-cost insurance. An optocoupled interface will protect the DSP or MCU from catastrophic power stage failures [15].

Optocoupler uses the light-to-current and current-to-light conversion property of photodiodes and LEDs to provide signal connection between two circuits without any need for electrical connections. Because diodes are nonlinear devices, the opto-isolator is not used in transmitting analog signals. However, opto-isolators find a very important application when on/off signals need to be transmitted from high-power machinery to delicate computer control circuitry. The optical interface ensures that potentially damaging large currents cannot reach delicate instrumentation. [21]

If multiple power switches are used in the circuit, their gate drive signals cannot share the same ground because their sources (for MOSFETs) or emitters (for BJTs) are at different voltage levels according to the operating principle of the circuit. Therefore, multiple power supplies will be necessary to provide different grounds.

In this design, a buffer 7407N is employed after DSP output signals to convert TTL voltage to CMOS voltage level. A high-speed (10Mbit/s) optocoupler HCPL2631 is input between output control signals from the DSP and inverter to protect DSP chip.

6.7 Controller Implementation with TMS320F2407A

Figure 6.9 shows the picture of the DC/AC converter's prototype. The prototype is made of two print circuit boards (PCB): the controller board and the power stage board. In this way, the high-voltage components and trace will be confined on the power stage board and on the low voltage components and trace on the controller board. Another benefit of this structure is that the power stage prototype need not change too much, but the controller board may change significantly. Making them into two different boards can make the optimization much easier. The drivers' circuit is on the power stage board to make sure that they are as near the MOSFETs as possible to eliminate the noise and parasitic inductance affections.

We can calculate the total loss on DC/AC inverter is 102W, which can easily dissipated by heat sink with fan cooling. Figure 6.9 is the prototype inverter with fan cooling which we designed and fabricated for 2 KW (Current RMS value is 65A) power output. Each heat sink is designed for 50W heat dissipation. It provides much better cooling performance with fan cooling. The PCB is 4 OZ heavy-copper PCB prototype board, which is specially designed for high current application. This board has been tested and worked greatly.

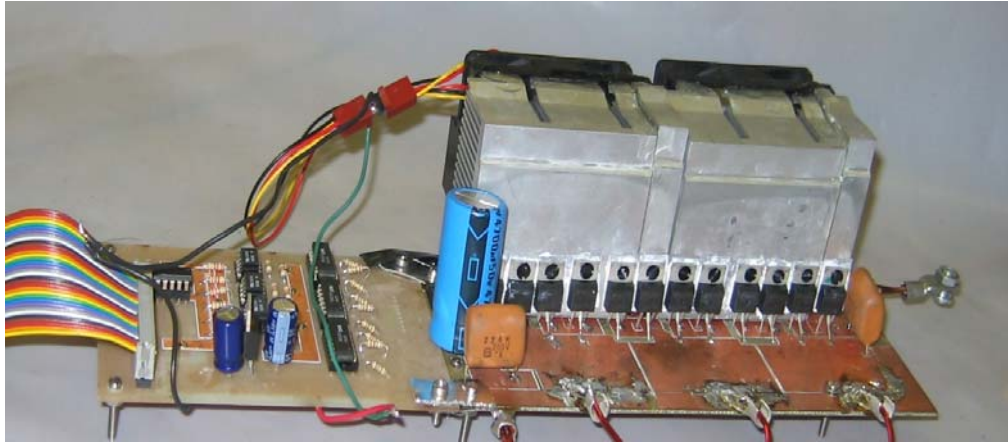


Figure 6.10 Prototype of inverter with heat sink

6.8 The Proposed Embedded System

The proposed super high-speed PMSM controller is based on DSP control, which produces the control signals based on SV PWM algorithm. Drive board provides drive power to the motor. A simple and easy to realize control method, constant volt per hertz (V/f) control scheme, is implemented to control motor speed. Due to the low phase inductance of the slot-less structure and inductance load requirement of PWM, an extra inductor low pass filter is used.

Space Vector PWM method is an advanced, computation-intensive PWM method and becomes widely applied in high performance application these years because of its superior performance characteristics. In space vector PWM method, voltage modulation

index, m , is chosen less than 0.952 to avoid over-modulation [8] [61]. A careful chosen switching frequency is helpful to realize higher speed and better performance. TI high-performance DSP TMS2000 will generate Space Vector PWM control signals and realize constant volts/hertz method, and PID compensation in feedback loop.

The proposed control scheme is implemented on the TMS320LF2407A. All the control routines are implemented using assembler language with fixed precision numerical representation. The control algorithm is synchronized by the DSP internal timers that generate interrupts. The software configuration is given as following.

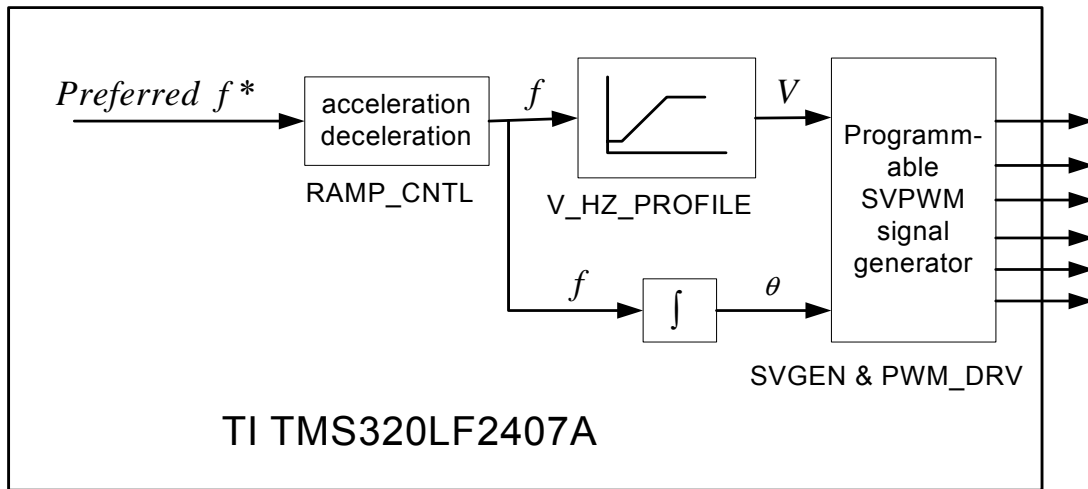


Figure 6.11 Software configuration

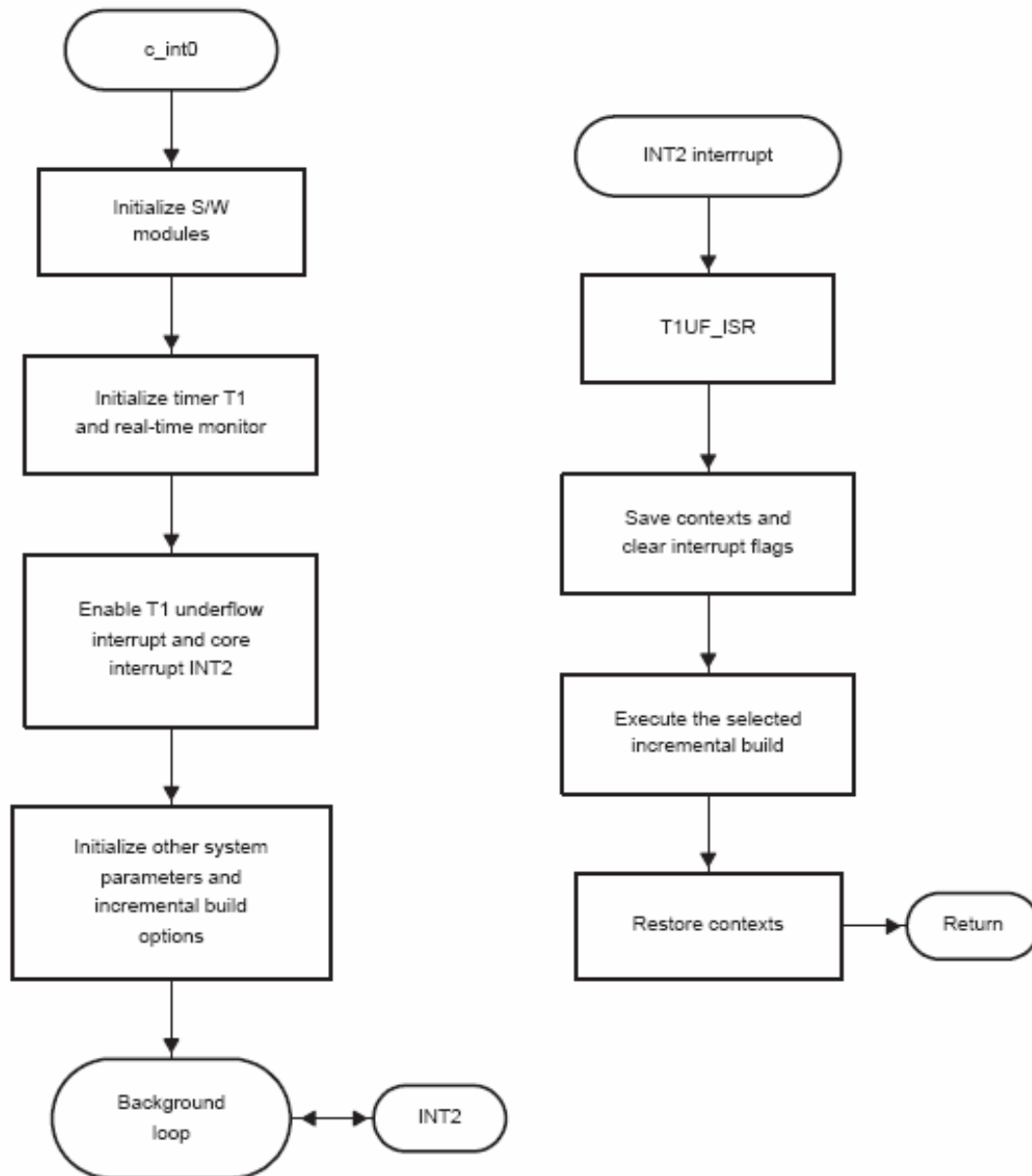


Figure 6.12 Software flow chart

6.8.1 Main blocks

RAMP_CNTL:

This module implements a ramp up and ramp down function. It is to make the output variable `setpt_value` equal the preferred input variable `target_value`.

V_HZ:

This module generates an output command voltage for a specific input command frequency according to the specified volts/hertz profile. This is used for variable speed implementation of AC motor drives.

SVGEN:

This module calculates the appropriate duty ratios needed to generate a given stator reference voltage using space vector PWM technique. The stator reference voltage is described by its magnitude and frequency.

PWM_DRV:

This module uses the duty ratio information and calculates the compare values for generating PWM outputs. The compare values are used in the full compare unit in 24x/24xx event manager (EV). This also allows PWM period modulation.

Optimization and debug are needed to make source code work correctly for the two super high-speed motors.

CHAPTER SEVEN: EXPERIMENTAL RESULTS AND ANALYSIS

The following test results and analysis are taken by the 100 Krpm motor first, and followed by the test results and analysis of 200 Krpm super high-speed motor.

7.1 Calibration of Current Probe

During test, we found our current meter has some attenuation as well as phase shift. We calibrated our AC current probe with another high-end AC and DC current probe (HP 1146A), oscilloscope and function generator.

We tested same sinusoidal signal using these two current probes and took HP 1146A as standard, which has no decay and shift in our applied frequency range. The test results of phase shift and attenuation in different frequency of ampere meter are shown in Figure 7.1.

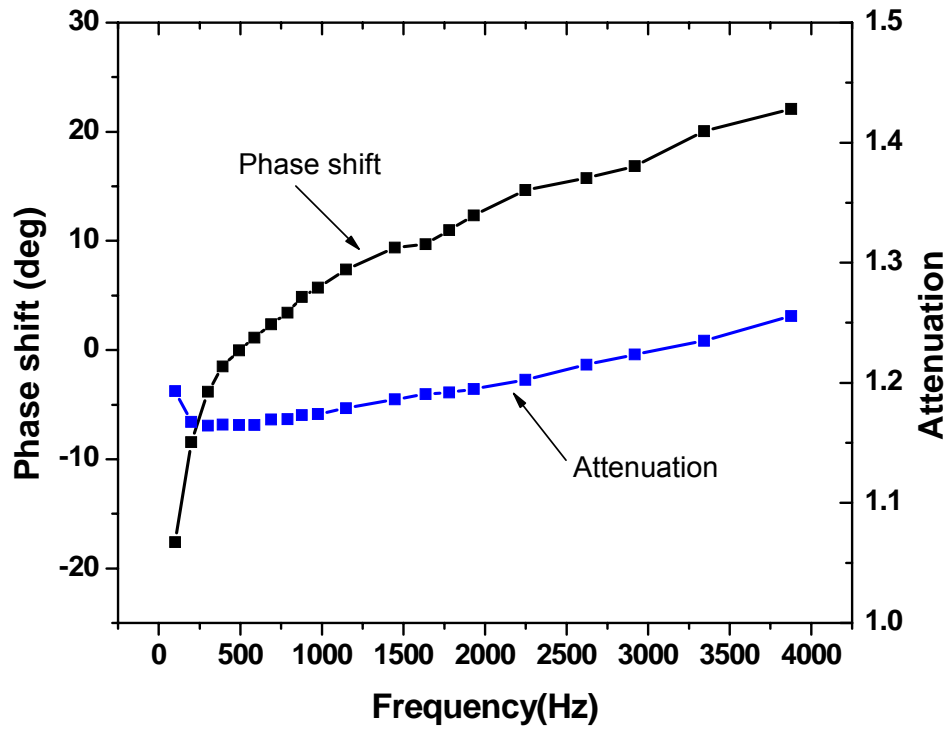


Figure 7.1 Phase shift and attenuation of AM Meter

The next figure shows the relationship of the ratio of the real current value over the reading value by our current probe with motor speed, which was test with real SV PWM control signals.

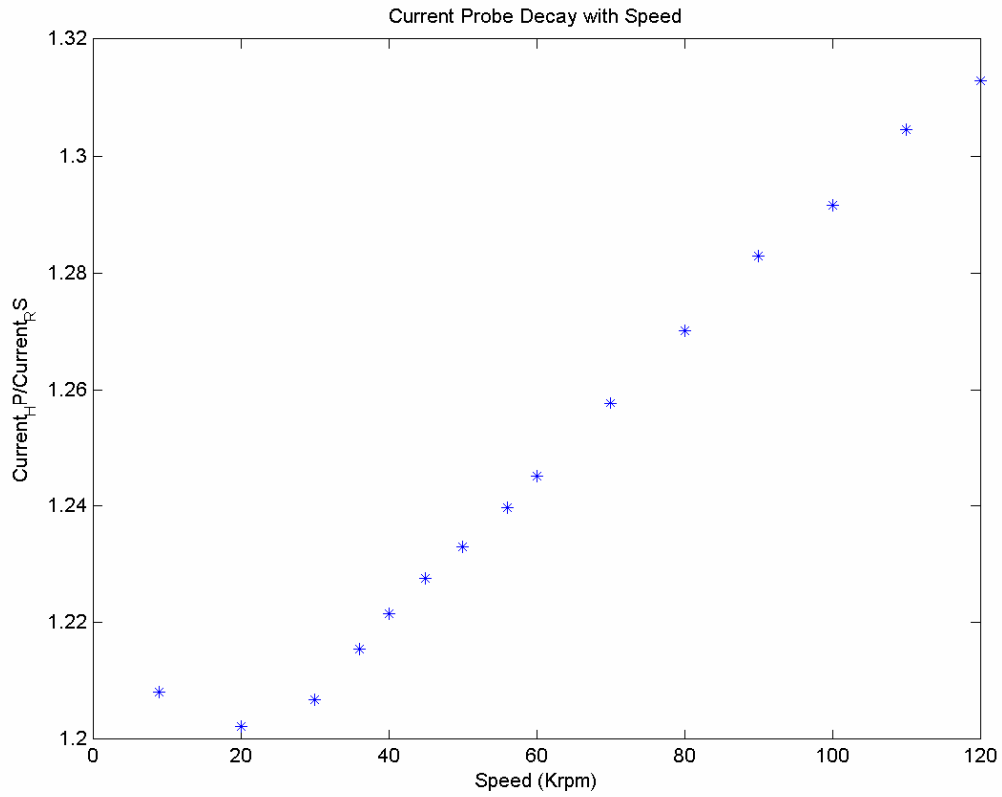


Figure 7.2 The real current value/ the reading value under different motor speed

After considering these phase shift and attenuation. The real input power to the motor can be calculated.

7.2 Experimental Results of Test Motor 1

The test was conducted up to about 87KRPM after increasing the input power to motor using open-loop control method. This speed limitation is mainly resulted from the

insufficient capability of the motor. With the new design and high efficiency 2000W super high-speed motor, the target speed (200 Krpm) was successfully achieved.

With the proposed optimal constant V/f control strategy, the motor has a much better dynamic performance, as shown in Figure 7.3, compared with motor phase current under original constant V/f control scheme and under the optimal V/f control scheme. Figure 7.4 shows excellent motor phase voltage and phase current sinusoidal waveforms at 50,000 RPM. The FFT analysis of the phase current I_c harmonics is given in Figure 7.5. The most prominent harmonic is 5th, whose normalized RMS value is only 5.88% and is negligible. In industry, it is all a rule of thumb – the harmonic is not harmful once it falls under 5%. The experimental results validate the effectiveness of the proposed scheme.

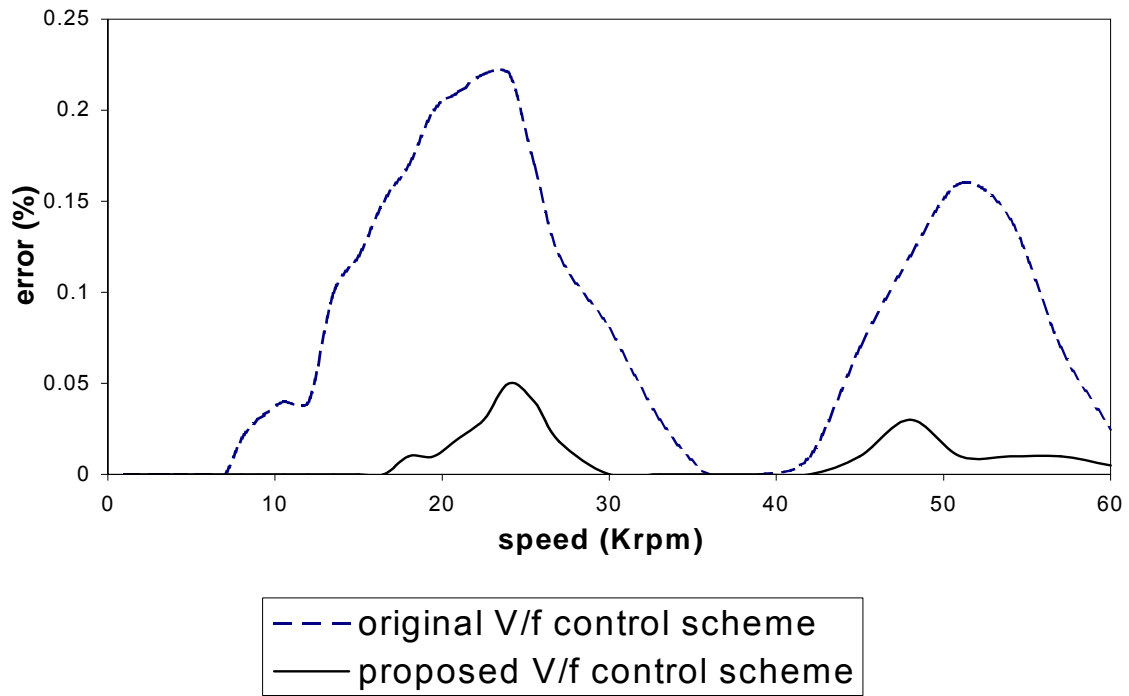
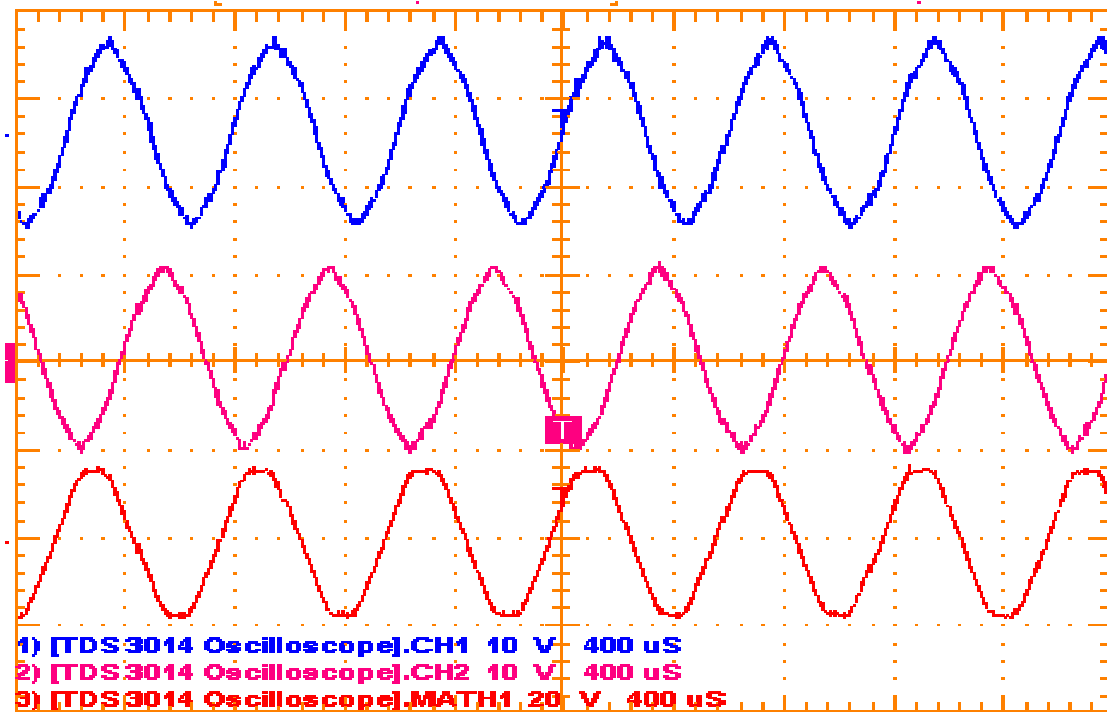


Figure 7.3 PMSM phase current ring error with mechanical speed (normalized) -- Real test results comparison



- PMSM phase voltage V_a waveforms
- PMSM phase voltage V_b waveforms
- PMSM phase current I_c waveforms

Figure 7.4 Motor phase voltage V_a , V_b and phase current I_c waveforms at 50,000 RPM

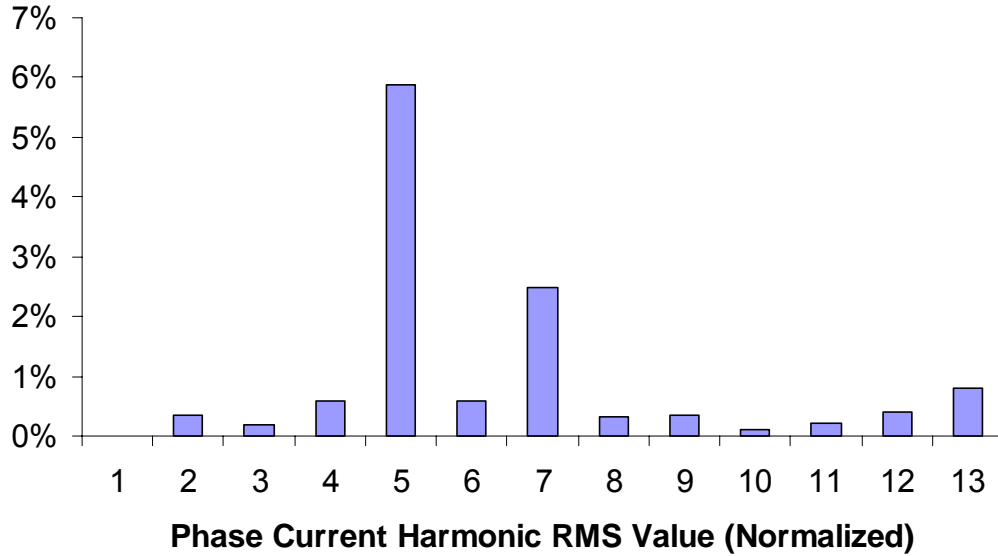


Figure 7.5 Phase current I_c harmonic FFT analysis (normalized)

Several system optimizations have been tested and employed. As we know, high switching frequency always yields good result in theory. However, more switching losses will dissipate in inverter with increasing switching frequency. More dv/dt noise also occurs. It also requires that every component in the whole system have excellent dynamic characteristics. But motor efficiency will increase due to lower core loss [65][66][67]. Simulation and tests are done to discover this balance. The result show that the system performance is almost the same when switching frequency is within some range.

Programmable dead time is added to PWM signals to avoid short circuit. This occurs in voltage source inverter due to the time spent on charging and discharging MOSFET input capacitors.

An extra low pass filter is needed to eliminate harmonics and also compensate low motor phase inductance. A 50uH inductance is chosen for the project.

7.3 Experimental Results of Test Motor 2

This super high-speed motor (2 KW, 200 Krpm) was tested under no load condition at first. With the further improvement of motor and controller, the super high-speed motor finally successfully reached the target speed -- 200 Krpm. Input power to PMSM at 200,000 rpm is 187 W. To further improve the efficiency of the 200,000 rpm motor, some modifications and tests have been done. The following figure shows the test results.

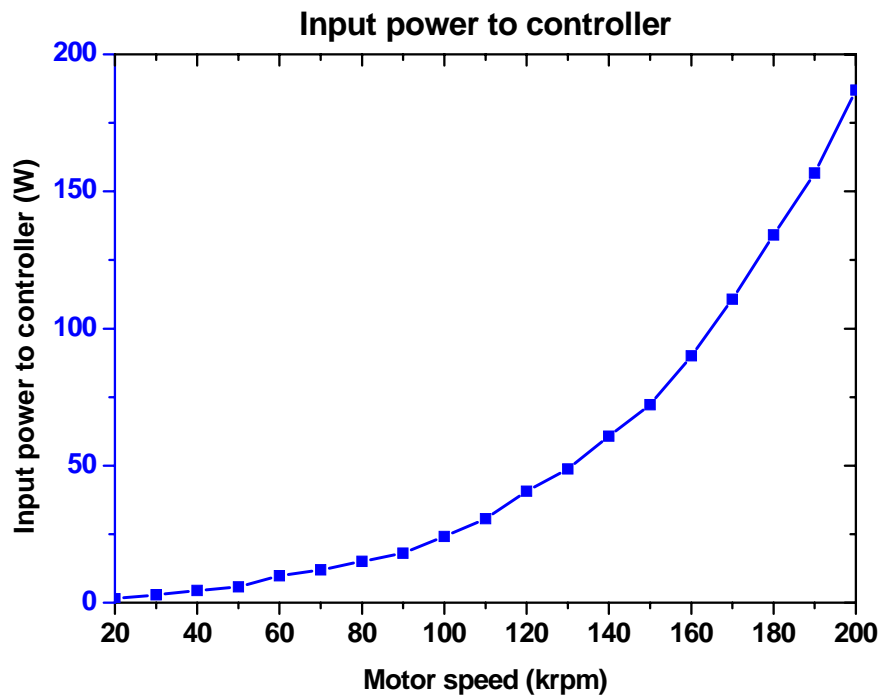


Figure 7.6 Input power to controller under different motor speed

7.4 Load Test Results and Analysis

Due to the huge phase current, the connection loss from connection lines and LPF can not be neglected. The resistance of connection line and LPF are tested with LCR meter.



Figure 7.7 LCR meter

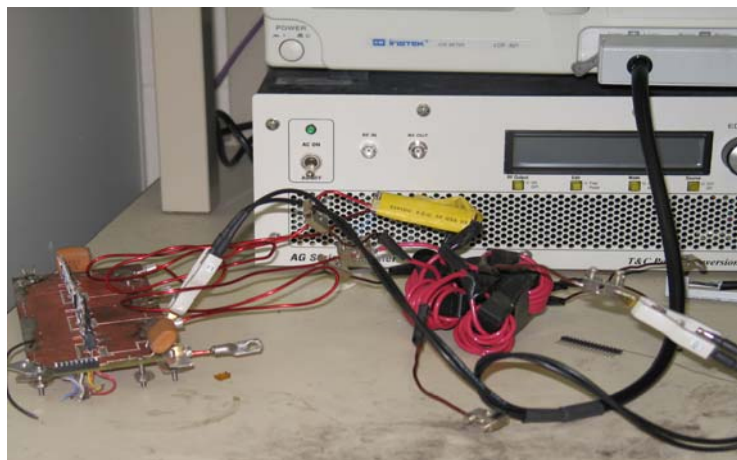


Figure 7.8 Test connection resistance with LCR meter

With these results, the super high-speed motor load test can be analyzed as follows:

Table 7.1 Load test results and analysis

| Motor Speed (krpm) | Input Current to motor (A) | Input Power to motor (W) | DC Voltage (V) | DC Current (A) | DC Power to controller (W) | Controller+LPF Efficiency (%) | Connection line + LPF resistance (mΩ) | Controller Efficiency (%) |
|-----------------------|-------------------------------|-----------------------------|----------------|----------------|-------------------------------|----------------------------------|--|------------------------------|
| 30.5 | 24.7 | 137.2 | 28.74 | 7.05 | 202.6 | 67.7 | 17 | 72.8 |
| 61 | 31.8 | 347.7 | 24.12 | 19.35 | 466.7 | 74.5 | 17.2 | 78.2 |
| 73.2 | 37.3 | 490.2 | 26.48 | 23.25 | 615.7 | 79.6 | 17.3 | 83.5 |
| 97.6 | 49.9 | 876.9 | 26.18 | 40.5 | 1060 | 82.7 | 17.4 | 86.8 |
| 109.8 | 40.3 | 785.7 | 26.94 | 33.3 | 897.1 | 87.6 | 17.4 | 90.7 |

The profile of controller efficiency can be drawn as Figure 7.9.

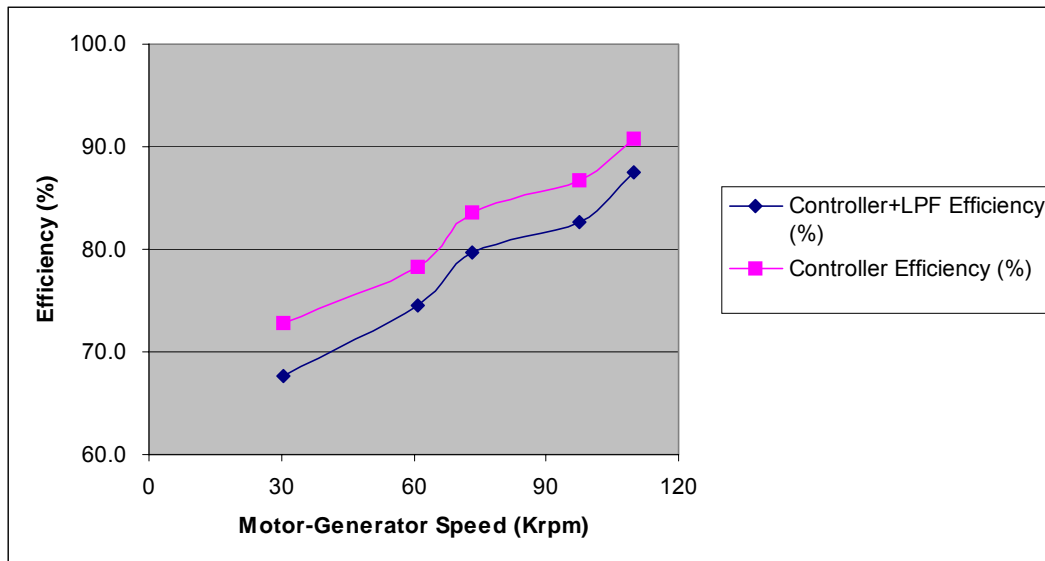


Figure 7.9 Controller efficiency with load

There are several possible solutions to further improve the system efficiency:

- Test system efficiency under premium status.
- With optimized parameters of source code, the system efficiency also can be improved. For different motor, the optimal values of the parameters are different. The optimum value can be found by test.
- Switching loss is linear with switching frequency and takes almost 30% of total loss. When the test is not with super high-speed, switching frequency can be lower to get a higher efficiency.
- When current goes high, the connection loss on connection line and LPF cannot be neglected. Shorter line, lower resistance and lower loss. Some motor control handbooks suggest directly installing controller on the motor to

reduce loss and harmonics caused by connection lines [15]. Loss pass filter is one component caused extra loss. But it cannot be removed because PWM signals need inductive load and inductance of our motor is too small.

7.5 Trouble Shooting

During the experiments, the high side of Driver IC IR2110 is latched up when the load increases. Due to the stray inductance on the trace between the high side and low side of MOSFET, V_s will undershoot less than zero, as shown in Figure 7.11(a). When $V_{BS_MAX} > 25V$, then the diode D_1 inside the driver will be latched up or even broken down. If V_B undershoots to a negative value, then diode D_2 will conduct, as shown in Figure 7.11(b). If no resistor in series, D_2 will latch up or even breakdown soon.

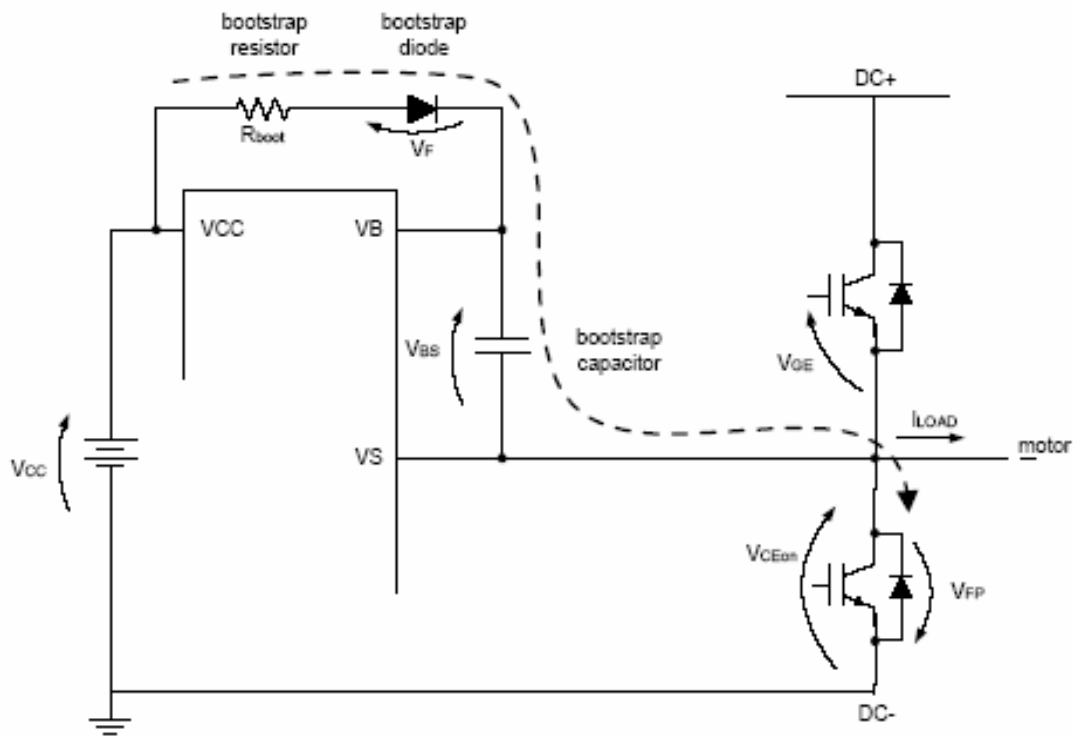
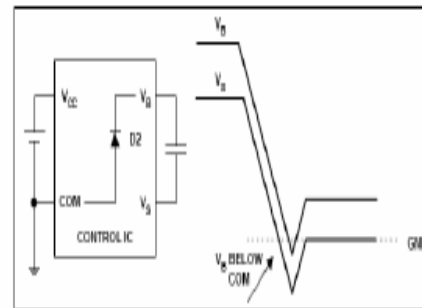
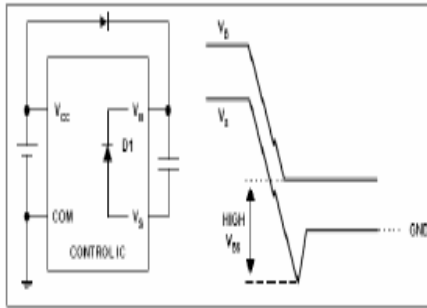


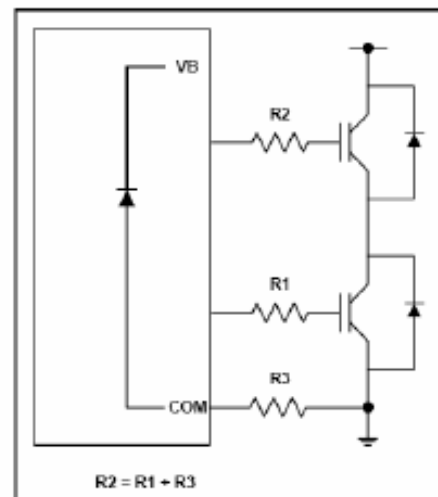
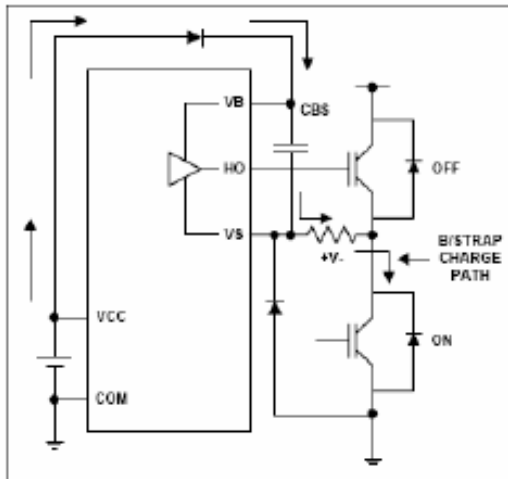
Figure 7.10 Bootstrap supply schematic [33]

To damp the ringing of V_S and V_B , two methods can be applied as shown in Figure 7.12. Experiment results show that the undershooting is damped. The undershooting of V_S and V_B will exaggerate when load increases. To avoid latch up at higher load, the undershooting of V_S and V_B should be strictly confined.



(a) Ideal Bootstrap Circuit (b) Practical Bootstrap Circuit with Floating Supply

Figure 7.11 Ring effect of V_B and V_s on drive IR2110 [32]



(a)

(b)

Figure 7.12 Two methods of V_s undershoot immunity [32]

CHAPTER EIGHT: CONCLUSION

8.1 Conclusion

In this dissertation, a approach for optimal digital controller for super high-speed PMSM is provided. Analysis on the effect of the PMSM parameters on its dynamic characteristics including stability and performance was performed. It was presented that super high-speed PMSM stability can be achieved over the full operating speed range. The stator resistance, R_s , which cannot be neglected, was taken into account to design a new optimized V/f control. An optimal nonlinear V/f schematic was derived.

Experimental experience gained from the DSP-based digital controllers for super high-speed PMSMs was also introduced in this dissertation. Testing systems for the super-high speed PMSM were built and feasibility has been examined.

LIST OF REFERENCES

- [1] Mouhoub Mekhiche, James L. Kirtley, Mary Tolikas, Edward Ognibene, Jerome Kiley, Evgeny Holmanskyy, and Francis Nimblett, "High Speed Motor Drive Development for Industrial Applications", Electric Machines and Drives, 1999. International Conference IEMD '99 9-12 May 1999 Page(s):244 – 248

- [2] M.A.Rahman, Fellow IEEE, Akira Chiba, Senior Member, IEEE and Tadashi Fukao, Fellow IEEE, "Super High Speed Electrical Machines – Summary", Power Engineering Society General Meeting, 2004. IEEE, 6-10 June 2004 Page(s):1272 - 1275 Vol.2

- [3] Shigematsu, K.; Oyama, J.; Higuchi, T.; Abe, T.; Ueno, Y., "The study of eddy current in rotor and circuit coupling analysis for small size and ultra-high speed motor", Power Electronics and Motion Control Conference, 2004. IPEMC 2004. The 4th International, Volume 1, 2004 Page(s):275 - 279 Vol.1

- [4] Morel, L.; Fayard, H.; Vives Fos, H.; Galindo, A.; Abba, G., "Study of ultra high speed switched reluctance motor drive", Industry Applications Conference, 2000. Conference Record of the 2000 IEEE, Volume 1, 8-12 Oct. 2000 Page(s):87 - 92 vol.1

- [5] Andrzej M. Trzynadlowski, "The Field orientation principle in control of induction motors", Kluwer Academic Publishers, 1994

- [6] P.D.C. Perera, F. Blaabjerg, J.K. Pedersen, P. Thogersen, "A sensorless, stable v/f control method for permanent-magnet synchronous motor drives" *Industry Applications, IEEE Transactions on*, Volume: 39 Issue: 3, pp. 783 -791, May-June 2003.
- [7] T.M. Jahns, "Motion control with permanent-magnet AC machines", *Proceedings of the IEEE*, Volume: 82 Issue: 8, pp. 1241 -1252, Aug. 1994
- [8] Bose. Bimal , "Modern Power Electronics And AC Drives," Prentice-Hall, 2002
- [9] Vas. Peter, "Sensorless Vector And Direct Torque Control," Oxford Science Publications, 1998
- [10] R.S.Colby, D.W. Novotny, "An efficiency-optimizing permanent-magnet synchronous motor drive," *Industry Applications, IEEE Transactions on* , Volume: 24 Issue: 3, pp. 462 -469, May-June 1988
- [11] Paul C. Kause, Oleg Wasynczuk and Scott D. Sudhoff, "Analysis of Electric Machinery", IEEE Press, 1995
- [12] D. Grahame Holmes and Thomas A. Lipo, "Pulse Width Modulation for Power Converter", IEEE Press Series on Power Engineering, IEEE Press, Wiley-Interscience, 2003
- [13] Ashfaq Ahmed, "Power Electronics for Technology", Prentice Hall, 1999

- [14] B. Jayant Baliga, "Power Semiconductor Devices", PWS Publishing Company, 1996
- [15] Richard Valentine, "Motor control electronics handbook", McGraw-Hill, 1998
- [16] Bon-Ho Bae, Seung-Ki Sul, Jeong-Hyeck Kwon, Jong-Sub Shin, "Implementation of sensorless vector control for super-high speed PMSM of turbo-compressor", Industry Applications Conference, 2001. Thirty-Sixth IAS Annual Meeting, Conference Record of the 2001 IEEE, Volume: 2, pp. 1203 -1209 vol.2, 30 Sep-4 Oct 2001.
- [17] G.R. Slemon, "On the design of high performance PM motors," Industry Applications Society Annual Meeting, 1992., Conference Record of the 1992 IEEE, pp. 279 -285 vol.1, 4-9 Oct. 1992.
- [18] Xu, L. and Wang, C., "Implementation and experimental investigation of sensorless control schemes for PMSM in super-high variable speed operation", Industry Applications Conference, 1998. Thirty-Third IAS Annual Meeting. The 1998 IEEE, Volume: 1, Page(s): 483 -489, 12-15 Oct 1998
- [19] A. Hughes, P. J. Lawrenson, "Simple Theoretical Stability Criteria for 1.8° Hybrid Motors", Proceeding of International Conference on Stepping Motor Systems, September 1979, pp. 127-135

- [20] Colby, R.S. and Novotny, D.W., "An efficiency-optimizing permanent-magnet synchronous motor drive", Industry Applications, IEEE Transactions on, Volume: 24 Issue: 3, Page(s): 462 -469, May-June 1988
- [21] Robert W. Erickson, and Dragan Maksimovic, "Fundamentals of Power Electronics", 2nd Edition, Kluwer Academic Publisher, 2000
- [22] Geof Potter, "An Introduction to Digital Control of Switching Power Converters", Emerson DCDC Technical White Paper, April 2004
- [23] Alberto Cavallo, Roberto Setola and Francesco Vasca, "Using MATLAB Simulink and Control System Toolbox", Prentice Hall, 1996
- [24] Duane Hanselman, Bruce Littlefield, "Mastering MATLAB 5", Prentice Hall, 1998
- [25] Thomas Gilmore and Raymond G. Sladky, "Ratings of Semiconductors for AC Drives", IEEE Transactions on Industry Applications, Vol. 37, No. 2, March/April 2001
- [26] Zhenyu yu, Texas Instruments, "Space-Vector PWM with TMS320c24x Using Hardware and Software Determined Switching Patterns", Application Report SPRA524,
- [27] Texas Instruments, Application Note BPRA044, "Digital Signal Processing Solution for Permanent Magnet Synchronous Motor"

- [28] Texas Instruments, Application Report Spru369, "TMS320C24x PWM Full Compare in Symmetric Mode"
- [29] International Rectifier, "Use Gate Charge to Design the Gate Drive Circuit for Power MOSFETs and IGBTs"
- [30] International Rectifier, "Gate Drive Characteristics and Requirements for HEXFETs"
- [31] Ned Mohan, Tore M. Undeland, and William P. Robbins, "Power Electronics- Converters, Applications, and Design", 2nd edition, John Wiley & Sons, Inc., 1995
- [32] Chris Chey, John Parry, "Managing Transients in Control IC Driven Power Stages," Design Tip #DT97-3, International Rectifier Corporation.
- [33] A. Merello, A. Rugginenti, M. Grasso, "Using monolithic high voltage gate drivers", Design Tip, DT04-4, International Rectifier,
- [34] George E. Danz, "HIP2500 High Voltage ($500V_{DC}$) Half-Bridge Driver IC," Application Note, No. AN9010.4, April 1994, Harris Intelligent Power.
- [35] Robert Mammano, "Switching Power Supply Topology Voltage Mode vs. Current Mode," Design Note #DN-62, October 1994, Unitrode Corporation.

- [36] Liping Zheng, "Super High-Speed Miniaturized Permanent Magnetic Synchronous Motor Design", Candidacy, University of Central Florida, 2002
- [37] Liping Zheng, "Design of a Super-High Speed Axial Flux Permanent Magnetic Synchronous Motor for Centrifugal Compressor", submitted to IEE Proc. Electric Power Applications
- [38] "SA828/838 Microprocessor Controlled PWM IC Family", Application Note, MITEL Semiconductor, January 1997
- [39] Texas Instruments, SPRA284A, "AC Induction Motor Control Using Constant V/Hz Principle and Space Vector PWM Technique with TMS320C240"
- [40] Limei Zhao, Chan Ham, et pl. "Design of Optimal Digital Controller for Stable Super-High-Speed Permanent-Magnet Synchronous Motor", to be published by IEE Proc. Electric Power Applications 2005, IEE proceedings online no. 20045266
- [41] Mohammed S Arefeen, David Figoli, Zhengyu Yu, Darnell.com PowerPulse, "Multiple Motor Control Using a Single DSP"
- [42] Issa Batarseh, "Power Electronic Circuits", Wiley, 2004

- [43] J. Holtz, "Pulse width modulation for electric power conversion", Proc. IEEE, Volume 82, Page(s):1194-1214, Aug. 1994
- [44] Texas Instruments, "TMS320F240 DSP Controllers Evaluation Module Technical Reference (Rev. B)", SPRU248B, 31 Jul 1999
- [45] Texas Instruments, "TMS320LF2407A, LF2406A, LF2403A, LF2402A LC2406A, LC2404A, LC2403A, LC2402A DSP (Rev. K)", SPRS145K, August 2005
- [46] Texas Instruments, "Implementing Triple Conversion Single-Phase On-line UPS using TMS320C240", Application Report SPRA589A
- [47] Texas Instruments, "Dead-Time Generation on the TMS320C24x"
- [48] Texas Instruments, "ACI3-2 Sensorless Variable Speed Three-Phase AC Induction Motor with Closed Loop Speed Control"
- [49] International Rectifier, "HEXFET Power MOSFET Designer's Manual - Application Notes and Reliability Data"
- [50] Vrej Barkhordarian, International Rectifier, "Power MOSFET Basics"
- [51] International Rectifier, "The Do's and Dont's of Using MOS-Gated Transistors"

- [52] International Rectifier, "Using MOS-Gated Power Transistor in AC Switching Application"
- [53] Isamu Sato, Koji Otani, Makoto Mizukami, Shigemitu Oguchi, Kunio Hoshiya, and Ken-ichiro Shimokura, "Characteristics of Heat Transfer in Small Disk Enclosures at High Rotation Speeds", IEEE Transactions on Components, Hybrids, and Manufacturing Technology, Vol. 13, NO.4, December 1990
- [54] International Rectifier, "Bootstrap Component Selection For Control IC's"
- [55] International Rectifier, "HV Floating MOS-Gate Driver ICs", INT978
- [56] International Rectifier, Data Sheet No. PD-6.011E, "IR 2110 High and Low Side Driver"
- [57] Fairchild, Datasheet, "FDP047AN08A0 / FDI047AN08A0 / FDH047AN08A0", June 2004
- [58] Mike Keagy, "Calculate Dissipation for MOSFETs in High-Power Supplies", Design Application, Electronic Design, October 2002
- [59] Jon Klein, "Synchronous Buck MOSFET Loss Calculations with Excel Model", Application Note, AN-6005, Fairchild Semiconductor, July 2003
- [60] Maxim Dallas Semiconductor, "Power Supply Engineer's Guide to Calculate Dissipation for MOSFETs in High-Power Supplies", Dec 2002

- [61] Dong-Choon Lee, and G-myoungh Lee, "A Novel Overmodulation Technique for Space-Vector PWM Inverters", IEEE Transactions on Power Electronics, Vol. 13, No. 6, Nov. 1998
- [62] Powerdesigners.com, "Recent Advances in Soft Switching Inverter Technology"
- [63] Deepak Shivaram Shet, "Sensorless Position Estimation in Sinusoidal Permanent Magnet Synchronous Motor", Thesis, Texas A & M University, December 1998
- [64] Fani S. Gunawan, "A Study of The Field-Oriented Control of a Permanent magnet Synchronous Machine With and Without Position Sensor", Thesis, The Ohio State University, 1997
- [65] S. Khomfoi, "Influence of PWM Characteristics on the Core Losses due to Harmonic Voltages in PWM Fed Induction Motors", IEEE Power Engineering Society Winter Meeting, Vol. 1, pp. 365-369, 2000
- [66] Jae-Young Choi, "Effect of Switching Frequency of Soft Switched Inverter on Electric Vehicle System", IEEE IECON 97, Vol. 2, pp. 658-663, 1997
- [67] T. Nergaard, H. Kouns, J.S. Lai, C. Konrad, "Optimal System Efficiency Operation of An Induction Motor Drive", IEEE Industry Applications Conference, 2002, Vol. 2 , pp.826 - 831

- [68] Alfio Consoli, Giuseppe Scarcella, and Antonio Testa, "Industry Application of Zero-Speed Sensorless Control Techniques for PM Synchronous Motors", IEEE Transactions on Industry Applications, Vol. 37, NO. 2, March/April 2001
- [69] Joao O. P. Pinto, A Neural-Network-Based Space-Vector PWM Controller for Voltage-Fed Inverter Induction Motor Drive, Industry Applications, IEEE Transactions on, Volume: 36 Issue, No. 6, Page(s): 1628-1636, Nov-Dec. 2000